CRITICAL TRANSITIONS IN FINANCIAL MODELS

BIFURCATION- AND NOISE-INDUCED PHENOMENA

Submitted by
Damian Smug
to the University of Exeter as a thesis for the degree of
Doctor of Philosophy in Mathematics
November 2018

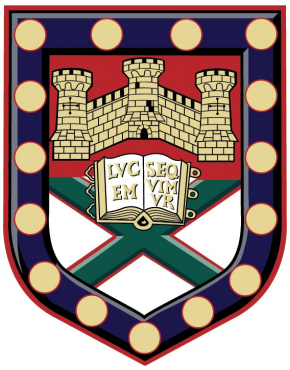

supervised by
Professor Peter Ashwin (University of Exeter)
Professor Didier Sornette (ETH Zürich)
Professor Jan Sieber (University of Exeter)

Abstract

A so-called Critical Transition occurs when a small change in the input of a system leads to a large and rapid response. One class of Critical Transitions can be related to the phenomenon known in the theory of dynamical systems as a bifurcation, where a small parameter perturbation leads to a change in the set of attractors of the system. Another class of Critical Transitions are those induced by noisy increments, where the system switches randomly between coexisting attractors. In this thesis we study bifurcation- and noise-induced Critical Transitions applied to a variety of models in finance and economy.

Firstly, we focus on a simple model for the bubbles and crashes observed in stock prices. The bubbles appear for certain values of the sensitivity of the price based on past prices, however, not always as a Critical Transition. Incorporating noise to the system gives rise to additional log-periodic structures which precede a crash. Based on the centre manifold theory we introduce a method for predicting when a bubble in this system can collapse.

The second part of this thesis discusses traders' opinion dynamics captured by a recent model which is designed as an extension of a mean-field Ising model. It turns out that for a particular strength of contrarian attitudes, the traders behave chaotically. We present several scenarios of transitions through bifurcation curves giving the scenarios a market interpretation.

Lastly, we propose a dynamical model where noise-induced transitions in a double-well potential stand for a company shifting from a healthy state to a defaulted state. The model aims to simulate a simple economy with multiple interconnected companies. We introduce several ways to model the coupling between agents and compare one of the introduced models with an already existing doubly-stochastic model. The main objective is to capture joint defaults of companies in a continuous-time dynamical system and to build a framework for further studies on systemic and individual risk.

Acknowledgements

I would like to express my deep gratitude to my main supervisor, Peter Ashwin, for fantastic collaboration and his clever guidance throughout my study. Moreover, I wish to thank my second supervisor, Didier Sornette, for bringing up millions of ideas and developing my financial and economic intuitions. Furthermore, many thanks to Jan Sieber for important insights and comments on my project. I would like to acknowledge my appreciation to the people who shared their time to discuss my work, especially to Florian Wagener, Egbert van Nes, Frank Kwasniok, Sebastian Wieczorek, Vladimir Levin, and to my fantastic office mates: Hassan, Courtney, Paul, Lamees and others who have crossed paths with me in the legendary office 201.

I am grateful for the opportunity to work within the CRITICS Innovative Training Network, which has received funding from the European Union's Horizon 2020 research and innovation programme under the Marie Skłodowska-Curie grant agreement No 643073. I truly benefited from the events within the network, therefore I am thankful especially to the trio who founded the network: Jeroen Lamb, Martin Rasmussen and Chris Richley. Moreover, to the people who led the courses during CRITICS meetings, to Gianfausto Salvadori, Frank Schilder, Kathrin Padberg-Gehle, Michel Crucifix, Christian Kühn and many others. Obviously, huge thanks to all the CRITICS students (Sajjad, Daniele, Michael, Johannes, Iacopo, Usman, Moussa, Karl, Christian, Flavia, Pablo, Kalle, Ke and Chun) for making this network a true cohort of friends.

Finally, I wish to thank my parents and sister for their support and constant trust in me. And lastly, I would like to dedicate this thesis to my wife Bogna for making my life an amazing adventure, for constantly inspiring me, and for making me reach higher than I would ever imagine.

Contents

List of Figures

List of Tables

Structure of the thesis

In Chapter 1 we list basic mathematical notions which appear throughout this thesis as well as mention several applications of critical transitions in financial models.

In Chapter 2 we explore a stock-bond model of Yukalov et al. [1] stating new findings on its relevance and discover noise-induced structures.

Chapter 3 introduces a method of predicting the time of a crash in the model in Chapter 2. This method, which can potentially be applied to a broad class of dynamical systems, is based on the centre manifold reduction and we test it against Monte Carlo methods.

In Chapter 4 we study an extension of mean-field Ising model applied to traders' decisions. We discover a rich set of bifurcations, which we interpret in terms of a variety of market scenarios.

In Chapter 5 we introduce a double-well coupled system to mimic statistics of companies' defaults. We analyse what kind of phenomena can lead to cascading bankruptcies and how the dependence there can be modelled with copulas.

Each of the Chapters 2-5 has a separate introduction and discussion sections. The aim of this structure is to enable the reader to study each of the chapters as an independent piece of work. We recommend to read the chapters in the order they appear in the thesis, however, this should not be necessary. The thesis concludes with a general discussion (Chapter 6), which puts together the findings presented in Chapters 2-5.

Contributions

Chapters 2 and 3 present the study described in the article: [*Damian Smug, Peter Ashwin and Didier Sornette.* ***"Predicting Financial Market Crashes Using Ghost Singularities"*** *(2018). PLoS ONE 13(3): e0195265]*.

Chapter 4 is based on the article: [*Damian Smug, Didier Sornette and Peter Ashwin.* ***"A Generalized 2D-Dynamical Mean-Field Ising Model with a Rich Set of Bifurcations (Inspired and Applied to Financial Crises)"*** *(2018). International Journal of Bifurcation and Chaos 28(4)]*.

Both manuscripts were prepared by the first author based on research directed by all the authors.

Chapter 1

General introduction

A *Critical Transition* is generally understood as a large and sudden change of the observed state of a system given a small change in the input of a system or a change in the conditions [2]. This phenomenon is often associated with an attractor vanishing as a parameter varies, leading to a jump to another attractor. This association generalises ideas developed in *catastrophe theory* [3] to dynamical systems that are not necessarily driven by a potential as *bifurcation-induced transitions* and can be thought of as an application of *bifurcation theory* [4]. However, the concept of Critical Transitions can also be extended to include transitions caused by noise-induced jumps between different attractors and rate-induced phenomena where the speed at which parameters vary leads the system to change state [5].

Critical Transitions have been applied to many different scientific fields for instance to ecology [6] or climate science [7] and were able to explain a variety of underlying mechanisms. However, in finance and economics the 'true' mechanisms are highly variable because they depend on human decisions and regulation which can affect the market and indeed its structure. Despite the fact that the underlying structures are highly volatile, there exist many simplistic theories which aim to explain market movements with linear models. For example, general equilibrium theory [8, 9] itself is nonlinear, however in applications the analysis is usually restricted to a neighbourhood of an equilibrium. There, the market simply follows an equilibrium with a linear response to perturbations. Nevertheless, linear models cannot be used to justify the spontaneous appearance of bubbles and crashes [10]. In this thesis we use nonlinear models and the mathematical

theory of Critical Transitions to try and explain these phenomena. We explore both bifurcation- and noise-induced Critical Transitions in several models originating from finance and economics.

The goal of this chapter is to introduce some of the mathematical background needed to understand the ideas presented in this thesis. We present some basics of dynamical systems and bifurcation theory, temporal discretisation schemes as well as continuation methods. Moreover, we discuss solutions of stochastic differential equations and provide numerical schemes for these. At the end of this chapter, we point to some examples of applications of Critical Transitions in finance and economics.

1.1 Deterministic dynamical systems

A *dynamical system* is a mathematical formulation of a rule which describes how a system evolves in time [11]. There are many ways to model such evolution with deterministic rules. In this thesis, we will use ordinary differential equations and iterated maps. While constructing a dynamical system to model certain real phenomena one often incorporates parameters. The selection of parameters can drastically change the dynamics of the system. This is related to the concept of a bifurcation, which we explain in Sec. 1.2. Common observed dynamics is convergence to a steady state or periodic oscillations, some systems however can exhibit more complicated behaviour such as chaos, which we introduce in Sec. 1.2.4.

Usually, the analytical approach to dynamical systems is not possible, as most nonlinear ordinary differential equations cannot be solved analytically. This has led to development of a wide range of numerical schemes which allow computers to approximate the solutions. The analysis of parameter dependence of solutions is even more complicated. Algorithms (continuation methods) have been developed to numerically appriximate this parameter dependence: see Sec. 1.3.

The world of deterministic dynamical systems includes continuous-time systems and discrete-time systems. The dynamics in continuous time we describe with ordinary differential equations (ODEs) in the form

$$\frac{dx(t)}{dt} = f(t, x(t)) \tag{1.1}$$

where $f(t,x) : \mathbb{R} \times \mathbb{R}^K \to \mathbb{R}^K$ for $K \in \mathbb{Z}_+$. We will consider f to be sufficiently smooth (Lipschitz-continuous) [12, Chapter 1], which implies that the ODE initial value problem has a well-defined and unique solution. In Eq. (1.1) x represents the vector of state (phase) variables and t represents time. Often, instead of $\frac{dx(t)}{dt}$ we write $\dot{x}$.

If the function f does not depend on time, the ODE (1.1) is called *autonomous*, otherwise, it is called *non-autonomous*. Throughout the thesis we will constrain the analysis of ODEs mainly to autonomous cases.

Systems with discrete time specify a rule describing how the system proceeds from one point in time to the next. This can be characterised as a *map* which is a function of the current time t and state of the system $x(t)$ whose value is the new state of the system at time $t+1$:

$$x(t+1) = m\,(t, x(t)) \tag{1.2}$$

where $m(t,x) : \mathbb{Z} \times \mathbb{R}^K \to \mathbb{R}^K$ for $K \in \mathbb{Z}_+$.

The Equation (1.2) is called a *difference equation*, and, similarly to the case for ODEs, difference equations are called *autonomous* if the function m does not depend on time. The relation (1.2) is sometimes written as $x \mapsto m(t,x)$ (or $x \mapsto m(x)$ when the function m does not depend on t).

Definition 1.1.1 (Evolution operator [4, Sec. 1.1.3])**.** *For given time $t \in T$ a map $\varphi^t : X \mapsto X$ defined in the state space X transforms some state $x_s \in X$ at time s into state $x_{s+t} \in X$ at time $s+t$ as follows:*

$$x_{s+t} = \varphi^t x_s. \tag{1.3}$$

The map φ^t is called an evolution operator. Moreover, $\varphi^0 = Id$ and $\varphi^t \circ \varphi^s = \varphi^{t+s}$ for all $t, s \in T$.

In continuous-time (for $T = \mathbb{R}$) the family $\{\varphi^t\}_{t\in\mathbb{R}}$ is called a flow. In discrete-time $\varphi^t = m^t = m(m(...))$ (t-times) denotes the t-th iterate of a map m ($T = \mathbb{Z}$ if the map m is invertible, otherwise $T = \mathbb{N}$).

Note that an autonomous ODE on X has solutions that can be viewed as a continuous time flow on X.

For a given flow or map the most basic way of graphically representing the

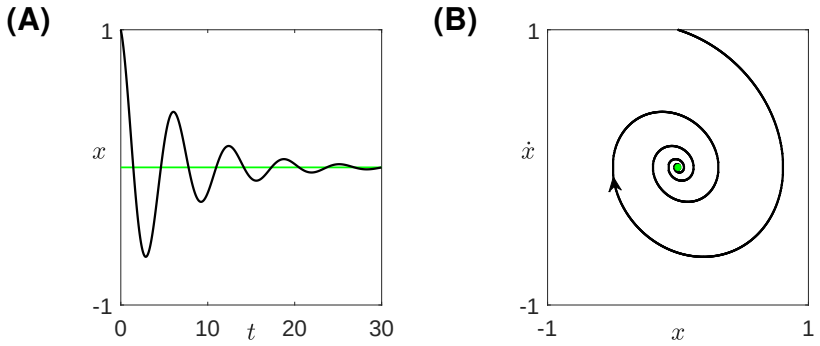

Figure 1.1: Sample representation of the dynamics of a damped pendulum shown (A) as a time series plot and (B) in phase space. Green denotes a fixed point and the arrow shows the direction in which the state of the system evolves with increasing time.

dynamics is a *time series plot*. For a chosen initial condition one simply shows its *orbit* (i.e. evolution in time) in a diagram where the X-axis represents the time and Y-axis the variable (phase) – see Fig. 1.1A. Another way is to show the trajectory in *phase diagrams*, where the axes represent the state variables (Fig.1.1B).

In Fig. 1.1B note that the trajectory converges to a point in phase space. This is an example of an attracting *fixed point* (*equilibrium*). Fixed points and *periodic orbits* are core objects appearing in studies of dynamical systems. The formal definitions of fixed points and periodic orbits are given below.

Definition 1.1.2 (Fixed point [12, Def. 1.6])**.**

1. *For flows – a point is a fixed point of a flow* φ *if and only if* $\varphi(x,t) = x$ *for all* t*.*

2. *For maps – a point is a fixed point of a map* m *if and only if* $m(x) = x$*.*

Definition 1.1.3 (Periodic point and periodic orbit [12, Def. 1.7])**.**

1. *For flows – a point* x *is periodic of (minimal) period* $T > 0$ *if and only if* $\varphi(x, t+T) = \varphi(x,t)$ *for all* t *and* $\varphi(x, t+s) \neq \varphi(x,t)$ *for all* $0 < s < T$*.*

2. *For maps – a point* x *is periodic of (minimal) period* $N = 1, 2, 3, ...$ *if and only if* $m^N(x) = x$ *and* $m^n(x) \neq x$ *for all* $0 < n < N$*.*

The orbit of a periodic point is called a periodic orbit.

A common way to relate specific flows to maps is to consider a *Poincaré map* or a *stroboscopic map*. The former is a map which takes a snapshot of the continuous system every time the trajectory crosses a certain section in phase space

[13, Sec. 10.1]. The latter is a map which takes a snapshot of the continuous dynamics every fixed time T [14] and is a useful simplification for studying periodic phenomena.

An important property of dynamical systems that allows to understand stability and bifurcations of fixed points is *hyperbolicity*.

Definition 1.1.4 (Hyperbolic fixed point)**.**

1. *For flows [12, Def. 4.6] – a hyperbolic fixed point is an equilibrium where the eigenvalues of the Jacobian have no real parts equal to zero.*

2. *For maps [13, Sec. 1.4] – a hyperbolic fixed point is a fixed point where the eigenvalues of the Jacobian do not lie on the unit circle.*

There are several concepts of stability, the most significant being the following one.

Definition 1.1.5 (Asymptotic stability [12, Def. 2.3])**.**

1. *For flows – a fixed point x is asymptotically stable if and only if both the following conditions apply:*

   - *the fixed point x is Lyapunov stable:*
     $\forall \varepsilon > 0 \, \exists \delta > 0 \, \forall y : |x - y| < \delta \implies |\varphi(x,t) - \varphi(y,t)| < \varepsilon \, \forall t \geq 0,$
   - *the fixed point x is quasi-asymptotically stable:*
     $\exists \delta > 0 \, \forall y : |x - y| < \delta \implies |\varphi(x,t) - \varphi(y,t)| \to 0$ *as* $t \to \infty$ *.*

2. *For maps – a fixed point x is asymptotically stable if and only if both of the following conditions apply:*

   - *the fixed point x is Lyapunov stable:*
     $\forall \varepsilon > 0 \, \exists \delta > 0 \, \forall y : |x - y| < \delta \implies |m^n(x) - m^n(y)| < \varepsilon \, \forall n \geq 0,$
   - *the fixed point x is quasi-asymptotically stable:*
     $\exists \delta > 0 \, \forall y : |x - y| < \delta \implies |m^n(x) - m^n(y)| \to 0$ *as* $n \to \infty$ *.*

The definition of stability presented above is often not straightforward to verify. However, one can use a definition of stability which is based on the eigenvalues of the Jacobian at the fixed point. Namely, a hyperbolic fixed point is *linearly stable* (resp. *strictly linearly unstable*) if:

1. for flows – all the eigenvalues of a fixed point have real parts less than 0 (resp. greater than 0) [12, Def. 4.8],

2. for maps – all the eigenvalues of a fixed point are inside (resp. outside) the unit circle [13, Sec. 1.4].

If a fixed point is linearly stable then it is asymptotically stable – see [12, Theorem 2.13]. We will call a stable fixed point a *sink*, strictly unstable a *source*, and, if a hyperbolic point is not a sink nor a source, it is called a *saddle* [12, Def. 4.8]. Note that a saddle point is an *unstable* (i.e. not stable) fixed point. Moreover, if at a source or a sink the eigenvalues have imaginary parts equal to zero, such a point is called a *node*. Otherwise, it is called a *focus*.

Fixed points and periodic orbits are examples of sets that have another important feature which may help to predict future states of a system: if a point starts in such a set, its evolution is restricted to this set. This property is called *invariance* [12, Def. 1.8] and plays a big role in simplifying or decoupling the dynamics in the neighbourhood of fixed points.

Following [13, Sec. 3.1], let us define three subspaces for a given fixed point in $\mathbb{R}^n$:

$$\begin{aligned} E^s &= span\{e_1, ..., e_s\} \\ E^u &= span\{e_{s+1}, ..., e_{s+u}\} \qquad\qquad (s+u+c=n) \\ E^c &= span\{e_{s+u+1}, ..., e_{s+u+c}\} \end{aligned} \tag{1.4}$$

where $\{e_1, ..., e_s\}$ are (generalised) eigenvectors corresponding to eigenvalues with negative real parts, $\{e_{s+1}, ..., e_{s+u}\}$ are (generalised) eigenvectors corresponding to eigenvalues with positive real parts and $\{e_{s+u+1}, ..., e_{s+u+c}\}$ are (generalised) eigenvectors corresponding to eigenvalues with real parts equal to zero (i.e. the Jacobian in the fixed point is singular). In discrete systems, instead of the condition that the real parts of eigenvalues are less/equal/greater than zero, one considers if the eigenvalues lie inside/on/outside of the unit circle, respectively [13, Sec. 3.3]. The subspace E^s is called the *stable subspace/eigenspace*, E^u is called the *unstable subspace/eigenspace* and E^c is called the *centre subspace/eigenspace*.

As mentioned earlier, sinks, saddles and sources are hyperbolic points, and, following the construction of E^c and the Def. 1.1.4, for hyperbolic points the centre subspace is dimensionless.

The subspaces E^s, E^u and E^c show only the stable, unstable and centre directi-

ons in the fixed point, they are not invariant manifolds. The existence of (local) invariant manifolds is given by the following theorem.

Theorem 1.1.6 (Centre Manifold Theorem for Flows [15, Theorem 3.2.1])**.** *Let f be a C^r vector field on $\mathbb{R}^n$, $f(0) = 0$ and the (generalised) eigenspaces E^s, E^u and E^c around the fixed point 0 are as given in Eq.* (1.4)*. Then:*

- *there exists a C^r s-dimensional stable invariant manifold W^s tangent to E^s at 0,*
- *there exists a C^r u-dimensional unstable invariant manifold W^u tangent to E^u at 0,*
- *there exists a C^{r-1} c-dimensional centre (local) invariant manifold W^c tangent to E^c at 0.*

The stable and unstable manifolds W^s and W^u specified above are unique, the centre manifold W^c does not need to be.

Remark 1.1.7*.* An interesting phenomenon can arise for saddle objects. As some of the eigenvectors of a saddle are stable and some are unstable, there is a possibility for existence of an orbit which is contained in both stable and unstable manifolds of the fixed point. It means that there can be an orbit which for time $t \to \infty$ and $t \to -\infty$ has the same limiting fixed point. This orbit is called a *homoclinic orbit* [12, Chapter 12].

Moreover, locally near the fixed point in Theorem 1.1.6, one can show [16] that there are coordinates x_s, x_u, x_c such that

$$\begin{cases} \dot{x}_s = A_s x_s + f_s(x_s, x_u, x_c) \\ \dot{x}_u = A_u x_u + f_u(x_s, x_u, x_c) \\ \dot{x}_c = A_c x_c + f_c(x_s, x_u, x_c) \end{cases} \tag{1.5}$$

for some functions f_s, f_u, f_c with no nonlinear part [15, Eq. (3.2.43)]. Then, the decoupled system can be simplified in the neighbourhood of a fixed point for instance by analysing only the dynamics on the centre manifold. This method is called *centre manifold reduction*. In order to perform it, one writes x_s or x_u in terms of the centre variable x_c and evaluates the flow on the centre manifold.

An example of a study of the dynamics on the centre manifold can be found in Sec. 3.3.

In many parametrised systems the centre manifold of an equilibrium will be nontrivial (i.e. such that the equilibrium is not hyperbolic) only for isolated sets of parameters. This change in hyperbolicity is associated with a bifurcation of equilibria, which we discuss, together with several other types of bifurcations, in the next section.

1.2 Bifurcations and chaos for flows and maps

In this section we will consider autonomous ODEs and autonomous maps allowing a smooth variation of parameter(s). It means that a continuous-time system can be written as

$$\frac{dx(t)}{dt} = f(x(t), p) \tag{1.6}$$

and the discrete-time system as

$$x(t) \mapsto m(x, p) \tag{1.7}$$

where x represents the vector of state variables and p is the vector of parameters.

When a parameter is varied, the behaviour of a dynamical system can change. If there exists a homeomorphism which maps the orbits in the system before the change of parameters to the orbits after the change, it means that there was no qualitative change of behaviour of the dynamical system. In such case one says that the two phase portraits and the two dynamical systems – before and after the parameter variation – are *topologically equivalent* [4, Sec. 2.1]. On the other hand, the appearance of phase portraits which are not topologically equivalent under a parameter change is called a *bifurcation* [4, Sec. 2.3]. In other words, a bifurcation is a qualitative change of behaviour of the dynamical system under a parameter change.

An example of a qualitative change in phase portraits is appearance of the centre manifold around a fixed point. In this case, for some parameter value p_c a fixed point is not hyperbolic as there exists a centre manifold of dimension greater or equal to 1. Yet, for another value of that parameter arbitrarily close to p_c the

fixed point is hyperbolic and therefore the centre manifold is dimensionless. The conclusion is that there must be a bifurcation in p_c as the two phase portraits are not topologically equivalent, because the centre manifold cannot be mapped to another manifold around the hyperbolic equilibrium. In general, the bifurcations of fixed points (i.e. *local bifurcations*) can occur only for parameter values where a fixed point is not hyperbolic [12, Chapter 8]. Hence, following Def. 1.1.4, to analyse local bifurcations it is enough to study the eigenvalues of the fixed points.

A bifurcation specifies only the difference between two phase portraits in terms of topological equivalence, hence different dynamical systems can undergo the same bifurcations. A 'simplest form' of a dynamical system of the same equivalence class of a bifurcation is called a *(topological) normal form* [4, Def. 2.16]. The 'simplest form' is a subjective term, thus for a given bifurcation there can be several common normal forms.

When one of the parameters is changed it is useful to present graphically how certain invariant objects vary for different parameter values. It is often done using (phase-parameter) *bifurcation diagrams* where the horizontal axis represents the parameter values and the vertical axis shows the phase values. If more parameters are varied at once, the bifurcations are visualised in two-parameter bifurcation diagrams where the state variables are not shown at all – only the information which bifurcations occur for which parameter values is presented. It is a useful method especially while presenting *codimension-two bifurcations*, i.e. where two parameters need to be varied for the bifurcation to occur. See Chapters 2–5 for a variety of bifurcation diagrams.

Below we describe several local and global bifurcations which appear throughout this thesis and provide the normal forms for local bifurcations. Moreover, we discuss their relevance to Critical Transitions based on the classification of bifurcations proposed in [17]: (i) *safe* – there is no jump between the attractors as well as no discontinuous change of their size, (ii) *explosive* – the existing attractor changes its size or form discontinuously, but the new attractor includes the old one, (iii) *dangerous* – the attractor disappears and causes a jump to another remote attractor. Categories (ii) and (iii) can be understood as a Critical Transition.

The bifurcations below are grouped separately for flows and maps. We will use λ or λ_1 and λ_2 to denote the eigenvalues at the point of bifurcation and in all cases the bifurcating fixed point of the system (1.6) or (1.7) is at $x = 0$ and $p = 0$.

1.2.1 Bifurcations for flows – local bifurcations

1. Saddle-node bifurcation (also called a *fold* or *limit point*)

   Normal form [4, Sec. 3.2]:

   $$\dot{x} = x^2 + p. \tag{1.8}$$

   Description: a bifurcation of two equilibria (a saddle and a node), which collide and disappear.

   Eigenvalue at the bifurcation point: $\lambda = 0$.

   Critical Transition: YES (dangerous bifurcation).

   Remark 1.2.1. A clarification on the name of this bifurcation is needed here. In a 1-dimensional system, there is no such object as a saddle and the actual collision at fold point is sink-source. In the N-dimensional (with $N \geq 3$) system, the actual collision can be saddle-saddle, but for the reduced 2-dimensional system at the bifurcation point it is still saddle-node.

2. Pitchfork bifurcation

   Normal form [12, Sec. 8.5]:

   $$\dot{x} = px \pm x^3. \tag{1.9}$$

   Description: at the bifurcation point one equilibrium splits into three. For two of the new equilibria the stability of eigenvectors is the same as for the equilibrium before the bifurcation. The third one differs in stability of one eigenvector. For example, if a one-dimensional sink undergoes a pitchfork bifurcation, after the bifurcation there will be two sinks and one source.

   Eigenvalue at the bifurcation point: $\lambda = 0$.

   Critical Transition: NO for supercritical pitchfork (i.e. a stable point splits into three), YES (dangerous bifurcation) for subcritical pitchfork (i.e. an unstable point splits into three).

3. Transcritical bifurcation

   Normal form [12, Sec. 8.4]:

   $$\dot{x} = px - x^2. \tag{1.10}$$

   Description: two equilibria meet at a bifurcation point. After the bifurcation both equilibria still exist, but they swap the stability.

   Eigenvalue at the bifurcation point: $\lambda = 0$.

Critical Transition: possible, depends on the exact shape of equilibria curves (either a safe bifurcation or a dangerous bifurcation). The two possibilities for a dangerous transcritical bifurcation are: the increasing stable branch lies above the increasing unstable branch, or, the decreasing stable branch lies below the decreasing unstable branch. A diagram of the latter can be found in [18, Fig. 2.8a].

4. (Andronov-)Hopf bifurcation

   Normal form [12, Sec. 8.8]:

$$\begin{cases} \dot{x}_1 = p_1 x_1 - p_2 x_2 \pm x_1(x_1^2 + x_2^2) \\ \dot{x}_2 = p_2 x_1 + p_1 x_2 \pm x_2(x_1^2 + x_2^2) \end{cases}. \tag{1.11}$$

   Description: at this bifurcation two of the eigendirections change their stability and a periodic orbit surrounding the equilibrium appears. In the 2-dimensional case, only sinks and sources can undergo a Hopf bifurcation. In higher dimensions it can happen also for saddles and then a saddle-periodic orbit appears.
   Real parts of eigenvalues at the bifurcation point: $\Re(\lambda_1) = \Re(\lambda_2) = 0$.
   Critical Transition: NO for supercritical Hopf (the periodic orbit is stable), YES (dangerous bifurcation) for subcritical Hopf (the periodic orbit is unstable).

5. Cusp bifurcation

   Normal form [4, Sec. 8.2]:

$$\dot{x} = p_1 + p_2 x \pm x^3. \tag{1.12}$$

   Description: it is a codimension-two bifurcation where two fold curves meet.
   Eigenvalue at the bifurcation point: $\lambda = 0$.

6. Bogdanov-Takens bifurcation (also called *double-zero eigenvalue bifurcation*)

   Normal form [4, Sec. 8.4]:

$$\begin{cases} \dot{x}_1 = x_2 \\ \dot{x}_2 = p_1 + p_2 x_1 + x_1^2 \pm x_1 x_2. \end{cases} \tag{1.13}$$

Description: it is a codimension-two bifurcation where a fold curve meets a Hopf bifurcation curve.
Eigenvalues at the bifurcation point: $\lambda_1 = \lambda_2 = 0$.

1.2.2 Bifurcation for maps – local bifurcations

1. Saddle-node bifurcation
   Normal form (see [4, Sec. 4.2] or [13, Sec. 21.1A]):

$$x \mapsto p + x \pm x^2. \tag{1.14}$$

   Description: a saddle fixed point collides with a node and both disappear.
   Eigenvalue at the bifurcation point: $\lambda = 1$.
   Critical Transition: YES (dangerous bifurcation).

2. Pitchfork bifurcation
   Normal form [13, Sec. 21.1C]:

$$x \mapsto x + px \pm x^3. \tag{1.15}$$

   Description: the bifurcation occurs at $p = 0$ where one fixed point splits into three. For two of the new fixed points the stability of eigenvectors is the same as for the fixed point before the bifurcation. The third one differs in stability of one eigenvector. For example, if a one-dimensional sink undergoes a pitchfork bifurcation, after the bifurcation there will be two sinks and one source.
   Eigenvalue at the bifurcation point: $\lambda = 1$.
   Critical Transition: NO for supercritical pitchfork, YES (dangerous bifurcation) for subcritical pitchfork.

3. Transcritical bifurcation
   Normal form [13, Sec. 21.1B]:

$$x \mapsto x + px \pm x^2. \tag{1.16}$$

   Description: two equilibria meet at a bifurcation point. After the bifurcation

both equilibria still exist, but they swap the stability.

Eigenvalue at the bifurcation point: $\lambda = 1$.

Critical Transition: possible depending on the exact shape of equilibria curves (either a safe bifurcation or a dangerous bifurcation).

4. Period-doubling bifurcation (also known as *flip bifurcation*)

   Normal form (see [4, Sec. 4.4] or [13, Sec. 21.2]):

$$x \mapsto -x - px + x^3. \tag{1.17}$$

   Description: a fixed point (i.e. period-1 point) or a periodic point doubles its period at the bifurcation point. This bifurcation can occur also in continuous systems, but only for periodic orbits.

   Eigenvalue at the bifurcation point: $\lambda = -1$.

   Critical Transition: NO for supercritical flip (stable point doubles its period), YES (dangerous bifurcation) for subcritical flip (unstable point doubles its period).

5. Neimark-Sacker bifurcation

   Normal form [4, Sec. 4.6]:

$$\begin{aligned}\begin{pmatrix} x_1 \\ x_2 \end{pmatrix} \mapsto (1+\alpha)\begin{pmatrix} \cos\theta & -\sin\theta \\ \sin\theta & \cos\theta \end{pmatrix}\begin{pmatrix} x_1 \\ x_2 \end{pmatrix} + \\ + \left(x_1^2 + x_2^2\right)\begin{pmatrix} \cos\theta & -\sin\theta \\ \sin\theta & \cos\theta \end{pmatrix}\begin{pmatrix} a & -b \\ b & a \end{pmatrix}\begin{pmatrix} x_1 \\ x_2 \end{pmatrix}.\end{aligned} \tag{1.18}$$

   For an alternative normal form see [13, Sec. 21.3].

   Description: periodic or quasi-periodic oscillations appear and the point changes its stability. This bifurcation is analogous to Hopf for flows, the complex conjugate eigenvalues cross the unit circle.

   Eigenvalues at the bifurcation point: $|\lambda_1| = |\lambda_2| = 1$.

   Critical Transition: NO for supercritical Neimark-Sacker bifurcation (stable oscillations), YES (dangerous bifurcation) for subcritical Neimark-Sacker bifurcation (unstable oscillations).

Remark 1.2.2. Adding higher order terms (for instance $O(\|x\|^4)$) to the right-hand side of Eq. (1.18) leads to a system which would exhibit qualitatively

different behaviour than the system (1.18) near the bifurcation. In an extended system there could be observed infinitely many periodic orbits (stable and unstable) and saddle-node collisions of these within a tiny parameter variation. Hence, one cannot call the form (1.18) a normal form of the Neimark-Sacker bifurcation generically, however, it describes in a simple way the key phenomenon: a creation of a periodic orbit from a point in a discrete dynamical system.

A local bifurcation of Eq. (1.6) at $x = x_c$ and $p = p_c$ is accompanied with appearance of a non-zero dimensional centre manifold of x_c at p_c. In order to understand changes with parameter, the system Eq. (1.6) can be extended by a trivial ODE for the parameter (see for instance [19, Example 2.]) to obtain:

$$\begin{cases} \dot{x} = f(x, p) \\ \dot{p} = 0 \end{cases} . \tag{1.19}$$

In this system the centre manifold of (x_c, p_c) has one more dimension than in Eq. (1.6), hence it is called an *extended centre manifold*. A consequence of such an extension is that the solutions of the system Eq. (1.19) on a centre manifold depend on p. Therefore, one can approximate analytically the solutions not only at the bifurcation for the original system given by Eq. (1.6), but also the dynamics as it varies with p. We use the analysis of a flow on an extended centre manifold in Sec. 3.3.

1.2.3 Bifurcations for flows – global bifurcations

Not every bifurcation happens locally. For instance, appearance of a homoclinic orbit (see Remark 1.1.7) does not change the phase portrait in the vicinity a fixed point. This is an example of a *global bifurcation*. In this thesis we mention only two global bifurcations, which are listed below.

1. Homoclinic bifurcation

   Description: it is a global bifurcation where a periodic orbit collides with stable and unstable manifolds of a saddle and a homoclinic orbit appears. The homoclinic orbit exists only at the bifurcation point and after the bifurcation the periodic orbit disappears [11, Sec. 8.4].

Critical Transition: YES (dangerous bifurcation) if the periodic orbit before the bifurcation is stable, NO if the fixed point inside the periodic orbit is stable.

2. Saddle-node on invariant circle

   Description: a saddle collides with a node and both disappear whereas a periodic orbit (an invariant circle) appears. This global bifurcation is also called *saddle-node homoclinic bifurcation* [4, Sec. 7.1.1] or *infinite-period bifurcation* [11, Sec. 8.4].

   Critical Transition: YES (explosive bifurcation).

1.2.4 Chaos

All the bifurcations described in Sections 1.2.1-1.2.3 affect two types of invariant sets: fixed points and periodic (or quasi-periodic) orbits. However, there is another important type of invariant set: a chaotic attractor, on which we will come across in Chapter 4. In order to explain chaotic behaviour, we use the definition of Lyapunov exponent presented below.

Definition 1.2.3 (Lyapunov exponent [20, Eq. (1.10)])**.** *Lyapunov exponent λ is the exponential rate of separation of trajectories on an invariant manifold given by*

$$\lambda(x_0, \delta x) = \lim_{t\to\infty} \frac{1}{t} \ln \left| (D\varphi^t(x_0))\, \delta x \right| \tag{1.20}$$

where δx indicates the direction of perturbation, D denotes the Jacobian, $|\cdot|$ stands for any vector norm and x_0 is an initial condition.

For computational purposes in this thesis we find the Lyapunov exponents using the numerical method given in [21].

Lyapunov exponents depend in principle on the choice of initial point x_0 and direction δx. However, it is typical that for points x_0 in a given basin of attraction and almost every δx the Lyapunov exponents are the same. Near to a stable fixed point the trajectories converge to each other, hence, as Lyapunov exponent represents the separation rate between two neighbouring trajectories, it is negative for these types of attractors [11, Sec. 10.5]. Moreover, every periodic orbit of an autonomous system has a zero Lyapunov exponent associated with phase shift

along the orbit. If the periodic orbit is stable then all other Lyapunov exponents are less than zero.

If the Lyapunov exponent is positive, but a given orbit is bounded in phase space, the attractor to which the trajectory converges is called *chaotic* [11, Sec. 10.5]. Following [12, Chapter 11], *chaos* can be understood as an aperiodic and bounded behaviour in a deterministic system that exhibits sensitive dependence on initial conditions (i.e. every two solutions which start arbitrarily close to each other get separated from each other). The main feature of deterministic systems exhibiting chaotic behaviour is that it is impossible to predict the evolution of state variables in the long run if there is even a tiny uncertainty about the initial condition.

1.3 Numerical schemes and continuation methods for deterministic systems

It is usually not possible to find an explicit analytical solutions of a set of nonlinear ODEs for a specific initial condition. For this reason we must turn to numerical approximation methods of the solutions. The simplest approximation scheme is called *Euler's method*, where given a previous step x_n the next one is approximated by $x_{n+1} = x_n + hf(t_n, x_n)$ for some small $h = t_{n+1} - t_n > 0$. However, because of the fact that Euler's method is often not very precise, throughout this thesis we use a different approximation scheme, which is outlined below.

Numerical scheme 1 (4^{th} order Runge-Kutta scheme [22, Sec. 6.10])**.** *The 4^{th} order Runge-Kutta numerical scheme for N points discrete in time and step-size $h = t_{i+1} - t_i$ is the following:*

$$x_{n+1} = x_n + \frac{h}{6}(V_1 + 2V_2 + 2V_3 + V_4) \tag{1.21}$$

where $V_1 = f(t_n, x_n)$, $V_2 = f(t_n + \frac{h}{2}, x_n + \frac{h}{2}V_1)$, $V_3 = f(t_n + \frac{h}{2}, x_n + \frac{h}{2}V_2)$ and $V_4 = f(t_n + h, x_n + hV_3)$ with initial condition $x_0 = x(0)$ and $n = 0, 1, ..., N-1$.

The precision of this approximation depends on h and it increases with decreasing h. For practical purposes though, one cannot use too low values of h as it

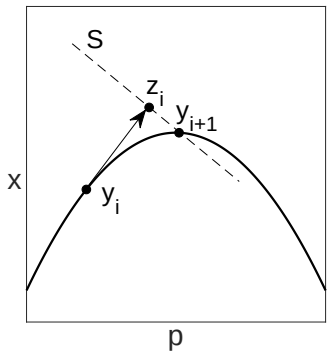

Figure 1.2: Graphical representation of pseudo-arclength continuation (Scheme 2). The predictor based on Euler scheme performed from point y_i is denoted by z_i. The corrected point y_{i+1} represents the intersection of equilibria curve and the hyperplane S orthogonal to the vector $\overrightarrow{y_i z_i}$.

can lead to numerical errors. We will further use 4^{th} order Runge-Kutta scheme with $h = 10^{-6}$.

If, instead of trajectories, we are interested in invariant sets and their bifurcations, we can use numerical continuation methods to approximately locate such solutions and find their bifurcations. A very common scheme is called *pseudo-arclength continuation* and it is implemented in continuation software `XPPAUT` [23] we use in the next chapters for continuation.

Numerical scheme 2 (Pseudo-arclength continuation [4, Sec. 10.2.1])**.** *Pseudo-arclength continuation is a method to continue solutions and it proceeds as follows:*

1. *Make a predictor z_i as in Euler's integration scheme in extended space (variables+parameter) from step y_i.*

2. *Correct the guess using Newton-Raphson solving scheme to y_{i+1} on a hyperplane S orthogonal to the vector attached in the predictor and connecting the initial point and the predictor.*

The schematic representation of this algorithm is provided in Fig. 1.2.

1.4 Stochastic differential equations

Sometimes, a purely deterministic model cannot explain features of a real system: this is especially the case if there is time-varying randomness in the system or

within the inputs to the system. In such a case it may be more appropriate to construct a model in the form of a stochastic differential equation (SDE) which describes the behaviour of a system with the deterministic and stochastic forcing as follows:

$$dx_t = f(t, x_t)\,dt + F(t, x_t)\,dW_t \tag{1.22}$$

with initial value x_0. Function $f : \mathbb{R} \times \mathbb{R}^K \to \mathbb{R}^K$ is called the *drift* whereas function $F : \mathbb{R} \times \mathbb{R}^K \to \mathbb{R}^{K \times L}$ is called *diffusion*, $K \in \mathbb{Z}$. dW_t is L-dimensional Wiener process. The solution x_t of the SDE (1.22) satisfies a stochastic integral equation

$$x_t = x_0 + \int_0^t f(s, x_s)ds + \int_0^t F(s, x_s)dW_s, \tag{1.23}$$

where we use the Itô representation of the integral $\int_0^t \cdot dW_s$. For more details on Itô integrals and other types of stochastic integrals see for instance [24].

In contrary to deterministic equations, the stochastic equations do not have unique solutions, but they have infinitely many solutions that depend not only on F and the initial condition, but also on the particular noise path W_t. Although there is no unique trajectory satisfying Eq. (1.22), it is still possible to extract some statistics of solutions for example by simulating an ensemble of trajectories with a set of 'typical' noise paths.

There is a big variety of approximation schemes for SDEs and one of the measures used to classify them is the *order of strong convergence*. Following [25, Eq. (9.6.2)], a time discrete approximation Y^δ with a step size δ is called *strongly convergent* to an Itô process X at time t if $\lim_{\delta \to 0} \mathbb{E}(|X_t - Y^\delta(t)|) = 0$.

Furthermore, strong schemes can be compared by their *order of convergence*. An approximation Y^δ is strongly convergent with order $\gamma > 0$ at time t if there exists $C > 0$ not dependent on δ and δ_0 such that for every $\delta \in (0, \delta_0)$

$$\mathbb{E}(|X_T - Y|) \leq C\delta^\gamma. \tag{1.24}$$

The simplest strong time discrete approximation is Euler-Maruyama scheme and it has order of convergence $\gamma = 0.5$.

Numerical scheme 3 (Euler-Maruyama approximation [25, Sec. 9.1])**.** *The Euler-*

Maruyama stochastic approximation for N points discrete in time is the following:

$$x_{n+1} = x_n + f(t_n, x_n)(t_{n+1} - t_n) + F(t_n, x_n)(W_{t_{n+1}} - W_{t_n}) \tag{1.25}$$

with initial condition x_0 and $n = 0, 1, ..., N-1$.

Because of its simplicity and thus low runtime, we use Euler-Maruyama scheme whenever we need to simulate large number of samples. In order to be consistent, for exploring certain features of individual paths we present our results given the same approximation scheme, but we also check if the results hold for a higher order scheme. For this purpose we use *Milstein scheme*, which is a strong time discrete approximation of order of convergence $\gamma = 1$. This scheme is presented below for F returning a square diagonal matrix of size $K \times K$.

Numerical scheme 4 (Milstein scheme with diagonal noise ($K = L$) [25, Sec. 10.3])**.** *For k-th component of $x_t = [x_t^1, ..., x_t^K]$ we have*

$$x_{n+1}^k = x_n^k + f^k \cdot (t_{n+1} - t_n) + F^{k,k} \cdot \left(W_{t_{n+1}}^k - W_{t_n}^k\right) + \frac{F^{k,k}}{2} \frac{\partial F^{k,k}}{\partial x^k} \left(\left(W_{t_{n+1}}^k - W_{t_n}^k\right) - (t_{n+1} - t_n)\right). \tag{1.26}$$

For readability in the statement above we have suppressed dependence on (t, x_t) in f^k and $F^{k,k}$.

Milstein scheme is computationally heavy for systems with more complicated than diagonal noise as at every time-step it computes multiple integrals of the form $\int_{t_n}^{t_{n+1}} \cdots \int_{t_n}^{s_2} dW_{s_1}^1 \cdots dW_{s_L}^L$ [25, Eq. (10.3.5)]. Therefore, if more than one Wiener process affects a single variable, one should consider correlating them (for instance with Cholesky decomposition) while keeping the diagonal form of the diffusion term F.

1.5 Critical Transitions in nonlinear models applied to finance and economics

As the last section of the introduction we will cover some of the applications of Critical Transitions (CT) focusing on finance and economics.

Bifurcation-induced transitions as a mathematical concept can be traced back to 1960s and 1970s to the work of Thom and Zeeman on catastrophe theory – the

branch of mathematics which relates to multistability and bifurcations in nonlinear deterministic systems defined by potential flows. Smale in his comprehensive review from 1978 [26] pointed out that however there were intuitions that catastrophe theory should be applicable to a variety of scientific fields, no data-based approach was presented at that time. Later, the concepts developed in catastrophe theory were popularised as *tipping points* mostly due to the book 'The Tipping Point' (2000) by Gladwell [27] in which the author suggested three key characteristics of a tipping point from networks perspective: i) contagiousness (the change is spreaded very quickly among the nodes), ii) little causes having big effects, iii) an instantaneous and dramatic response. Interestingly, in this book there was no recollection of the work by Thom and Zeeman, even though it discussed very similar phenomena as catastrophe theory, but from case-study point of view. Next, the two complementing theories were linked together in the book 'Critical Transitions in Nature and Society' [2] and now the term *tipping point* is used interchangeably with the term *Critical Transition*.

It is worth mentioning that the characteristic i) of a tipping point, contagiousness, in the theory of Critical Transitions is often replaced by positive feedback, especially when discussing simple systems which can tip. One example of such simple systems is a boat which has two stable states – standing straight or being completely upside down [2]. If the wind becomes too strong or the load becomes too large, this boat can tip over. When thinking of the load weight as of a parameter, there is some critical value of the weight below which the boat will not turn upside down, whereas for a small increase of this weight it can tip. The positive feedback causes the tipping to accelerate just after passing the unstable steady state. This is an example of a Critical Transition since 'little causes have big effects' and the 'response is instantaneous and dramatic' despite no 'contagiousness'.

Given the description of a Critical Transition, which says that a CT is a large and rapid change of the observed state of a system given a small change of conditions, the Critical Transitions are not confined to bifurcation-induced only. For instance, if tiny noisy increments lead to a jump from one attractor to another, this transition is called *noise-induced tipping/CT*. This approach is often illustrated as stochastic jumps between wells in a potential system (as in Chapter 5).

Another type of Critical Transition occurs if a deterministic system does not tip

for an infinitely small change of conditions, whereas it does tip if this change is quick enough. This class of tipping is called *rate-induced tipping/CT*. The classification into bifurcation-, noise- and rate-induced tipping has been suggested in [5], however there might be another classes of Critical Transitions which have not been described yet. In this thesis we focus mainly on bifurcation- and noise-induced Critical Transitions applied to finance and economics – as far as we know there has not been designed any model which would justify usage of rate-induced Critical Transitions in these areas yet, however we discuss potential usage of such type of CT in General discussion.

1.5.1 Bubbles and crashes – what are they?

Applications of Critical Transitions in finance and economics focus mainly on explaining or predicting *crashes*, but what are those and how are they determined? For instance, Wikipedia (as on 9.07.2018) does not give a precise definition of a crash at all: *"A stock market crash is a sudden dramatic decline of stock prices across a significant cross-section of a stock market, resulting in a significant loss of paper wealth." Sudden*, *dramatic*, *significant* – one can see that from the mathematical point of view this definition is not useful as it is not quantitative at all. Others try to give a more quantitative description: according to [28], crash is an instantaneous financial event usually identified with a large decrease of value of an index or a stock. Definition of *large decrease* is still fuzzy, so some quantify a crash for instance as at least 15% correction of market value of an asset or index in three weeks period [29]. Of course, there can be much smaller and rapid movements which would intuitively be identified as crashes and would not fit the former definition, as for example the 2010 Flash Crash [30]. Another interesting concept of what a crash is was developed in a series of papers by Johansen and Sornette [31–34]. The authors point out that crashes, i.e. extreme market drawdowns, are outliers (often referred to as 'dragon-kings' [35]) which do not belong to the same distributions as small and intermediate losses.

Another phenomenon related to crashes is a *financial bubble* – it can be understood as either a price which grows super-exponentially [29, 36], or as a difference between the market price and the fundamental price [37]. The fundamental price is a pure value of an asset without addition of any speculation-driven incre-

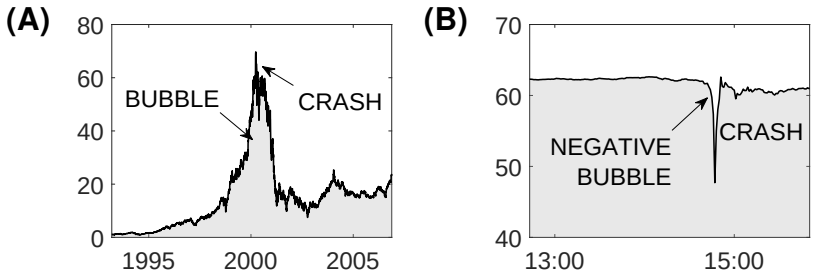

Figure 1.3: Two examples of crashes. (A) Dot-com bubble and a crash afterwards (CISCO Systems), (B) the 2010 Flash Crash (6th May 2010) with a negative bubble preceding the crash (Procter & Gamble).

ment, but it is only a theoretical concept, which might not be observable in reality [38]. A different approach to bubbles was presented recently in [39] – a market price process has a bubble when it deviates from an efficient market hypothesis (i.e. the price mirrors all the available information and no earnings can be done basing ones trading only on advantage in knowledge [28]). In this approach the authors model separately the pre-drawdown bubble (as a possibly explosive process which does not need to follow the efficient market hypothesis) and the drawdown as a correction to the fundamental price efficient market. This kind of inefficient bubbles could be observed for instance during a super-exponential acceleration of prices which is followed by a crash.

The latter definition fits well the study we present in Chapter 3 where we approximate an arising bubble with a function exhibiting a finite-time singularity at some predicted time of a crash.

Importantly, all the aforementioned definitions of bubbles do not mean that a bubble always ends with a crash [37], and that a crash does need to be preceded by a bubble. Furthermore, the bubbles could be as well positive as negative and they could occur on timescales of significantly different magnitudes (see Fig. 1.3).

In the following sections we will cover several models where bifurcation theory or Critical Transitions in dynamical systems framework are applied to finance and economy.

1.5.2 Zeeman (1974)

The first model explaining crashes as Critical Transitions was presented by Zeeman [40]. The author models the dynamics of some generic stock index I assuming that $\dot{I} > 0$ represents the bull market and $\dot{I} < 0$ the bear market. The main

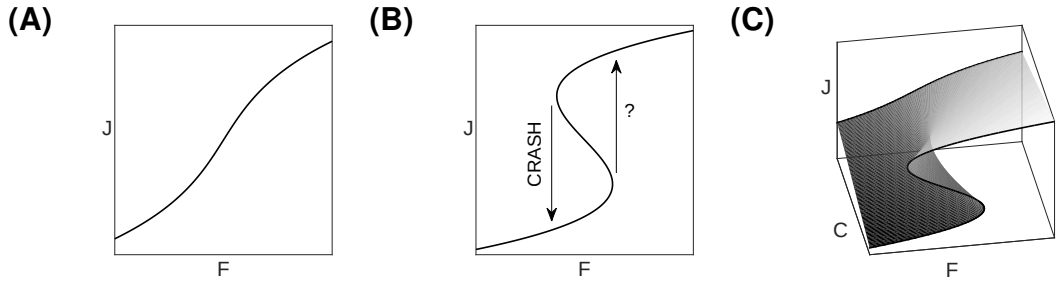

Figure 1.4: Classic introductory example of the idea of a critical transition where a small parameter shift leads to a large response in the variable with application as presented in [40]. (A) Small parameter change → small response, (B) small parameter change → large response (crash/? – the author does not elaborate on the jump opposite to the crash), (C) 3-D representation. One can notice the change of regimes between the one where no rapid change occurs and regime with a jump.

variable is the derivative of I, namely $J = \dot{I}$. Moreover, the dynamics is governed by two group of investors – *fundamentalists* (F) and *chartists* (C). Fundamentalists base their investments on the economic factors and follow the dynamics of an underlying fundamental value of the index. On the other hand, chartists (also called trend followers) think that the market trend will not change – they tend to buy an asset when the price grows believing it will grow even further. The manifold of equilibria (called also *slow manifold*) in this model is given by

$$J^3 - (C - C_0)J - F = 0 \tag{1.27}$$

where C, C_0 and F practically play a role of parameters. For some values of C, one can observe in the plane (J, F) that there is no bifurcation and J changes gradually depending on F. In another regime of C the variable J can fall down rapidly under a small variation of F due to a fold bifurcation. Bringing back F to the state from before the jump does not make the system jump back – much bigger change is needed. This kind of behaviour is known as *hysteresis* or *hysteresis loop*. See Fig. 1.4 for a graphical explanation.

The interpretation of the results is that for a small number of chartists the market moves smoothly from bull regime to bear regime in response to the number of fundamentalists. On the other hand, for larger values of chartists the market under the variation of number of fundamentalists can crash and jump from one attractor to another.

1.5.3 Lux (1995)

The deterministic model presented in [41] explains the nonlinearities and positive feedbacks observed in the markets by the notion of *herding* among the traders. This concept assumes that the traders tend to follow other traders especially when there is lack of sufficient information. The model by Lux [41] is thought to be one of the first models of bubbles and crashes based on the herding of traders. According to its author, investors' opinions about the future price change with certain probability which depends on the amount of positive or negative beliefs among others. It is described as a kind of 'contagion' in beliefs within uninformed traders. The model uses simple transition probabilities between groups of traders who believe that the price will go up or down. Lux assumes that the spread of beliefs is transported in both directions, but with different strength depending mainly on the amount of positive and negative opinions. The obtained system describes coupled continuous dynamics of spread of news between traders and the asset price formation. In such system, due to the bifurcations, there can exist one, two or three equilibria and, in some cases and certain initial conditions, the system converges to a stable periodic orbits and bubbles (understood here as the price which exceeds the fundamental price). Moreover, Lux sees the switches between positive and negative opinions in the way that Zeeman did for price variation, namely, as Critical Transitions from one attractor to another resulting from a fold bifurcation [40]. Lux's dynamical system is a Van der Pol oscillator with large damping term (see [42]). The factor that causes the nonlinearities is the heterogeneity among the traders.

1.5.4 Brock and Hommes (1998)

The model by Brock and Hommes [43] describes price dynamics in the case in which traders can choose to invest in either a risky or a risk-free asset. The investors have heterogenus beliefs on what can happen to the price. The realised returns depend on stochastic dividends, hence the traders can decide to buy more or less risky assets relying on their strategy (which can be quantified by some measure of fitness). Moreover, the speed of switching between strategies is governed by the main parameter β, which is called the *intensity of choice* – for infinite β everybody uses the same fittest strategy and for $\beta = 0$ the strategies are

chosen evenly.

The authors study several scenarios with traders of the following types:

- rational agents who possess perfect knowledge on the future price;
- fundamentalists who believe that the price will come back to the fundamental value;
- trend chasers who believe that the trend will not change (they can be biased);
- contrarians who believe that the trend will revert (they can be biased);
- purely biased traders who do not follow the trend and only believe that the fundamental value is different than the (unknown to them) true one.

The scenarios are divided by the composition of different types of traders on the market:

1. *rational agents* versus (un-biased) *trend chasers*:
   the full knowledge of rational agents is driving the price to an equilibrium. The equilibrium is either the fundamental price for smaller values of β, or one of two non-zero equilibria (due to a pitchfork bifurcation) for larger values of β;

2. *fundamentalists* versus *trend chasers*:
   the model for some values of β produces oscillations which are very similar to the time series presented in Fig. 1.3A and can be understood as repetitive bubbles and crashes. Due to the influence of noise, negative bubbles are also possible. Moreover, for larger values of β chaotic behaviour is observed;

3. *fundamentalists* versus *contrarians*:
   for small values of β all the trajectories are attracted to a unique stable equilibrium. Increasing β leads at first to the Hopf bifurcation and then to a period-doubling cascade ending with chaotic behaviour;

4. *fundamentalists* versus *positively biased* versus *negatively biased* traders:
   the increase of β leads from an equilibrium through a Hopf bifurcation and several period-doubling bifurcations to (quasi-)periodic behaviour;

5. *fundamentalists* versus *unbiased trend chasers* versus *trend chasers with positive bias* versus *trend chasers with negative bias*:
   no additional phenomenon is observed in this scenario. There is a Hopf bifurcation and chaotic behaviour in certain parameter regimes.

Finally, the authors identified the following causative relationship between the presence of certain types of traders and the occurring bifurcation:

- trend chaser → pitchfork bifurcation,
- contrarian → period doubling bifurcation,
- opposite biased beliefs → Hopf bifurcation.

It is worth noticing that most of the above bifurcations are not bifurcation-induced Critical Transitions; only the emergence of a chaotic attractor in points 2, 3 and 5 is. However, in the model presented in [43] the stochastic fluctuations lead to jumps between attractors and to the occurrence of bubbles even in the non-bubble regimes. Both of these phenomena can be classified as noise-induced Critical Transitions.

1.5.5 Yukalov, Sornette and Yukalova (2009)

In order to account for the significant amount of random fluctuations (noise / stochasticity) observed in financial data, it is common to use SDE models for financial processes (see Sec. 1.4). The paper [44] presents a model describing the relative price of a single asset (x) and its trend (y). Relative price of an asset is defined as the difference between the log-price and the fundamental log-price, which is a logarithmic version of one of the definitions of the bubble price presented in Sec. 1.5.1. The state variables are given by the following equations:

$$\begin{cases} dx = ydt + \sigma dW \\ dy = f(x, y, t)dt + \sigma' dW' \end{cases} \tag{1.28}$$

where W and W' are two independent Wiener processes.

By making a few assumptions and simplifications of f (Taylor expansion, additivity, symmetry and self-similar first-order exponential approximation) and neglecting the influence of σ' comparing to the deterministic trend, the system (1.28)

is transformed into:

$$\begin{cases} dx = ydt + \sigma dW \\ \frac{dy}{dt} = \alpha x + \beta y + Ax^3 \exp(-\frac{x^2}{\mu^2}) + By^3 \exp(-\frac{y^2}{\lambda^2}) \end{cases} . \tag{1.29}$$

The interpretation of parameters in Eq. (1.29) is the following:

- α – strength of mean reversing ($\alpha < 0$), or strength of speculative behaviour leading to appearance of bubbles ($\alpha > 0$);
- $\beta < 0$ – market friction;
- A – collective behaviour; correction of mispricing for $A < 0$, or further speculation away from equilibrium for $A > 0$;
- μ – measure of uncertainty in the fundamental value (μ small means that the investors are well informed). It tempers the nonlinear term in order to avoid finite-time singularities;
- B – speculative trading behaviour, if $B > 0$ the investors believe that the trend will be preserved;
- λ – liberalisation: "the larger it is, the easier are the changes of mispricing drift" [44].

Similarly to [41, 45–47], herding and speculative behaviour in this model is the largest source of nonlinear feedback. After an analysis of many different scenarios (i.e. different sets of parameters) the crucial observation is that the noise increments cause a Critical Transition from an equilibrium to a stable periodic orbit which is identified as a business cycle. Moreover, (stochastically blurred) basins of attraction in the model (1.29) are larger for stable cycles than for stable equilibria. It means that an asset price should spend more time following a cycle than staying close to an equilibrium.

1.5.6 Tramontana, Westerhoff and Gardini (2010)

Tramontana, Westerhoff and Gardini in [47] model the market as a step-by-step system. In every iteration the price is recalculated using a certain algorithm and

log-price is created every time by a market maker equation as a sum of previous log-price and the demand of different types of investors:

$$P_{t+1} = P_t + D_t^{C_1} + D_t^{C_2} + D_t^{F_1} + D_t^{F_2}. \tag{1.30}$$

In that system there are four types of traders. Two of them, C_1 and C_2, are chartists, who believe in market trend in a very simple way – they want to buy an asset when the market price exceeds the fundamental price, which is assumed to be known. The chartists are split into two groups: C_1 – those who always trade a constant volume of an asset, and C_2 – those who scale their demand to the difference between the market price and the fundamental price. The other type of traders are fundamentalists and they are split into two groups (F_1 and F_2) similarly as chartists, however, fundamentalists' beliefs are completely opposite – they believe that the price will go eventually back to the fundamental one. To account for speculations the orders can be of different sizes for the price above and below the fundamental, hence the map (1.30) can be discontinuous in 0.

Similarly to [43], the article [47] presents a spectrum of scenarios given existence of some groups of traders only. It studies four simplified cases of demand creation:

1. presence of chartists C_1 and fundamentalists F_1 causes the convergence of the price to the fundamental price or divergence of prices to infinity;

2. presence of chartists C_2 and fundamentalists F_2 leads to either the convergence to the fundamental price or convergence to (quasi-)periodic and very regular oscillations;

3. all types of investors coexist and $\#C_1 > \#F_1$ and $\#F_2 > \#C_2$ – the dynamics is either chaotic exhibiting irregular bubbles and crashes or explodes to infinity. The shift from the region with chaos to the divergent region can happen for an infinitely small change of a parameter (i.e. it is a Critical Transition);

4. coexistence of all types of investors and $\#F_1 \gg \#C_1$ and $\#C_2 \gg \#F_2$ leads to bistability between a fixed point and chaotic dynamics. In the chaotic regime the market shifts irregularly from bear to bull market.

1.5.7 Bischi et al. (2006)

Some models are designed just to mimic the price and demand dynamics, but other also describe the evolution of the expected asset price. Bischi et al. [45] present a completely different view on the market than Tramontana et al. [47]. They do not base any study on the concept of fundamental price nor they divide the traders into chartists and fundamentalists. In [45] the authors assume, that all of the traders are differentiated only by stochastic terms. The final price is determined from the demand which accounts for all the beliefs and decisions and, based on the law of large numbers, it leads to a deterministic model:

$$\begin{cases} \omega_{t+1} = \tanh\left[\beta \cdot J(|q_t|) \cdot \omega_t - \beta \cdot q_t\right] \\ q_{t+1} = (1-\rho)q_t + f(\omega_t) \end{cases}, \tag{1.31}$$

where ω is the average of all decisions to buy $(+1)$ or sell (-1) and $q_t = p_t - \bar{p}_t$ is the difference between the current price and the expected price.

The main analysis presented in [45] studies the behaviour of fixed points and possible trajectories. It is found that for the system (1.31) there might be i) one stable fixed point, ii) two stable and one unstable fixed points, iii) unstable focus with a stable periodic orbit around it (possibly bubbles). The identified bifurcations are supercritical pitchfork and supercritical Neimark-Sacker, what means that in the deterministic approach in this model no Critical Transition is possible. On the other hand, for the regime with two stable fixed points noise-induced transitions are possible if the system is stochastically forced. It is worth noting that in the regime i) the different values of initial demand ω_0 can lead to different fixed points of price p_t because the expected price $\bar{p}_t$ is not a fixed value.

Interestingly, a very similar mathematical formulation of averaged opinion dynamics was presented in [48]:

$$\begin{cases} s_{t+1} = \tanh(a \cdot s_t + b \cdot H_t) \\ H_{t+1} = \theta \cdot H_t + (1-\theta)s_t \end{cases}, \tag{1.32}$$

however in this case the second variable, H, is interpreted as a measure of momentum of the opinion dynamics. We perform a bifurcation study of the model (1.32) in Chapter 4.

1.5.8 Discussion

As presented above, there has been a lot of effort put in modelling bubbles and crashes with bifurcation-induced phenomena. The three main types of invariant sets which seem to be crucial in financial dynamical models are: i) a fixed point identified with the fundamental price, ii) stable (quasi-)periodic oscillations identified with bubbles and crashes, iii) chaotic attractors. The bubbles in the aforementioned models appear due to parameter change through supercritical Hopf or supercritical Neimark-Sacker bifurcations, which we do not interpret as Critical Transitions. However, some of the models explain rapid shifts in the market as a saddle-node bifurcation. In Sec. 1.2 there was mentioned one more bifurcation which leads to creation of a stable periodic orbit – a SNIC bifurcation which indeed is a Critical Transition. An example of a system with this bifurcation is presented in Chapter 2.

Some of the bifurcations occurring in the quoted dynamical systems are not Critical Transitions, but they cause bistability. It means that adding noise to the system can make the system tip from one attractor to another. Moreover, if the system is close to a bifurcation which will cause appearance of periodic behaviour, but does not exhibit bubbles and crashes in the deterministic framework, introducing noise will actually blur the bifurcation boundaries and allow the periodic-like phenomena to occur even in the non-crash regime in the parameter space.

Chapter 2

Modelling bubbles and crashes with a stock-bond dynamical system

We analyse the behaviour of a nonlinear model of coupled stock and bond prices exhibiting periodically collapsing bubbles. By using the formalism of dynamical system theory, we explain what drives the bubbles and how foreshocks or aftershocks are generated. A dynamical phase space representation of that system coupled with standard multiplicative noise rationalises the log-periodic power law singularity pattern documented in many historical financial bubbles.

This chapter, together with Chapter 3, presents the study described in the article [*Damian Smug, Peter Ashwin and Didier Sornette.* ***"Predicting Financial Market Crashes Using Ghost Singularities"*** *(2018). PLoS ONE 13(3): e0195265]*.

2.1 Introduction and literature review

Forecasting market behaviour has been a topic of general interest for hundreds of years. At the same time, given the complexity of financial markets, mathematical models have been limited to explore in a rather fragmented way some of the many mechanisms and dynamics at play in the real world. Following the review presented in Sec. 1.5, there are models exploring the impact of the dynamics between traders (see e.g. [41, 45, 47, 49–51]), other models attempt to capture the effects of feedbacks between financial information and investment strategies using various stochastic nonlinear processes (see e.g. [1, 37, 44, 52]).

These references can be conceptually linked to the pioneering work of [43, 53–57] describing the dynamical behaviour of heterogeneous markets with many trader types using dynamical system concepts, including limit cycles as the large type limit of interaction agents, bifurcation routes to instability and strange attractors in evolutionary financial market models. This variety suggests that the concepts and methods of complex dynamical systems could be useful in the area of financial markets. A certain type of nonlinearity is of particular interest due to its large impact in generating what are arguably the most visible deviations from normally (quasi-)efficient financial markets, namely financial bubbles. During financial bubbles, positive feedback mechanisms give rise to the so-called super-exponential acceleration of prices [29, 58–60], followed by the burst of the bubble in large drawdowns [31, 32, 34], i.e. crashes. A parsimonious representation of this super-exponential dynamics takes the form of finite-time singularity models [61–65].

In this chapter we revisit the model of coupled stock and bond prices introduced by [1], which exhibits periodically collapsing bubbles in a certain domain of the parameter space.

The chapter is constructed as follows. In Section 2.2, we explain the construction of the model and build basic intuitions on the bubbles and crashes for the deterministic version. Furthermore, in Sec. 2.3, we investigate thoroughly the parameter space explaining which kind of bifurcations one should expect and how exactly the bubbles emerge. Next, in Sec. 2.4, we present a short analytical study of scaling laws governing the period and the amplitude of the bubbles in certain limits. Section 2.5 introduces stochastic extension of the main system in a form of SDE and then, in Sec. 2.6 we justify dynamically several stylised facts observed in financial markets. Section 2.7 concludes.

2.2 Nonlinear dynamical system of stocks and bonds

In this section, we recall the dynamical system of [1] and provide dynamical explanations for a variety of market events. We also point out the existing bifurcations and how the system responds to parameter shifts. The latter will be quantified in the neighbourhood of bifurcation lines. The system is extended into a version with multiplicative noise to model stochastic price fluctuations.

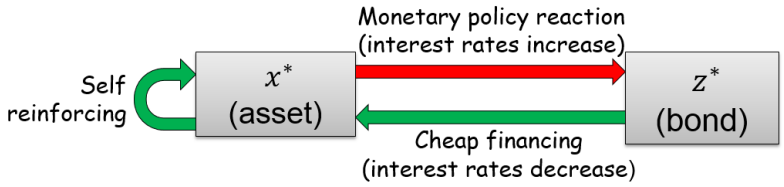

Figure 2.1: Schematic diagram showing the feedback loops governing the prices $x(t)$ and $z(t)$ for the model (2.1) of [1]. An increasing bond price means mechanically a lower interest rate and thus a lower borrowing cost, which favours further stock price increase (term e^{-bxz} with $b > 0$). A large stock price leads to a reaction of the central bank to increase the interest rates and thus decrease the bond price (term e^{-gx} with $g < 0$). A larger stock price is also assumed to feedback positively on itself (term e^{-bxz} with $b > 0$).

A dynamical system of a coupled pair of one bond and one asset is introduced in [1]:

$$\begin{cases} \dot{x} = x - x^2 \cdot e^{-bxz} \\ \dot{z} = z - z^2 \cdot e^{-gx} \end{cases} . \tag{2.1}$$

The system is designed from a self-financing portfolio and links the price of an asset/stock (x) with the price of a bond (z), the latter quantifying the cost of borrowing. As can be observed later, the amplitude of variations of z is too large to be directly interpreted as a real bond price and one can treat z as the investors confidence for further growth of stock market. Although qualitatively the bond price is positively correlated with the confidence, we keep to an analysis of the model presented in [1] and leave its generalisation to future work.

Parameter $b > 0$ stands for the sensitivity of the fundamental asset price on asset and bond prices, while parameter $g < 0$ is the sensitivity of the fundamental bond price to asset prices. The scheme of feedback loops governing the equilibria of these two variables is presented in Fig. 2.1 and is more thoroughly explained by [1]. One can think of the terms e^{-bxz} and e^{-gx} as quantifying the amplitudes of the forces that tend to push the prices back to their fundamental values. Depending on the parameters in system (2.1), three different scenarios can be observed for the same initial conditions: convergence to a stable fixed point, divergence to infinity (only for $g > 0$) or convergence to a stable periodic orbit. In the following, we classify the different bifurcations exhibited by system (2.1), making more precise and extending the analysis of [1]. We shall focus on the nonlinear periodic orbits as their properties make them reasonable candidates to represent bubbles and crashes in real financial markets.

Definition of bubbles: We shall call 'bubble' each transient part of a periodic

orbit during which the price x accelerates in a super-exponential fashion, and which is followed by a fast correction. In the deterministic version (2.1) of the model, these bubble regimes occur only for certain periodic orbits. The bubbles are thus occurring periodically, hence the title of 'periodically collapsing bubbles' in [1].

2.3 Bifurcations of fixed points and periodic orbits

In a macroscopic view of the two parameter plane for the system (2.1), one can observe two lines of bifurcations of fixed points – saddle-node and Hopf [1], which are presented in Fig. 2.2A. However, taking a closer look at the region where these two lines meet, it turns out that it is not a single point, but a set of points where bifurcations of codimension-two occur (more information on the appearance of these codimension-two bifurcations can be found in [66–69]). From an economic point of view, this means that a very small change in the market conditions can move the system from a stable regime to one with regular bubbles and crashes. When the sensitivity of the stock price b grows, then the term e^{-bxz} decays and thus the systems moves further away from the underlying logistic behaviour with attraction to a stable equilibrium. At a certain point, the influence coming from the term e^{-bxz} is weak enough to hold the stock price static and as a result consecutive periodic bubbles can be observed. A different feedback is observed for $g < 0$ growing. In this situation the term e^{-gx} decreases and hence the z term is less influenced by dynamics of x. However, if stock price rises high enough, it will compensate for small $|g|$, what consecutively will affect the bond price and lead to the collapse of stock price allowing z to rise again and so on in an oscillatory manner. Of course, the boundaries between different regimes will be smoothed out somewhat when a stochastic component is added (see e.g. [18]).

After tracking certain bifurcation paths varying b with fixed g, we have noticed that the bubbles are not necessarily born from a Hopf bifurcation, but some arise after having at first an infinite period. Two cases must thus be considered:

1. The saddle is always present. The periodic orbit grows until it hits the saddle and the homoclinic connecting orbit appears (see Sec. 1.2.3). For one parameter value, the stable and unstable separatrix of the saddle are con-

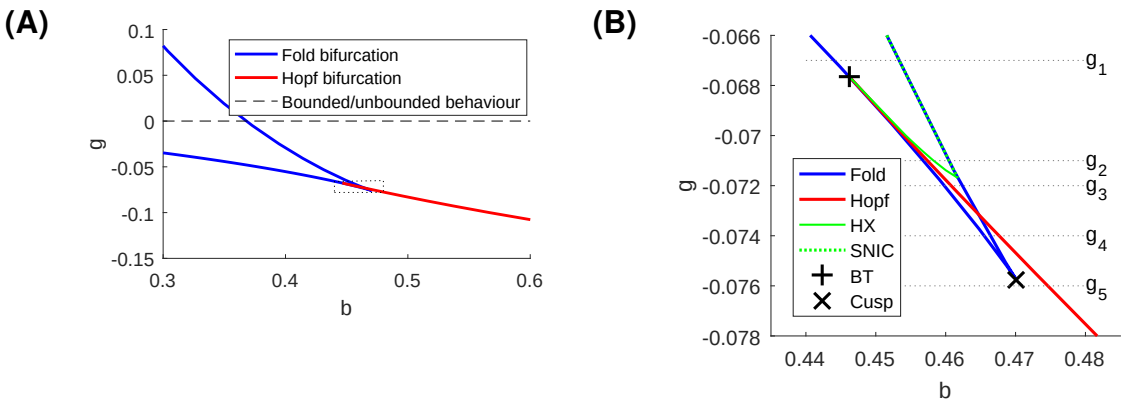

Figure 2.2: (A) Two-parameter bifurcation diagram, (B) zoom-in on the marked rectangle in panel. (A). The dotted lines represent certain bifurcation paths, which are shown in Fig. 2.3. BT means Bogdanov-Takens point. Bifurcations are computed using `XPPAUT` [23].

nected. To refer to this situation, we will use the abbreviation HX. Following Sec. 1.2.3, this bifurcation is a Critical Transition, because the system under infinitely small change of parameter jumps to another attractor.

2. The other possibility is that a periodic orbit is born from a collision of a saddle and a node, which makes both equilibria disappear. The set of parameters for which the collisions occur forms a saddle-node invariant circle (denoted SNIC). Following Sec. 1.2.3, this bifurcation can be considered as a Critical Transition, because the system under infinitely small change of parameter starts to follow much larger attractor.

The HX bifurcation line was tracked in the two-parameter plane by following an orbit of large period, whereas the SNIC coincides with a saddle-node branch. In Fig. 2.2B, both lines are indicated.

In order to show how changes of parameter affect the stability of the fixed points and of the periodic orbits, Fig. 2.3 presents a set of bifurcation diagrams where chosen paths for different values of g are shown to determine the bifurcation order. The selected parameter values exhaust all the possible situations. Note that the periodic orbits always emerge if either a saddle collides with a stable node or via a Hopf bifurcation.

In the system (2.1) there are also two points where codimension-two bifurcation occurs. One of them is the Bogdanov-Takens point (further information can be found in Sec. 1.2.1). For the Bogdanov-Takens point, the Jacobian has a

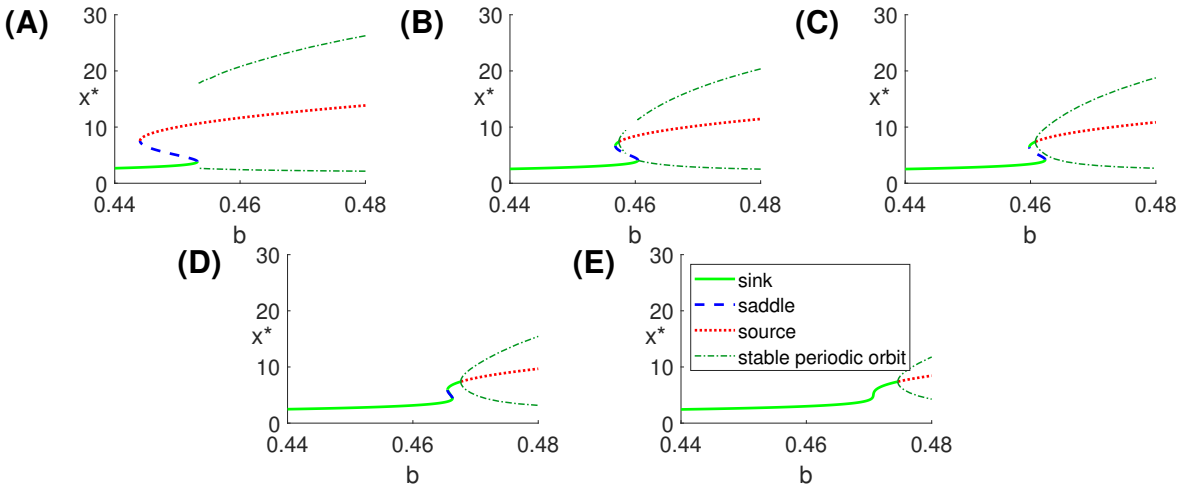

Figure 2.3: Phase-parameter bifurcation diagrams for fixed $g < 0$, (A) $g = -0.067$, periodic orbits appear when a saddle collides with a sink, (B) $g = -0.071$, periodic orbits appear via a Hopf bifurcation, exist until a homoclinic bifurcation occurs and then appear again when a saddle collides with a sink (further analysis of the periods for that situation is presented in Section 2.4), (C) $g = -0.072$, periodic orbits emerge from a Hopf bifurcation point, which occurs between two fold bifurcations, (D) $g = -0.074$, the fold bifurcations are approaching each other, (E) $g = -0.076$, only the Hopf bifurcation remains, from which periodic orbits appear.

double-zero eigenvalue, hence it is possible to derive the analytical coordinates for that point, which are the following:

$$\begin{cases} x^*_{BT} = e^2 \approx 7.389 \\ z^*_{BT} = e^{-\frac{1}{2}} \approx 0.6065 \\ b_{BT} = 2e^{-\frac{3}{2}} \approx 0.4463 \\ g_{BT} = -\frac{1}{2}e^{-2} \approx -0.06767 \end{cases} . \tag{2.2}$$

The second codimension-two bifurcation point is a cusp (see Sec. 1.2.1). The analytical values of its coordinates are as follows:

$$\begin{cases} x^*_{cusp} = e^{\frac{1+\sqrt{5}}{2}} \approx 5.043 \\ z^*_{cusp} = e^{\frac{\sqrt{5}-3}{2}} \approx 0.6825 \\ b_{cusp} = \frac{1+\sqrt{5}}{2}e^{1-\sqrt{5}} \approx 0.4701 \\ g_{cusp} = \frac{\sqrt{5}-3}{2}e^{-\frac{1+\sqrt{5}}{2}} \approx -0.07574 \end{cases} . \tag{2.3}$$

2.4 Analysis of scaling laws governing the period and the amplitude of the bubbles

The scaling laws governing the period and the amplitude help to quantify some properties of the system. They may be useful, for instance, to localise a given real system in the parameter plane. Moreover, knowledge of the scaling law governing the period of a bubble could help to distinguish in practice which bifurcation is approached. A numerical study of the period and amplitude of bubbles in the vicinity of certain singularity lines is documented in [1]. In here we present a confirmation of their result.

2.4.1 Period

As defined in Section 2.2, a necessary condition for a bubble to occur is the presence of a periodic orbit (in the deterministic version (2.1) of the dynamical system). We find that oscillations are born in Hopf bifurcation and remain until a HX bifurcation, then they appear again in a SNIC. Following the literature [11, 70], we conclude that the result in [1] is correct in terms of the period only in certain parameter regimes, namely in the neigbourhood of SNIC bifurcation. In the bifurcation diagram 2.3B, there are two disjoint intervals where bubbles occur. The authors of [1] did not locate the homoclinic bifurcation. These two situations are governed by different scaling laws depending on the distance from the bifurcation:

1. approaching HX (see [70]) for $0 < \Delta = b_{hx} - b \ll 1$:

$$f_{hx}(\Delta) = c \cdot |\ln(\Delta)|\,, \tag{2.4}$$

2. approaching SNIC (see [11, Ex. 4.3.1]) for $0 < \Delta = b - b_{snic} \ll 1$:

$$f_{snic}(\Delta) = c \cdot \Delta^{-1/2}\,. \tag{2.5}$$

In the second case, adding higher order terms gives actually a better fit. Fig. 2.4 shows good agreement of these approximations and the simulated data.

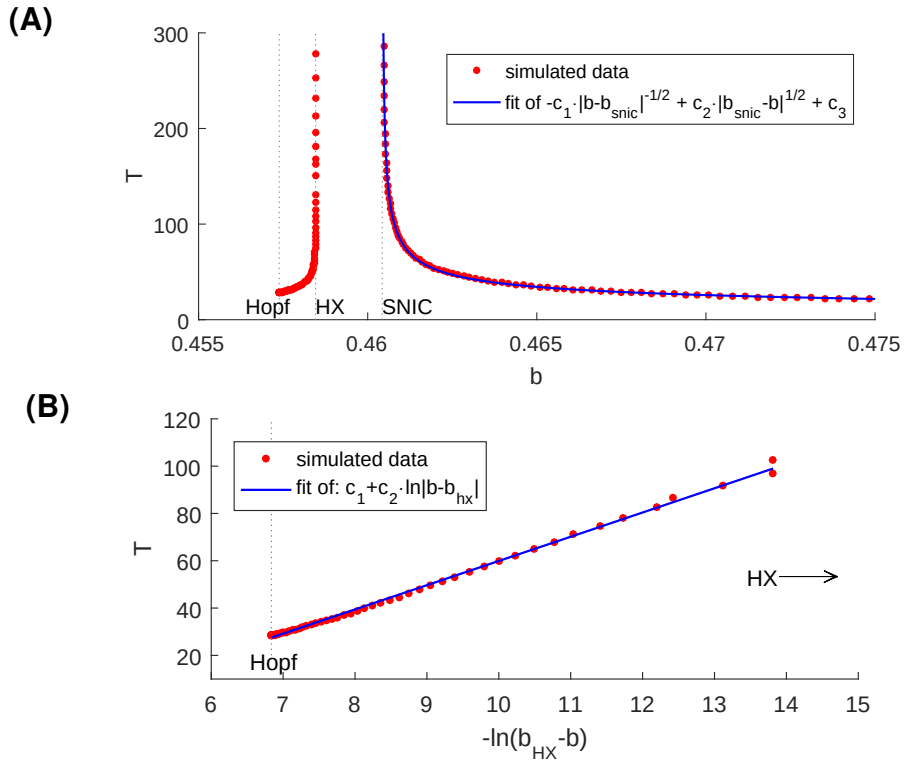

Figure 2.4: Analysis of the orbit's periods for $g_2 = -0.071$ as in Fig. 2.3B. (A) Scenario 1 of approaching HX (left series of dots) and scenario 2 of approaching SNIC (right series of dots fitted by expression (2.5)); (B) Scenario 1 of approaching HX: logarithmic transformation of the distance from the bifurcation point approximated by a linear function.

2.4.2 Amplitude

The numerical analysis of an amplitude of the bubbles in [1] relies on the observation that the relation $\frac{\ln(\text{amplitude})}{\ln|g|}$ is asymptotically linear. Our analytical study below confirms such a result not for the amplitude, but for the unstable equilibrium inside the stable periodic orbit. However, we are able to transfer this result to amplitude by numerical observation that the relation of the stock price at the unstable equilibrium to the amplitude converges to a constant. In order to determine how high can a bubble rise, let us first find a lower bound for the amplitude. Let x_{max} be the maximal value of x and x_{eq} be a non-trivial equilibrium point – both marked in Fig. 2.5. Obviously, $x_{max} \geqslant x_{eq}$.

We can obtain the parameter g depending on x_{eq} and b at the crosspoint of the nullclines:

$$\begin{cases} 0 = x_{eq} - x_{eq}^2 \cdot e^{-b x_{eq} z} \\ 0 = z - z^2 \cdot e^{-g x_{eq}} \end{cases} . \tag{2.6}$$

which yields

$$\begin{cases} x_{eq} = e^{bx_{eq}z} \\ z = e^{gx_{eq}} \end{cases}, \tag{2.7}$$

and thus

$$|g| = \frac{\ln(bx_{eq}) - \ln(\ln(x_{eq}))}{x_{eq}}. \tag{2.8}$$

As $x_{eq} \to \infty$, $|g| \to 0^+$.

What is more,

$$\forall \varepsilon > 0 \;\; \exists \hat{x} \;\; \forall x_{eq} > \hat{x} \quad \frac{c_1}{x_{eq}^{1+\varepsilon}} \leqslant |g| \leqslant \frac{c_2}{x_{eq}^{1-\varepsilon}}, \tag{2.9}$$

where c_1 and c_2 are some positive constants. We will use the notation $|g| \sim \frac{1}{x_{eq}}$ to represent the relation (2.9). Translating the previous statement for x_{eq}, we obtain

$$x_{eq} \sim \frac{1}{|g|}. \tag{2.10}$$

From the numerical calculations presented in Fig. 2.6, we conclude that

$$\frac{x_{max}}{x_{eq}} \xrightarrow[g \to 0^-]{} c, \tag{2.11}$$

where $c \in [1, 2)$ is a constant. The data points for $\frac{x_{max}}{x_{eq}}$ shown in Fig. 2.6 can be fitted very well by the function

$$\frac{x_{max}}{x_{eq}}(g) = \frac{1}{(-\log_{10}|g|)^{\alpha}} + 1, \tag{2.12}$$

where for $\alpha = 0.8328$, $R^2 = 0.9991$. It implies that $c = 1$.

Finally, from (2.10) and (2.12), we deduce that

$$x_{max} = \frac{x_{max}}{x_{eq}} \cdot x_{eq} \sim 1 \cdot \frac{1}{|g|} = \frac{1}{|g|}. \tag{2.13}$$

2.5 Stochastic dynamical system of stocks and bonds

In order to investigate the extent to which the classification of the different regimes of the deterministic system (2.1) informs us on the behaviour of prices in the presence of a stochastic component we analyse an SDE version of (2.1) with

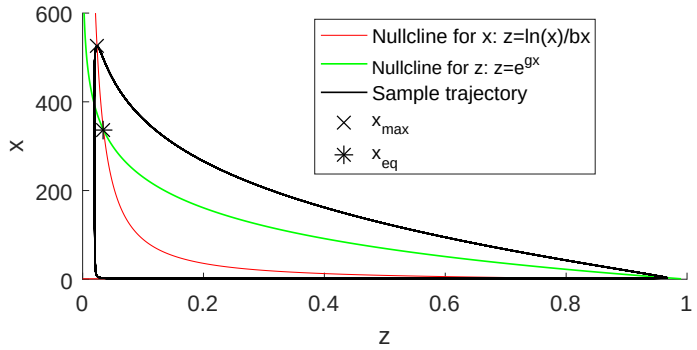

Figure 2.5: Nullclines for the system (2.1) with marked x_{max}, x_{eq} and a sample periodic trajectory. Parameters are $b = 0.5$ and $g = -0.01$. As $g \to 0^-$, the nullcline for z shifts to the right, so that the crosspoint with the nullcline for x (the equilibrium point x_{eq}) goes to infinity.

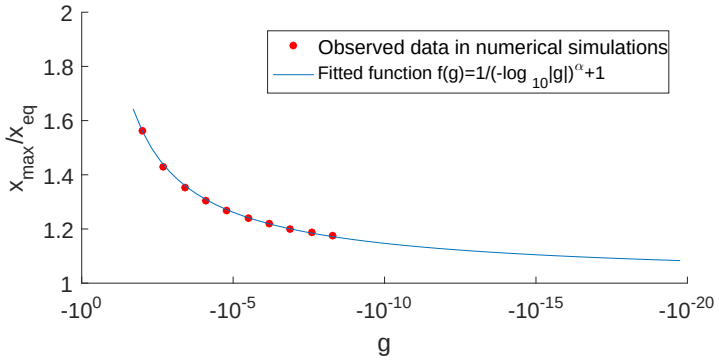

Figure 2.6: Change of the ratio of the top of bubble to the non-trivial equilibrium point depending on g. Here $b = 0.5$. One can notice extremely good approximation of fitted curve with $R^2 = 0.9991$.

multiplicative noise. Specifically, we study the following system of SDEs:

$$\begin{cases} dx = \left(x - x^2 \cdot e^{-bxz}\right) dt + \sigma_x \, x \, dW_t^{(1)} \\ dz = \left(z - z^2 \cdot e^{-gx}\right) dt + \sigma_z \, z \, dW_t^{(2)}. \end{cases} \tag{2.14}$$

The two new terms $\sigma_x \, x \, dW_t^{(1)}$ and $\sigma_z \, z \, dW_t^{(2)}$ correspond to the standard multiplicative proportional stochastic components of financial price models. For $b, g \to +\infty$, the two nonlinear terms vanish, and the system (2.14) reduces to two standard geometric Brownian motions (GBM). Nevertheless, in the system we analyse, the natural value of g resides in the interval $(-\infty, 0)$. Making $|g|$ small ($g \to 0^-$) corresponds to decreasing the sensitivity of bond price on stocks. Further growth of g above 0 means that the sensitivity is actually inverted and $g \to +\infty$ should be understood as not large sensitivity, but an inverted way with which the stocks have an impact on the bonds. Moreover, $g \to +\infty$ implies that z grows exponentially towards infinity and thus $e^{-bxz} \to 0$. Then, for larger times the stock price decouples from the bond price and even for small fixed positive values of b the GBM for x can be recovered. It is important to notice, that both $b \to \infty$ and $b = 0$ lead to such decoupling, but in the latter case x is bounded since the deterministic part is a pure logistic equation in x. The z dependence for $b > 0$ thus amounts to decreasing the impact of the bound, in other words, increases the bound for the price x.

Here, the volatilities σ_x and σ_z are constant and the two Wiener processes $dW_t^{(1)}$ and $dW_t^{(2)}$ are correlated with a constant correlation coefficient of 0.5. This value is justified as, according to [71], correlations between postwar returns in stock and bond prices were around 0.4 in the U.S. and around 0.6 in the U.K. However, during bubbles and crashes, correlations tend to vary a lot [72–74], hence it would be interesting to investigate the impact of regime switches in the amplitude of the correlation coefficient. We leave this for a future work.

In our simulations, we analyse the stochastic dynamics close to the saddle-node bifurcation at an arbitrarily chosen point $b = 0.42$ and $g = -0.04$. We use the empirical evidence that the daily standard deviation for stock prices (resp. bond prices) is of the order of a few percent, say 3% (resp. a few basis point, i.e. a few hundreds of a percent, say 0.05%). Taking the reduced time unit of our model to correspond to approximately three months of the real world, this yields that

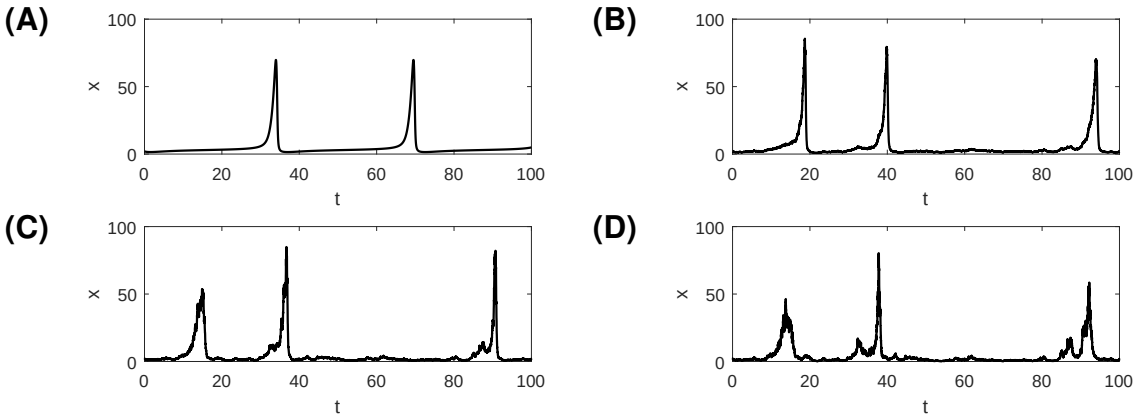

Figure 2.7: Sample bubbles generated with system (2.14) with various noise levels for the same realisations of the random increments $dW_t^{(1)}$ and $dW_t^{(2)}$. The parameters are $b = 0.42$, $g = -0.04$, $\mathrm{Corr}\left(\mathrm{W_t^{(1)}}, \mathrm{W_t^{(2)}}\right) = 50\%$, initial conditions: $x_0 = 2$, $z_0 = 0.3$, (A) $\sigma_x = 0.0$, $\sigma_z = 0.00$, (B) $\sigma_x = 0.2$, $\sigma_z = 0.01$, (C) $\sigma_x = 0.4$, $\sigma_z = 0.01$, (D) $\sigma_x = 0.6$, $\sigma_z = 0.01$.

reasonable values of σ_x should lie in the interval $[0.2, 0.6]$ and of σ_z in the interval $[0, 0.01]$.

The values of σ_x could be retrieved in another way as well. Assuming that the typical standard deviation in the GBM model of stock prices with daily time units is approximately of order 10^{-4} (say 0.0004) and one time unit in our model is around 100 days, rescaling the variance proportionally to the time we obtain the new value of $\bar{\sigma} = \sqrt{100} \cdot 0.0004 = 0.004$ and the GBM can be written in the new time units as $dp = \mu p dt + \bar{\sigma} p dW_t$. If we take the drift coefficient μ to be of order 1% in 100 days (around 3% in a year), we obtain $dp = 0.01 \cdot p dt + 0.004 \cdot p dW_t$ and the proportion for stock price $\frac{\bar{\sigma}}{\mu} = 0.4$ is the same as in the model (2.14) with $\frac{\sigma_x}{1} = 0.4$.

Fig. 2.7 shows four trajectories obtained by numerical integration of (2.14) for different levels of noise (different values of σ_x and σ_z). The first observation is that the stochastic system also exhibits recurring bubbles with qualitatively similar shapes to the deterministic case. However, rather than being precisely periodic, one can observe some variability in the waiting times between them. This can be rationalised by viewing stochastic innovations as providing effective changes of initial conditions along the price paths. Stochasticity also introduces randomness in the amplitude of the bubbles, some being smaller and others larger than in the deterministic periodic case. Another interesting observation is that, as the noise amplitude increases, bubbles are accompanied by 'foreshocks' and 'aftershocks', namely significant price activities before and after a main price peak. These qualitative observations will be explained thoroughly in Section 2.6.

2.6 Dynamical bubble – genesis

In order to rationalise the qualitative properties illustrated in Fig. 2.7, let us study an arising bubble in phase space instead of in the time domain. The way a bubble grows or deflates can be driven by a variety of forces that can be investigated conveniently in phase space. The phase diagrams of Fig. 2.8B and Fig. 2.8D present the crucial drivers of bubbles, which are now listed.

- **Nullclines** (the curves where either $\dot{x} = 0$ or $\dot{z} = 0$) and their intersection – unstable fixed point. As the nullcline for x (red curve) is the most important for the stock price dynamics, to ensure the clarity of the graphical representation, the nullcline for z is not included. When the trajectory lies close to the nullcline for x, the dynamics of the stock price becomes almost entirely driven by the stochastic component. Close to the equilibrium fixed point (red dot) or in the neighbourhood where the equilibria collided ($x \approx 0, z \approx 0.9$), the deterministic trend of the bond price disappears as well.

- **Deterministic bubble path** to which the stochastic trajectories are attracted (blue bold curve). The system evolves clockwise and the density of dots represents the inverse of the speed of the representative point (one dot is plotted every fixed time period). For small x, the price changes happen at a much slower pace than for higher values of x and the largest speed is reached when x collapses in what can be termed as a crash.

- **Other sample deterministic trajectories**, marked in light blue, help understanding the future evolution of the system. Every trajectory spirals clockwise, some of them prematurely abort the bubble, whereas other trajectories approach the bubble much further from the equilibrium ghost point and will be instantly directed to take the loop around.

These terms are useful in explaining what really drives the development of each specific bubble. In the presence of noise, there are various patterns occurring in the system, which in turn capture several stylised facts observed in real financial markets. Let us focus on the three main stages of the development of a bubble. The numbers in curly brackets stand for certain situations presented in Fig. 2.8.

Foreshocks. When a bubble begins, stochastic fluctuations can push the trajectory above or below its underlying deterministic version. If x happens to be

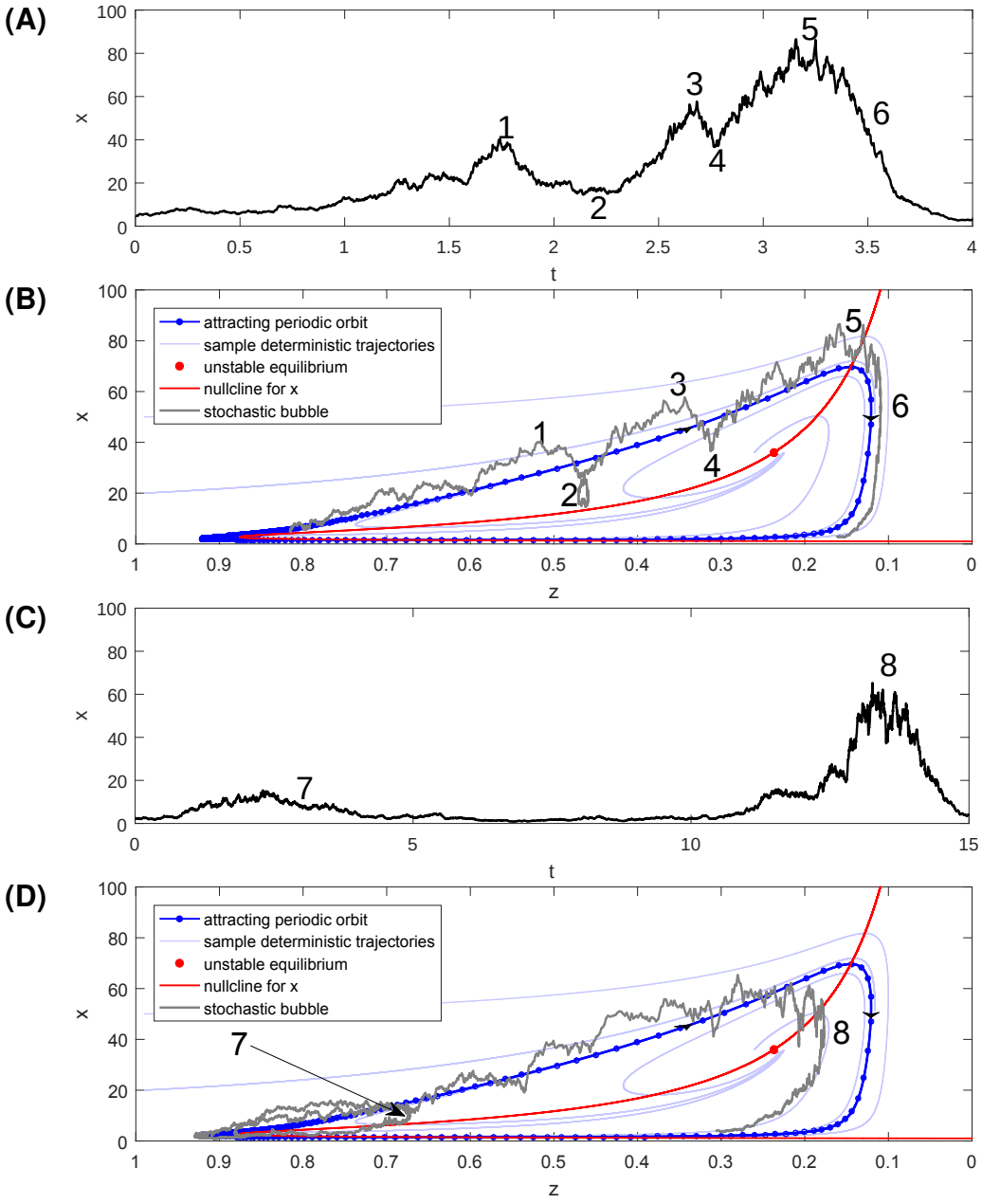

Figure 2.8: Schematic representation showing different phases and outcomes of stochastic bubbles for (2.14) with $b = 0.42$, $g = -0.04$, $\sigma_x = 0.6$, $\sigma_z = 0.0$. The bold blue line represents a deterministic stable orbit with blue dots at fixed time intervals. (A) and (B) Foreshocks {1/2} and {3/4} preceding the main crash {5/6} are clearly visible. The time intervals between the consecutive local peaks and corrections decrease as a result of at least two factors: first, until around $z = 0.2$, the price x accelerates making it prone to take a time consuming detour for smaller x {2} that becomes less impactful compared to when x is larger {4}. (C) and (D) The noise can push the dynamics to enter the region where deterministic forces drag trajectories back to the region of small x, thus aborting the bubble {7} before it fully develops. The same kind of behaviour for higher x levels can shorten the life of a bubble in the regime close to the unstable fixed point where the price dynamics can oscillate temporarily before the main crash {8}.

pushed down intensively in a small time period, the dynamics may be driven back and terminate the bubble, leading to the abortion of the main loop – see point {7} in Figs. 2.8C and 2.8D. The shape of the deterministic vector field shows that, for smaller values of x, the burgeoning bubble trajectory can be pushed back to the ghost fixed point $(x = 0, z = 0.9)$ with relatively smaller levels of noise (the bubble aborts). For other trajectories tracking the deterministic bold blue line, much larger levels of noise are needed to push the price along such a detour, unless the system approaches the end of bubble or the unstable equilibrium when the deterministic force will gradually make x decrease.

On the other hand, the dynamics of x can withdraw partially, spiral out and create another bubble again {2}. The latter situation can occur several times {2,4} before the main crash {6} happens. Moreover, the higher the level of x, the quicker the progression along the underlying deterministic bubble path. As x increases, the price trajectory becomes influenced by underlying deterministic trajectories spiralling out that changes in shape, compared to the phase space region for smaller x's. The higher x is, the smaller can be a partial detour away from the deterministic trajectory. As the noise is multiplicative, the same Wiener increments give larger variations of x as the dynamics evolves, so that more structures can be observed along the bubble growth. Faster evolution leads to a decrease in the time intervals between the consecutive price peaks. For instance, when price peaks are observed in phase space for $x = 10$, $x = 20$ and $x = 30$, in time space the latter two will be closer to each other than the first two.

All those factors add up and lead to the birth of smaller structures with accelerating periodicity preceding the end of the bubble and the start of the main crash. These patterns are reminiscent of those observed in real financial bubbles, in particular the joint acceleration of price and of price oscillations captured by the log-periodic power law singularity model (i.e. if taken the logarithm of the time remaining to the occurence of a singularity, the oscillations are periodic) [28, 61, 75, 76]. To support this observation we produce Lomb-periodograms (Fig. 2.9) of the trajectories presented in Fig. 2.8 (for more information on log-periodicity see [33, 77, 78]). A Lomb-periodogram is a common way of analysing the spectrum of a signal with unevenly sampled time series, hence it is a more general tool than a Fast Fourier Transform. For a short introduction to Lomb-periodograms see for instance [79, Sec. 13.8].

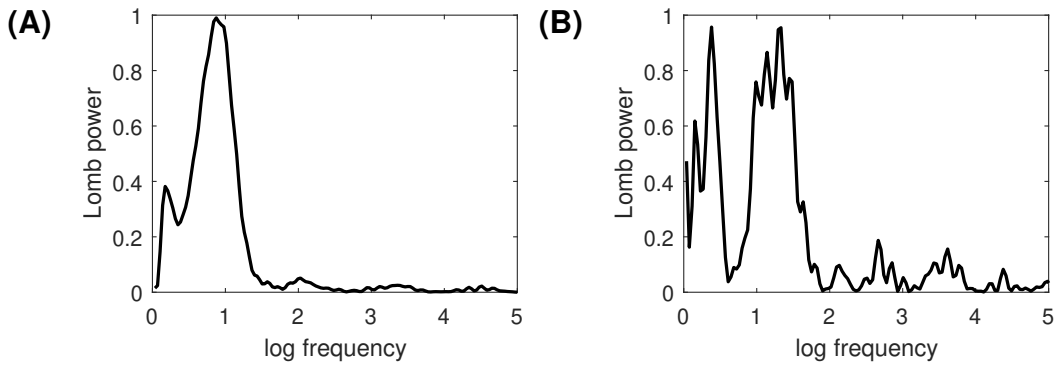

Figure 2.9: Lomb-periodograms for the trajectories presented in Fig. 2.8. The selection of t_c is done through scanning different possible values between the maximum of the time series until the end of sample and then by picking the one giving the highest peak in the Lomb-periodogram. (A) The optimised $t_c = 3.46$, which is in the middle of the deflating bubble, (B) the optimised $t_c = 13.26$, which is the top of the bubble. In the second case the sample was shortened so it begins at time 11.5, when the bubble starts to develop.

The spectral analysis is performed on the residuals $R(t)$ of the logarithmic series $\ln(x(t))$ as a function of the variable $\ln(t_c - t)$ optimised for the highest peak in the Lomb-periodogram with respect to t_c. The residuals are obtained through a transformation given in Equation (18) from [75]:

$$R(t) = \frac{\ln(x(t)) - A - B(t_c - t)^\beta}{C(t_c - t)^\beta} \tag{2.15}$$

with $A = 10$, $B = 1.0$, $C = 0.76$, $\beta = 0.10$ for the series presented in Fig. 2.9A and $A = 4.5$, $B = 1.0$, $C = 0.34$, $\beta = 0.44$ for the series presented in Fig. 2.9B. In both diagrams one can spot a clear peak characterising the most common log frequencies which suggests the presence of log-periodicity.

The peaks presented in Fig. 2.9 at frequencies around $0.1 - 0.3$ correspond to remains of the slow trend over the whole time interval of analysis. The peaks at $f_1 \approx 0.9$ in Fig. 2.9A and $f_2 \approx 1.3$ in Fig. 2.9B are the signal associated with genuine log-periodicity. The corresponding angular frequencies are $\omega_1 = 2\pi f_1 \approx 5.7$ and $\omega_2 = 2\pi f_2 \approx 8.2$, whereas the preferred scaling ratios are $\lambda_1 := e^{1/f_1} \approx 3.0$ in the first case and $\lambda_2 := e^{1/f_2} \approx 2.2$ in the second one. λ_1 and λ_2 quantify the ratio between the shrinking intervals defined by successive price peaks. The results are not sensitive to the method for selecting the critical time t_c. Picking t_c close to the maximum of the price results in basically the same position of the second peak close to $f = 1$, only the size of the peak changes somewhat.

It is important to mention how our findings relate to actual empirical results. As a benchmark we take the research presented in [78]. It is an interesting obser-

vation to note that the series shown in Fig. 2.9A visually very well matches most of the real data based Lomb-periodograms from [78]. The scaling we obtained in the first case is however slightly larger – 3.0 compared to 2.0. We expect that varying the parameters b and σ_x can influence the log-frequency of the foreshocks. The first parameter governs the periodicity of the bubbles (see Equations (2.4) and (2.5)) whereas the second one should be large enough for the foreshocks to appear (as presented in Fig. 2.7), however, we leave detailed testing of this hypothesis for further work. In the second Lomb-periodogram (Fig. 2.9B), one can observe two major peaks – it means that the low frequencies in residuals were not perfectly removed. This series can be compared to the outlying NASDAQ100 in Fig. 11 from the aforementioned paper. In fact, the frequency of the peak corresponding to the log-periodicity well matches the data presented in [78] – 2.2 versus 2.0.

Main crash. The stochastic component modulates the growth of the amplitude of each bubble. Small excursions outwards of a deterministic bubble speed up the evolution and are multiplied by the nonlinear forces (see the furthest right part of the deterministic trajectory in Fig. 2.8B). This can lead to a rapid crash without any preliminary small corrections. On the other hand, if the trajectory gets pushed inwards by stochastic innovations, it enters the region with a smaller influence from the underlying deterministic dynamics, which can then generate aftershocks.

Aftershocks. The aftershocks are purely noisy structures occurring close to the unstable fixed point. The trajectory can wobble around the nullcline or an equilibrium point for an extended period of time. This could be interpreted as a market hesitating on whether to accept that the price has peaked and is due for a correction or a crash, or rather developing some wishful thinking that this is just a temporary consolidation before a new rally starts. Adding noise also in the bond price dynamics can lead to augmenting the variety of consecutive aftershocks.

2.7 Conclusions

Revisiting the nonlinear model of coupled stock and bond prices exhibiting periodically collapsing bubbles recently proposed by [1], we have been able to prove

and document a number of novel important properties. We have extended the previous analysis of [1] concerning the classification of a set of bifurcations in the two-parameter space of this model, organised by codimension-two cusp and Bogdanov-Takens points. We have also confirmed analytically the numerical results concerning the bubble amplitude scaling as $1/|g|$ as a function of the parameter g quantifying the sensitivity of the fundamental bond price to asset prices, when it approaches 0 from below. Moreover, following [11, 70], we conclude that there are two bifurcation paths along which a periodic orbit has its period diverging, which are associated with two different scaling laws: depending on the distance $\Delta = |p - p_{bif}|$ from the bifurcation line, the period diverges as $|\ln \Delta|$ for an homoclinic bifurcation or as $\Delta^{-\frac{1}{2}}$ for a saddle-node invariant circle, which are both present in the studied system.

Using a detailed phase space representation and spectral analysis, we have been able to characterise the forces controlling the bubble growth and deflation in the presence of stochastic multiplicative noise. We found that the characteristics of the acceleration of the dynamics in phase space and the shape of the deterministic vector field are two major causes of the price patterns resembling the log-periodic power law singularity structures observed in real financial prices.

Chapter 3

Ghosts of finite-time singularities – from derivation to application

This chapter presents an extension of the study of the stock-bond dynamical system given by Eq. (2.1) in Chapter 2. We extract the underlying finite-time singularities close to the saddle-node bifurcation and use the associated trajectories to develop a method to predict the bubble collapses.

This chapter, together with Chapter 2, presents the study described in the article [*Damian Smug, Peter Ashwin and Didier Sornette.* ***"Predicting Financial Market Crashes Using Ghost Singularities"*** *(2018). PLoS ONE 13(3): e0195265]*.

3.1 Brief introduction

The concept of ghosts of singularities emerges from studying stable periodic solutions in the neighbourhood of a saddle-node bifurcation. We realised that, even if the trajectory close to the saddle-node point can be well approximated by a truncated normal form, further away, the differences might become infinitely large (for instance, if the periodic orbit stays bounded and the normal form approximation exhibits a blow up in finite time), but the period can still be well estimated. In general, we will use the notion of *ghosts* of finite-time singularities to describe the rapid changes in periodic solutions of the exact family, for which the truncated normal form (approximating family) leads to *real* finite-time singularities that are not observable in the original system. A key insight is that, even if we cannot ap-

proximate the exact shape of the periodic function, we are able to obtain another piece of information that is almost as important – its periodicity. We show that the knowledge about the period of oscillations can indeed help to forecast the time of a crash.

First, in Sec. 3.2, we show how the notion of a ghost of a finite-time singularity can be applied for a simple nonlinear ODE and then, in Sec 3.3, we provide more sophisticated analysis of approximating the trajectories in the stock-bond system. We develop our formalism and technique to provide credible predictions of the stock price falls in the deterministic case. Furthermore, we perform several tests and fits in order to determine how exactly the approximation should be parametrised (Sections 3.4 and 3.5). We then test the forecasting skill of this method on different stochastic price realisations and compare with Monte Carlo simulations of the full system – Sec. 3.6. Remarkably, the approximate normal form is significantly more precise and less biased. Moreover, the method of ghosts of singularities is less sensitive to the noise realisation, thus providing more robust forecasts. We finish this chapter with concluding remarks in Sec. 3.7.

3.2 A simple example

We start with an example explaining what we call *ghosts of finite-time singularities*. We present a study of an ODE known as the *theta model* for a spiking neuron [80, Eq. (3.6)]. We consider the following simplified system with one parameter λ:

$$\dot{\theta} = 1 - \cos(\theta) + \lambda\,. \tag{3.1}$$

The solution of the equation (3.1) with $\lambda > 0$ can be found explicitly, choosing a continuous branch of $\arctan$ for:

$$\theta(t) = 2\arctan\left(\frac{\sqrt{\lambda^2+2\lambda}}{\lambda+2}\tan\left(t\sqrt{\frac{\lambda^2}{4}+\frac{\lambda}{2}}+const.\right)\right) \tag{3.2}$$

where the constant term is determined by the initial condition. On the other hand, one can look for the normal form of the saddle-node bifurcation, which is $\dot{x} = x^2+\lambda$.

Such a form is easily obtained by a Taylor expansion of the cosine function,

$$\cos(\theta) = 1 - \frac{\theta^2}{2} + O(\theta^4)\,, \tag{3.3}$$

and the ODE (3.1) can be approximated by

$$\dot{\theta} = \frac{\theta^2}{2} + \lambda \tag{3.4}$$

with the explicit solution

$$\theta(t) = \sqrt{2\lambda}\tan\left(t\sqrt{\frac{\lambda}{2}} + const.\right). \tag{3.5}$$

This solution exhibits a singular behaviour for the times t_n such that $t_n\sqrt{\lambda/2} + const. = (2n+1)\pi/2$ becomes an odd multiple of $\pi/2$. In contrast, the exact solution (3.2) does not have such a divergence, with θ remaining finite at all times. Rather than showing a divergence at these times t_n, θ slows down close to the neighbourhood where the equilibria collided and accelerates further away. Close to these times t_n but not too close such that $\tan\left(t\sqrt{\lambda/2} + const.\right)$ is sufficiently smaller than 1 so that one can expand the $\arctan$ to equal its argument, and neglecting terms of order λ^2 compared to λ and terms of order λ compared to 1, then the exact solution (3.2) reduces to the solution (3.5) of the approximating normal form. This shows that the approximate solution shadows the true trajectory very close to the singular times t_n. We refer to the acceleration of the true dynamics as the ghost of the singularity exhibited by the underlying normal form approximating it.

In equation (3.5), the constant term plays an important role. If the initial condition in the original system (3.1) is not directly observable (for instance it might be out of the stable periodic orbit), the constant term in (3.5) can be used to obtain reliable estimates of the time of the next ghost singularity.

We assume that $\lambda > 0$, hence the system exhibits periodic behaviour – see Fig. 3.1. From equations (3.2) and (3.5), it is a simple calculation to obtain the periods, which are not identical due to the differences in the argument of the tangent function. But, the smaller the absolute value of λ, the smaller is the difference in periodicity and the more accurate the predictions obtained from the normal form approximation (3.4) of the full system (3.1). We conclude that the

approximation of the true solution leads to a good estimation of the period even if its amplitude does not match that of the original system. This result can be used to make predictions on the future state of the system with no need for simulations.

It is important to mention that in the model (3.1) the dynamics is described on a circle. For graphical convenience in Fig. 3.1 we present θ in the arbitrary interval $[-\pi, \pi]$ and align the instant of the largest change of θ with the singularity time. Nevertheless, for any other choice of the interval used for graphical explanation, the singularities of the red curve will match the highest variation of the true solution. This is caused by the fact that both the approximating and the original solution spend most of the time close to the remainder of the equilibria and perform only a very short, and thus quick, detour. It hints, that our result is generic with respect to other approximating forms in the same equivalence class for a bifurcation as long as they produce periodic behaviour, whereas the original bifurcation is not only a saddle-node collision, but actually a SNIC (see Sec. 1.2.3).

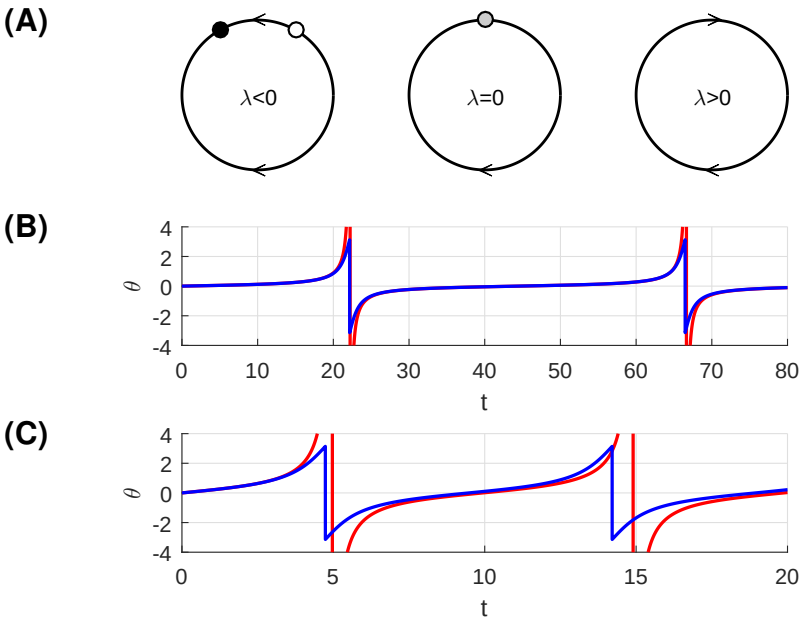

Figure 3.1: Example of ghosts of finite-time singularities and real finite-time singularities. (A) Schematic bifurcation diagram of the flow of system (3.1). For $\lambda < 0$, there are two equilibria – one stable (black) and one unstable (white), for $\lambda = 0$, a saddle-node bifurcation occurs and for $\lambda > 0$ (if we allow discontinuities in the solutions), one can observe periodic orbits between $-\pi$ and π. In the two-dimensional case, discontinuities are not necessary to obtain a periodic behaviour. Panels (B) and (C) show the sample solutions for systems (3.1) and (3.4). The blue curve is the original accurate solution of the full dynamics, where no finite-singularity occurs. The red one is the approximation based on the saddle-node normal form. In the solution based on normal form, there are finite-time singularities whereas, in the original one, bubbles and crashes are bounded. The jump behaviour exhibited by the exact solution of the full system is called the *ghost of the singularity* associated with the normal form approximation. Parameter values are: (B) $\lambda = 0.01$ and (C) $\lambda = 0.2$.

3.3 Centre manifold expansion for an emerging bubble

This section, similarly to the previous one, provides analytical derivation of the bubble trajectory in the vicinity of a SNIC bifurcation in the system (2.1) from the previous chapter, namely:

$$\begin{cases} \dot{x} = x - x^2 \cdot e^{-bxz} \\ \dot{z} = z - z^2 \cdot e^{-gx} \end{cases} . \tag{3.6}$$

In order to find a good approximate function of the price dynamics $x(t)$ of a bubble, we calculate $x(t)$ for parameters close to the upper saddle-node branch shown in Fig. 2.2A. On the upper part of the saddle-node curve, let us consider parameters (b^*, g^*) and the corresponding non-trivial equilibrium point (x^*, z^*). We fix b^* and vary only parameter g, so instead of (3.6), we consider the following system:

$$\begin{cases} \dot{x} = x - x^2 e^{-b^* xz} \\ \dot{z} = z - z^2 e^{-(g^*+\delta)x} \end{cases} . \tag{3.7}$$

Next, we move the system to the origin so that the equilibrium point is placed at $(0, 0)$:

$$\begin{cases} X = x - x^* \\ Z = z - z^* \\ b = b^* \\ g = g^* + \delta \end{cases} \tag{3.8}$$

and, by taking into account the derivative $\frac{d\delta}{dt}$, we obtain

$$\begin{pmatrix} \dot{X} \\ \dot{Z} \\ \dot{\delta} \end{pmatrix} = \begin{pmatrix} (X + x^*) - (X + x^*)^2 e^{-b^*(X+x^*)(Z+z^*)} \\ (Z + z^*) - (Z + z^*)^2 e^{-(g^*+\delta)(X+x^*)} \\ 0 \end{pmatrix} = \begin{pmatrix} F(X, Z, \delta) \\ G(X, Z, \delta) \\ 0 \end{pmatrix} . \tag{3.9}$$

The Jacobian in the equilibrium point is

$$J := J(X,Z,\delta)\Big|_{(0,0,0)} = \begin{pmatrix} \frac{\partial F}{\partial X} & \frac{\partial F}{\partial Z} & 0 \\ \frac{\partial G}{\partial X} & \frac{\partial G}{\partial Z} & \frac{\partial G}{\partial \delta} \\ 0 & 0 & 0 \end{pmatrix}_{(0,0,0)} \overset{(*)}{=} \begin{pmatrix} p_1 & p_2 & 0 \\ p_3 & \frac{p_2 p_3}{p_1} & p_4 \\ 0 & 0 & 0 \end{pmatrix}, \tag{3.10}$$

where the substitution $(*)$ is performed in order to simplify the notations for the saddle-node equilibrium point where the Jacobian $\begin{pmatrix} \frac{\partial F}{\partial X} & \frac{\partial F}{\partial Z} \\ \frac{\partial G}{\partial X} & \frac{\partial G}{\partial Z} \end{pmatrix}$ is singular. J has eigenvalues $(\lambda_c, \lambda_s, \lambda_c) = \left(0, \frac{p_1^2+p_2p_3}{p_1}, 0\right)$ and the eigenvectors for the two first eigenvalues are

$$v_{c_1} = \begin{pmatrix} -\frac{p_2}{p_1} \\ 1 \\ 0 \end{pmatrix} \quad \text{and} \quad v_s = \begin{pmatrix} \frac{p_1}{p_3} \\ 1 \\ 0 \end{pmatrix}. \tag{3.11}$$

For the third eigenvalue λ_c, we need to find the generalised eigenvector v_{c_2}

$$Jv_{c_2} = v_{c_1} \quad \Longrightarrow \quad J^2 v_{c_2} = Jv_{c_1} = 0\,, \tag{3.12}$$

hence, we calculate the eigenvectors of J^2 for the eigenvalue λ_c. One is of course v_{c_1} and the other is

$$v_{c_2} = \begin{pmatrix} -\frac{p_2 p_4}{p_1^2+p_2p_3} \\ 0 \\ 1 \end{pmatrix}. \tag{3.13}$$

In the vector basis $P := (v_{c_1}, v_s, v_{c_2})$, new coordinates can be obtained by the following transformation

$$\begin{pmatrix} X \\ Z \\ \delta \end{pmatrix} = P \begin{pmatrix} U \\ V \\ \delta \end{pmatrix} = \begin{pmatrix} -\frac{p_2}{p_1} & \frac{p_1}{p_3} & -\frac{p_2 p_4}{p_1^2+p_2p_3} \\ 1 & 1 & 0 \\ 0 & 0 & 1 \end{pmatrix} \begin{pmatrix} U \\ V \\ \delta \end{pmatrix} \tag{3.14}$$

and on the other hand

$$\begin{pmatrix} U \\ V \\ \delta \end{pmatrix} = P^{-1} \begin{pmatrix} X \\ Z \\ \delta \end{pmatrix} = \begin{pmatrix} -\frac{p_1 p_3}{p_1^2+p_2p_3} & \frac{p_1^2}{p_1^2+p_2p_3} & -\frac{p_1 p_2 p_3 p_4}{(p_1^2+p_2p_3)^2} \\ \frac{p_1 p_3}{p_1^2+p_2p_3} & \frac{p_2 p_3}{p_1^2+p_2p_3} & -\frac{p_1 p_2 p_3 p_4}{(p_1^2+p_2p_3)^2} \\ 0 & 0 & 1 \end{pmatrix} \begin{pmatrix} X \\ Z \\ \delta \end{pmatrix}. \tag{3.15}$$

Hence, in the new coordinates, the dynamical system becomes

$$\begin{pmatrix} \dot{U} \\ \dot{V} \\ \dot{\delta} \end{pmatrix} = \begin{pmatrix} \frac{dU(X,Z)}{dt} \\ \frac{dV(X,Z)}{dt} \\ 0 \end{pmatrix} = \begin{pmatrix} (P^{-1})_{11}\dot{X} + (P^{-1})_{12}\dot{Z} \\ (P^{-1})_{21}\dot{X} + (P^{-1})_{22}\dot{Z} \\ 0 \end{pmatrix}. \tag{3.16}$$

Using the multivariate Taylor expansion for $\dot{U}$, $\dot{V}$ and $\dot{\delta}$ at the point $(0,0,0)$, we obtain

$$\begin{aligned} \begin{pmatrix} \dot{U} \\ \dot{V} \\ \dot{\delta} \end{pmatrix} &= \begin{pmatrix} 0 & 0 & \mu_1 \\ 0 & \mu_2 & 0 \\ 0 & 0 & 0 \end{pmatrix} \begin{pmatrix} U \\ V \\ \delta \end{pmatrix} + \\ &+ \begin{pmatrix} a_1U^2 + a_2UV + a_3U\delta + a_4V^2 + a_5V\delta + a_6\delta^2 \\ b_1U^2 + b_2UV + b_3U\delta + b_4V^2 + b_5V\delta + b_6\delta^2 \\ 0 \end{pmatrix}, \end{aligned} \tag{3.17}$$

where the coefficients μ_i (for $i \in \{1,2\}$), a_i and b_i (for $i \in \{1,...,6\}$) are known. It is important to mention that the Jacobian of the system (3.17) has two vanishing eigenvalues and forms a Jordan normal form with separated centre (U_c, δ_c) and stable (V_s) parts.

The flow on the stable manifold can be approximated by

$$V_s(U_c, \delta_c) = \alpha U_c^2 + \beta U_c\delta_c + \gamma\delta_c^2, \tag{3.18}$$

hence

$$\dot{V}_s(U_c, \delta_c) = \frac{\partial V_s}{\partial U_c}\dot{U}_c + \frac{\partial V_s}{\partial \delta_c}\dot{\delta}_c = (2\alpha U_c + \beta\delta_c)\dot{U}_c. \tag{3.19}$$

In order to determine α, β and γ we need to compare coefficients in $\dot{V}_s(U_c, \delta_c)$ and $\dot{V}(U_c, \delta_c)$:

$$\begin{aligned} &\mu_2V_s + b_1U_c^2 + b_2U_cV_s + b_3U_c\delta_c + b_4V_s^2 + b_5V_s\delta_c + b_6\delta_c^2 = \\ &= (2\alpha U_c + \beta\delta_c)(\mu_1\delta_c + a_1U_c^2 + a_2U_cV_s + a_3U_c\delta_c + a_4V_s^2 + a_5V_s\delta_c + a_6\delta_c^2) \end{aligned} \tag{3.20}$$

When inserting (3.18) into (3.20), it is enough to compare the coefficients up

to quadratic terms:

$$\begin{aligned}
\boldsymbol{U_c^2}: &\quad \mu_2\alpha + b_1 = 0 \implies \alpha = -\frac{b_1}{\mu_2} \\
\boldsymbol{U_c\delta_c}: &\quad \mu_2\beta + b_3 = 2\alpha\mu_1 \implies \beta = -\frac{2b_1\mu_1 + b_3\mu_2}{\mu_2^2} \\
\boldsymbol{\delta_c^2}: &\quad \mu_2\gamma + b_6 = \beta\mu_1 \implies \gamma = -\frac{2b_1\mu_1^2 + b_3\mu_1\mu_2 + b_6\mu_2^2}{\mu_2^3}.
\end{aligned} \tag{3.21}$$

Finally, in order to obtain the flow on the centre manifold, we insert (3.18) with determined coefficients (3.21) into $\dot{U}$ (3.17):

$$\begin{aligned}
\dot{U}_c = f(U_c,\delta_c) = \mu_1\delta_c + a_1U_c^2 + a_2U_c(\alpha U_c^2 + \beta U_c\delta_c + \gamma\delta_c^2) + a_3U_c\delta_c + \\
+a_4(\alpha U_c^2 + \beta U_c\delta_c + \gamma\delta_c^2)^2 + a_5(\alpha U_c^2 + \beta U_c\delta_c + \gamma\delta_c^2)\delta_c + a_6\delta_c^2 = \\
= \mu_1\delta_c + a_6\delta_c^2 + \gamma a_5\delta_c^3 + \gamma^2 a_4\delta_c^4 + U_c(a_3\delta_c + a_2\gamma\delta_c^2 + a_5\beta\delta_c^2 + 2a_4\beta\gamma\delta_c^3) + \\
+U_c^2(a_1 + a_2\beta\delta_c + a_5\alpha\delta_c + 2a_4\alpha\gamma\delta_c^2 + a_4\beta^2\delta_c^2) + U_c^3(a_2\alpha + 2a_4\alpha\beta\delta_c) + U_c^4a_4\alpha^2 \quad .
\end{aligned} \tag{3.22}$$

In order to approximate the function describing the time dependence of the price of an arising bubble, we integrate $\dot{U}_c$:

$$\frac{dU_c}{dt} = f(U_c,\delta_c) \quad \implies \quad \frac{dU_c}{f(U_c,\delta_c)} = dt \quad \implies \int \frac{1}{f(U_c,\delta_c)}dU_c = \int dt + const. \tag{3.23}$$

hence

$$\int \frac{1}{f(U_c,\delta_c)}dU_c = t + const.. \tag{3.24}$$

Without dropping higher order terms, it might not be possible to obtain U_c explicitly, hence we assume, that $\delta_c = \varepsilon$ and as U_c is expected to vary faster than the parameter, we take $U_c = U_{c_0}\sqrt{\varepsilon} + O(\varepsilon)$. Then, for the function f, we truncate all terms of order higher than $O(\varepsilon)$, hence $f(U_c,\delta_c) = \mu_1\delta_c + a_1U_c^2 + O\left(\delta_c^{\frac{3}{2}}\right)$. From Equation (3.24), using the simplified form of f, we obtain

$$\frac{1}{\sqrt{a_1\mu_1\delta_c + O\left(\delta_c^{\frac{3}{2}}\right)}}\arctan\left(\sqrt{\frac{a_1}{\mu_1\delta_c + O\left(\delta_c^{\frac{3}{2}}\right)}}U_c\right) = t + const., \tag{3.25}$$

which gives

$$U_c = \sqrt{\frac{\mu_1\delta_c}{a_1}}\tan\left(t\sqrt{a_1\mu_1\delta_c} + const.\right) + O\left(\delta_c^{\frac{3}{2}}\right). \tag{3.26}$$

The error term is found by Taylor expansion of tangent function close to the equilibrium as its argument, i.e. $tan(x) \approx x$ for small x.

Inserting (3.26) into (3.18) leads to

$$V_s = \alpha U_c^2 + \beta U_c \delta_c + \gamma \delta_c^2 =$$
$$= \alpha \left(\sqrt{\frac{\mu_1 \delta_c}{a_1}} \tan\left(t \sqrt{a_1 \mu_1 \delta_c} + const. \right) \right)^2 + \beta \left(\sqrt{\frac{\mu_1 \delta_c}{a_1}} \tan\left(t \sqrt{a_1 \mu_1 \delta_c} + const. \right) \right) \delta_c + \gamma \delta_c^2 + O\left(\delta_c^{\frac{5}{2}} \right) =$$
$$= \gamma \delta_c^2 + \beta \delta_c^{\frac{3}{2}} \sqrt{\frac{\mu_1}{a_1}} \tan\left(t \sqrt{a_1 \mu_1 \delta_c} + const. \right) + \alpha \delta_c \frac{\mu_1}{a_1} \tan^2\left(t \sqrt{a_1 \mu_1 \delta_c} + const. \right) + O\left(\delta_c^{\frac{5}{2}} \right). \tag{3.27}$$

Then, from (3.14), (3.26) and (3.27) one obtains

$$X = -\frac{p_2}{p_1} U_c + \frac{p_1}{p_3} V_s - \frac{p_2 p_4}{p_1^2 + p_2 p_3} \delta_c = \frac{p_1}{p_3} \gamma \delta_c^2 - \frac{p_2 p_4}{p_1^2 + p_2 p_3} \delta_c +$$
$$+ \left(\frac{p_1 \beta \sqrt{\mu_1} \delta_c^{\frac{3}{2}}}{p_3 \sqrt{a_1}} - \frac{p_2 \sqrt{\mu_1 \delta_c}}{p_1 \sqrt{a_1}} \right) \tan\left(t \sqrt{a_1 \mu_1 \delta_c} + const. \right) + \frac{p_1 \alpha \mu_1 \delta_c}{p_3 a_1} \tan^2\left(t \sqrt{a_1 \mu_1 \delta_c} + const. \right) + O\left(\delta_c^{\frac{3}{2}} \right) =$$
$$= -\frac{p_2 p_4}{p_1^2 + p_2 p_3} \delta_c - \frac{p_2 \sqrt{\mu_1 \delta_c}}{p_1 \sqrt{a_1}} \tan\left(t \sqrt{a_1 \mu_1 \delta_c} + const. \right) + \frac{p_1 \alpha \mu_1 \delta_c}{p_3 a_1} \tan^2\left(t \sqrt{a_1 \mu_1 \delta_c} + const. \right) + O\left(\delta_c^{\frac{3}{2}} \right), \tag{3.28}$$

where all parameters in the above expression are known. Finally, we need to shift back X by the position of the equilibrium according to (3.8): $x = X + x^*$.

3.4 Fitting parameters of the approximated form of a bubble

The detailed analysis from the previous section leads to the final form

$$x_{app}(t) = A + B \tan(C(t - D)) + E \tan^2(C(t - D)), \tag{3.29}$$

where all parameters but D are given explicitly in terms of b and g. The parameter D cannot be computed in the same way as the others, since it determines the movable singularity of $x_{app}(t)$. Such singularities are at positions that strictly depend on the initial condition of the system – see for instance [81]. Hence, given a certain trajectory the parameter D needs to be found by means of curve fitting.

Obviously, one could simply skip the analytical approach of Sec. 3.3 and fit all

the parameters A–E. However, in such an approach one needs to find a proper slope (governed by parameters B and E) and, more importantly, the period (governed by the parameter C) of the function (3.29). Losing the information about the period means that we actually lose information about the timescales of occurences of bubbles that was coming from the approximating normal form in the neigbourhood of a bifurcation.

In order to validate numerically the approximate form (3.29) we choose two sets of parameters b and g in the vicinity of the saddle-node branch. For these values we simulate trajectories of a stable periodic orbit in the system (3.6) and we extract only the increasing part of variable x. Then, we align the function (3.29) to the simulated series. Parameters A, B, C and E for each set of b and g are obtained directly from the Eq. (3.28). However, in order to provide greater flexibility in the fitting scheme and to approach the fact that the trajectories have a tendency to progress very slowly for low values of x, we allow in the fitting procedures a vertical correction. It means that we allow to fit the parameter A as well. We denote it in Table 3.1 by A^*. The curve fitting procedure is performed in `GraphPad Prism 7` (Nonlinear Regression; least squares fitting method; quantification of goodness-of-fit based on R square) and its results are presented in Tab. 3.1.

b	g	A	$\boldsymbol{A^*}$	B	C	$\boldsymbol{D}$	E
0.4	−0.029	3.042	2.977	0.1744	0.02637	62.03	$-0.5416 \cdot 10^{-3}$
0.38	−0.0117	2.819	2.812	0.03683	0.006325	251.8	$-0.8509 \cdot 10^{-5}$

Table 3.1: Parameters for the best fits of the functions family (3.29) to the numerical solutions. Parameter A^* replaces A as explained in the text. Only the parameters marked in bold were fitted.

The two fits are presented in Fig. 3.2 where we show the mean square error of fit in terms of the distance from the underlying saddle-node equilibrium. The neighbourhood of the saddle-node equilibrium is where the trajectories spend the most time.

The exceptionally low value of parameter E in Tab. 3.1 suggests that it might be worth to drop the higher order term in the function (3.29) and analyse the approximation of the form:

$$\hat{x}_{app}(t) = A + B\tan(C(t-D))\,. \tag{3.30}$$

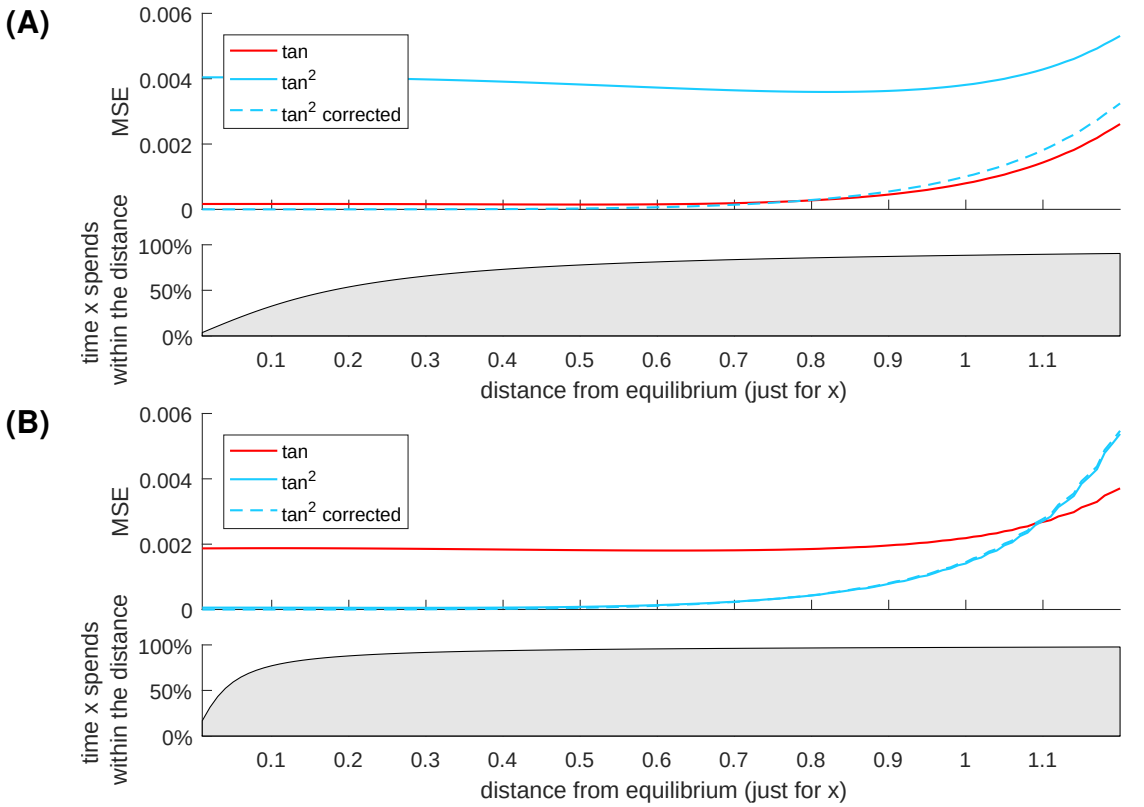

Figure 3.2: Comparison of the MSE (mean squared error) for (3.29) and (3.30) as a function of the distance from the saddle-node equilibrium, with the percentage of time that the asset price spends within that distance for (A) $b = 0.4$, $g = -0.029$ and (B) $b = 0.38$, $g = -0.0117$. From the diagram one can deduce that application of vertical correction can decrease the error of the fitted function significantly in some cases but not always. The percentage of time that the asset price spends within a certain distance (bottom panels of (A) and (B)) suggests that the system resides far from an equilibrium only during a very short period. On the other hand, this period is extremely important as it is the time when the bubbles arise and collapse. Comparison of the blue and red curves implies that even though close to the equilibrium $\tan^2$ gives small MSE, further on it is outperformed by the simplified function $(\tan)$ and that function with a vertical correction is used for the predictions presented in Section 3.2.

Because in Fig. 3.2A the vertical correction incorporated in the fitting of (3.29) significantly improved the goodness-of-fit, we allow to fit parameter A in (3.30) as well. The parameters for the function $\hat{x}_{app}(t)$ are presented in Tab. 3.2 and were obtained in the same way as these for the form with higher order term.

Both the tangent function (3.30) and the formula (3.29) with the quadratic term provide good fits to the bubble price in the close neighbourhood of the equilibrium. One can see that formula (3.29) gives a very small error close to the equilibrium point, however, the error increases much faster than for the tangent function (3.30) when moving further from the equilibrium. This means that, in order to approximate the trajectory the best results would be obtained by using (3.29) close to the saddle-node equilibrium and then switch to (3.30) further away. However, for

b	g	$\boldsymbol{A}$	B	C	$\boldsymbol{D}$
0.4	−0.029	2.991	0.1744	0.02637	62.07
0.38	−0.0117	2.855	0.03683	0.006325	251.3

Table 3.2: Parameters for the best fits of the functions family (3.30) to numerical solutions. The parameters marked in bold – A and D were found by fitting method, whereas the parameters B and C are obtained through (3.28).

simplicity, we restrict to the usage of the approximation given by Eq. (3.30) only.

In the analysis outlined above the functions were fitted to the full bubble trajectory, however, in order to make use of the approximated form we need to verify how well the tangent function (3.30) can actually perform predictions of the crash time. We denote by t_c the crash time (i.e. the ghost of finite-time singularity) observed in the trajectory, whereas t_p denotes the predicted time of a crash (the real singularity) calculated from some given sample within the time interval $[t_1, t_2]$. This sample is treated as current knowledge, whereas t_2 is understood as current time. From the tangent function (3.30) it is straightforward to find t_p. Knowing that $\tan(\frac{\pi}{2} + k\pi) = \infty$, t_p is determined by the condition $C(t_p - D) = \frac{\pi}{2} + k\pi$, which gives

$$t_p(t_2) = \inf\left\{\frac{\pi/2 + k\pi}{C} + D > t_2 : k \in \mathbb{N}\right\}. \tag{3.31}$$

In Fig. 3.3 we illustrate a sample application of the method of predicting ghosts of finite-time singularities in the deterministic system (3.6).

3.5 Selection of the optimal window length

Before one applies the above results, there is one more parameter to determine – the window length w of the time series to which the function (3.30) is fitted. It is important to realise that one should not use the whole price history, but only the rather recent one when the price starts to accelerate and a bubble develops. Before that, the price is close to its ghost equilibrium fixed point and is mostly exhibiting a random walk. Moreover, as the function (3.30) exhibits periodic finite-time singularities, when one wants to predict the next singularity, including the previous one in the analysis will be highly disruptive to the search algorithm (in our case: Levenberg-Marquardt). The simple solution to avoid such situation is to bound the window length from above, for instance to 70% of the fitted function's

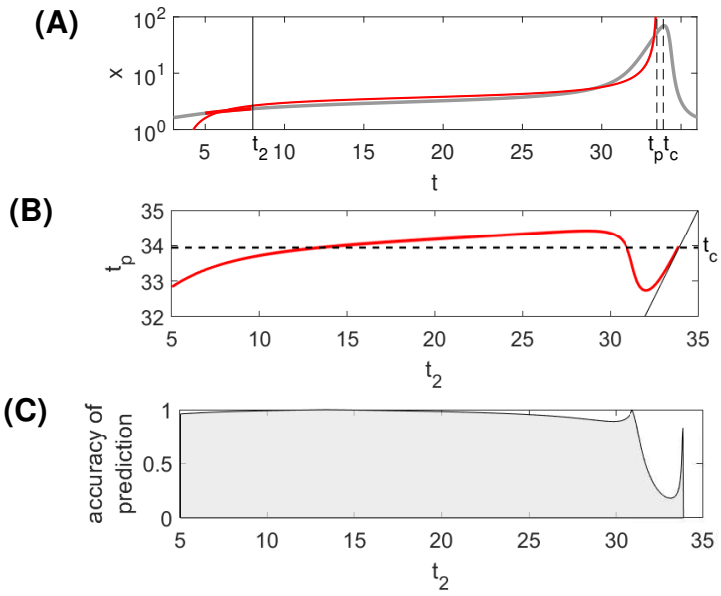

Figure 3.3: Sample application of the ghosts of finite-time singularities in the deterministic system (3.6) for parameters $b = 0.42$ and $g = -0.04$. (A) Presentation of one fit (thin red line) for a small sample set representing current knowledge (bold red) up to 'present' time $t_2 = 8$ (solid black line) compared with the true price trajectory (grey). The predicted time of the crash (i.e. where the finite-time singularity occurs in (3.30) – indicated by the dashed black line) is very close to the peak of the bubble and therefore provides an accurate forecast. (B) Time t_p of the predicted crash (red) as a function of the 'present' time t_2 compared with the exact crash time t_c. We apply here a sliding window of arbitrary length $w = 3$. Section 3.5 explains the methodology that we follow to choose the optimal window length. When the bubble starts to grow rapidly (around $t = 30$), the predicted crash time t_c decreases towards the 'present' time t_2 and, as t_2 increases, t_p remains close to t_2 as can be seen by the line $t_p = t_2$ (solid black). The price acceleration thus tends to induce the calibration to believe that the crash is looming, exaggerating the imminence of the danger. (C) Accuracy of crash prediction measured by $1 - |t_c - t_p|/|t_c - t_2|$. The prediction accuracy is remarkably high already very far from the crash, and does not improve significantly over most of the lifetime of the bubble. However, when time passes 30, the accuracy deteriorates dramatically. It is caused by the fact that the predictions are based on the normal form truncation close to the equilibrium. This is not the case after time 30 when the system grows exponentially.

period and to check several initial guesses picking the one with the least mean square error or the smallest predicted time of a crash following the final (i.e. 'present') time t_2 of the sample. In our computation, the second criterion is used, as our objective is to predict the singular time t_p of the bubble collapse.

On the other hand, the window length cannot be too small as even a tiny perturbation would cause t_p to vary significantly and the outcome would not be reliable anymore. In order to avoid any a priori bias, we propose to scan both window lengths w and end of sample time t_2 on 100 randomly generated bubbles. Afterwards, for each time window, the prediction error is quantified as $\frac{|t_p - t_c|}{|t_2 - t_c|}$, with the top and bottom 10% cases being put aside to remove outliers and ensure

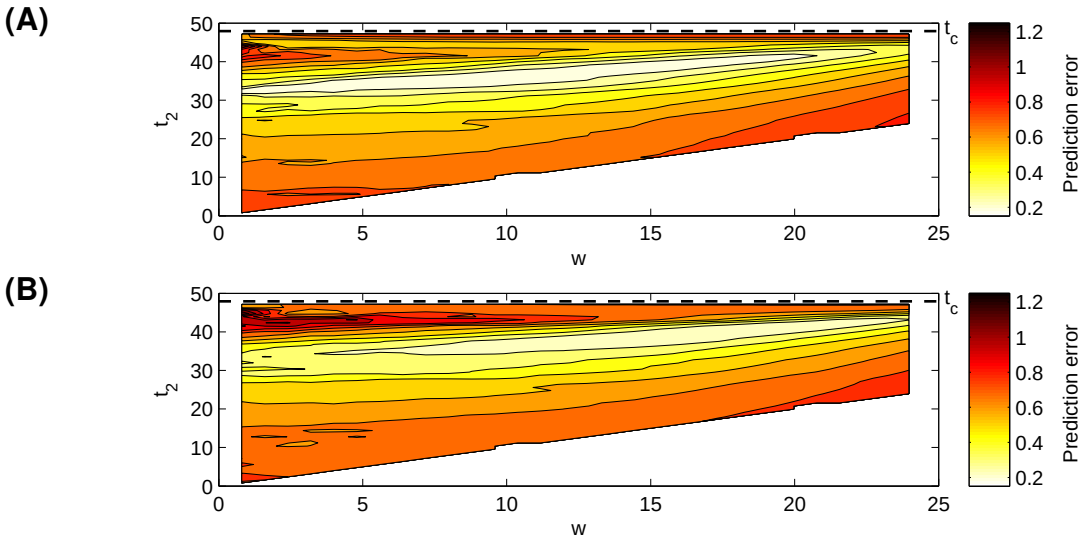

Figure 3.4: Dependence of the prediction error $\frac{|t_c - t_p|}{|t_c - t_2|}$ as a function of window size w and end t_2 of window. (A) For $\sigma_x = 0.2$, the optimal window length is around 10 – i.e. where the error values are the lowest. (B) For $\sigma_x = 0.4$, the optimal window length is around 15. The parameters of the model are $b = 0.42$, $g = -0.04$, $\sigma_z = 0.01$, $\delta(W_t^{(1)}, W_t^{(2)}) = 50\%$. For both selected window sizes, the error just before the time of a crash t_c does not significantly differ in comparison to larger w and, moreover, the smaller w is, the faster the system responds to new information. There is thus a trade-off between responsive adaptation of the fits and error size.

robust results, and the rest is averaged. The procedure maps one prediction error value to each pair (w, t_2). Fig. 3.4 presents the final results.

Based on Fig. 3.4, for the following simulations presented in the next Section 3.6, we will use window size $w = 10$ for $\sigma_x = 0.2$ and $w = 15$ for $\sigma_x = 0.4$. For these selected values of w, the prediction errors are the smallest over the widest range of window size w and window ends t_2, making the results robust.

3.6 Application of ghosts of finite-time singularities to simulated data

When all parameters are estimated, we can finally determine how the methodology of ghosts of finite-time singularities can work in practice. Firstly, we generate a single trajectory with a sufficiently long price history preceding a crash from the SDE model (2.14) studied in the previous chapter:

$$\begin{cases} dx = \left(x - x^2 \cdot e^{-bxz}\right) dt + \sigma_x \, x \, dW_t^{(1)} \\ dz = \left(z - z^2 \cdot e^{-gx}\right) dt + \sigma_z \, z \, dW_t^{(2)} . \end{cases} \tag{3.32}$$

The variable x is shown as the grey line in Fig. 3.5 with its scale given on the left-hand side vertical axis. The knowledge of the model parameters, as determined in Sec. 3.3, gives explicitly the period and the slope of the tangent function (3.30) used to approximate the emerging bubbles.

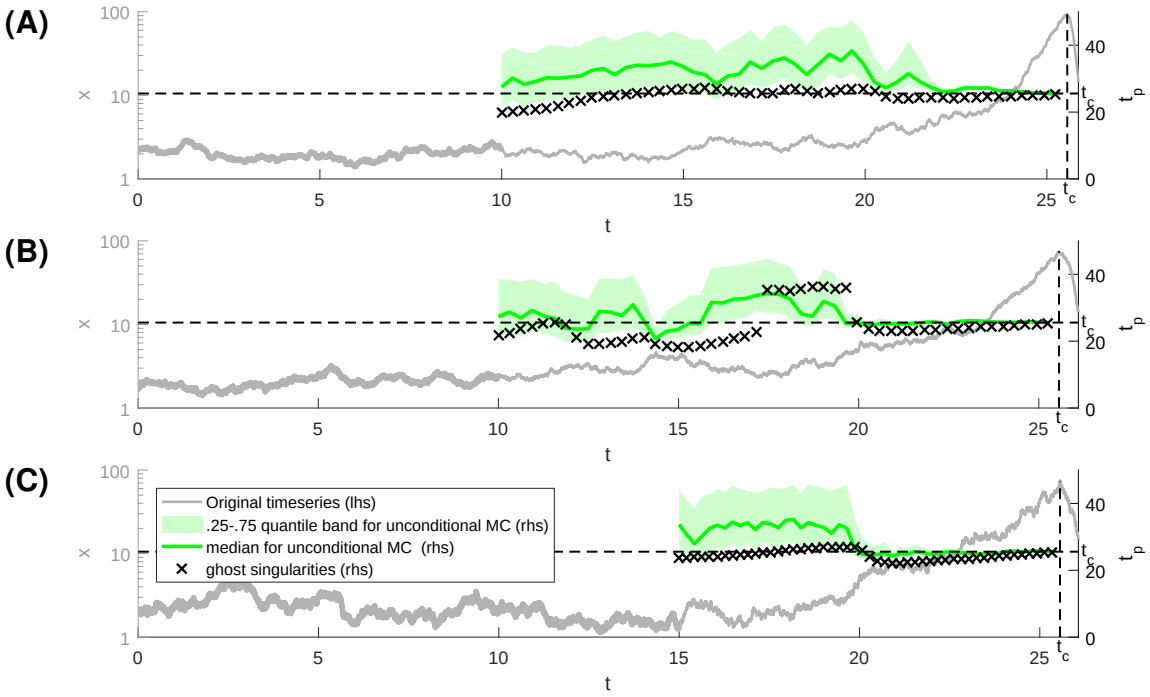

Figure 3.5: Test of the methodology using the ghosts of finite-time singularities in comparison with Monte Carlo method. (A) and (B) correspond to two different realizations of the price process for $\sigma_x = 0.2$ and $\sigma_z = 0.01$, (C) corresponds to one realisation generated with $\sigma_x = 0.4$ and $\sigma_z = 0.01$. The stochastic price trajectory is plotted (grey line) with its scale given on the left-hand side vertical axis. The scale of the crash time predictions is given by the right-hand side vertical axis. The symbols 'x' stand for the predicted time t_p, using the history from time $t - w$ until time t to perform the calibration with the singular model. The criteria used to select the window size w for different noise amplitudes are given in Section 3.5.

Then, based on the considerations presented in Section 3.5, the size of the sliding window of analysis is chosen. For $\sigma_x = 0.2$, it is $w = 10$, hence the first prediction (or calibration) is done at time $t_2 = 10$, which allows us to take into account the history in the window $t \in [0, 10]$. This initial window is shown as a bold grey line close the horizontal axis in Fig. 3.5. The corresponding predicted crash time $t_p(t_2 = 10, w = 10)$ is indicated by the first black 'x' marker (with its scale given on the right-hand side vertical axis). Thereafter, the calibration window is shifted, while keeping its size fixed, which mimics the passing of time as the bubble develops and we accumulate data to perform real-time forecasts, while removing data of the far away past. Implementing this procedure gives us the evolution of t_p as a function of 'present' time t_2, offered as a forecast for the real

time t_c of the crash. We continue the procedure until t_2 approaches close to the true t_c.

The forecasts obtained by using the tangent function (3.30) are compared with those of the following Monte Carlo scheme using the exact equations (3.32). We integrate 500 trajectories with the known exact parameters and initiated in the current state (x_t, z_t), and record the time $t_p^{MC,i}$ $(i = 1, ..., 500)$ of the first crash that appears in each trajectory. Operationally, we define a crash by the occurrence of a maximum of a bubble that rose above 50% and then collapsed to a value below 20% of the underlying deterministic stable bubble that would exist for the same parameter values. For the selected level of noise, this criterion has been found to be very reliable. Then, the forecast t_p^{MC} is the median value of the all crash times $t_p^{MC,i}$ over this population of 500 price trajectories (green line in Fig. 3.5). The ensemble $t_p^{MC,i}$ $(i = 1, ..., 500)$ also allows us to give the inter-quartile interval of confidence (the light green band in Fig. 3.5).

To determine the influence of the amplitude of the noise process on the quality of the forecasts, we present two different outcomes for the same noise value $\sigma_x = 0.2$ (Fig. 3.5A-B) and one for $\sigma_x = 0.4$ (Fig. 3.5C). It is noteworthy that these diagrams differ significantly. In the first case (Fig. 3.5A), the price trajectory happens to be very regular, and the predictions are found to be very accurate over a large time interval. For the second price realisation (Fig. 3.5B) that exhibits stochastic foreshocks, the forecasts are more unstable, as a result of the influence of disjoint local attractors in the parameter space. The disappearance of one of them with the lowest t_p leads visually to a discontinuous transition towards a different state around time $t = 17$. On the other hand, the forecasts are definitely closer to the true t_c than the Monte Carlo scheme. One can also note that the forecasts become visually excellent when t_2 passes the value 20 beyond which the price starts its characteristic bubble acceleration. However, following Fig. 3.3C, this phenomena is often accompanied by low accuracy of prediction.

For the higher level of noise (Fig. 3.5C), two regimes can be observed. First, t_p steadily increases as a function of t_2. Then, around $t_2 = 20$, one can observe a quick decreasing phase, which is caused by a sudden escalation of the variable x. This suggests that the method of ghosts of finite-time singularities provides a cautious approach as it quickly reacts to variable changes while being on the conservative side with t_p in general smaller than the true t_c. In contrast, the Monte

Carlo forecast errs towards larger values up to $t_2 = 20$ and then converges quickly to the correct value.

The diagrams in Fig. 3.5 suggest that the Monte Carlo method tends to overestimate the crash time, however, this is not a correct interpretation. The stochastically forced system (3.32) tends to spend significant amount of time in the close neighbourhood of the remainder of the equilibrium, and thus extracting time series with a bubble and some history beforehand is in a way biasing the experiment. On the other hand, our approach will always claim that a crash will occur in a certain time which, by the construction of our predictor, is lower than the period of the tangent function (3.30). Hence, we suggest to interpret t_p as a measure of risk for a certain time series rather than an exact crash time.

In summary, it is remarkable that the method of ghosts of singularities provides in general a better forecast than the full integration of the true dynamical stochastic equation. By reducing the complexity and focusing on the key ingredient underlying the forecast skill, namely the time to the bubble, the method of ghosts of singularities seems to be less sensitive to idiosyncratic noise realisations, thus providing more robust forecasts. This can be interpreted as a kind of effective coarse-graining of the dynamical equations, a process that, when done intelligently, has been shown in the past to improve predictability [82–85].

3.7 Conclusions

We have provided an analysis to show how dramatic shifts in a stochastically forced dynamical system can be predicted. By expanding the system in the neighbourhood of the saddle-node bifurcation, we obtained a function that approximates an arising bubble. This function exhibits finite-time singularities and, therefore, it cannot be used to predict the precise system state far from the equilibrium trajectory. Nevertheless, its periodicity still matches well that of the original system. This property gives a simple tool to predict when the system is going to crash.

We have shown by considering a few realisations of the stochastic price process how the idiosyncratic occurrence of noise innovations and increasing volatility impact the performance of the predictions. We have introduced the notion of ‘ghosts of finite-time singularities’, based on a normal form approximating the true

dynamics and which exhibits a finite-time singularity while the true system does not. But it turns out that the time of the peak of the bubble in the true system is very well approximated by the singularity time of the approximating normal form. Hence, the peak of the bubble can be viewed as a kind of 'ghost' of the finite-time singularity expressed in the approximating normal form. It turns out that this concept is very useful to predict the time of crashes by estimating the remaining time to the end of an evolving bubble, using the approximated normal form valid close to a bifurcation point.

Finally, we have tested the forecasting skill of the method of 'ghosts of finite-time singularities' on different stochastic price realisations, in comparison with the full integration of the true dynamical stochastic equation. Remarkably, we have found that the former is significantly more precise and less biased than the construction of many scenarios built on the full integration of the exact stochastic differential equations. The mechanism underlying this augmented performance has been argued to result from a reduction of complexity that focuses on the key ingredient underlying the forecast skill, namely a ghost singular behaviour, which leads to a smaller sensitivity to idiosyncratic noise realisations, thus providing more robust forecasts.

Chapter 4

A generalised mean-field Ising model with a rich set of bifurcations

In this chapter we present an analysis of an extended version of the dynamical mean-field Ising model. Instead of classical physical representation of spins and external magnetic field, the model describes traders' opinion dynamics [48]. The external field is endogenised to represent a smoothed moving average of the past state variable. This model captures in a simple set-up the interplay between instantaneous social imitation and past trends in social coordinations. We show the existence of a rich set of bifurcations as a function of the two parameters quantifying the relative importance of instantaneous versus past social opinions on the formation of the next value of the state variable. Moreover, we present thorough analysis of chaotic behaviour, which is exhibited in certain parameter regimes. Finally, we examine several transitions through bifurcation curves and study how they could be understood as specific market scenarios. We find that the amplitude of the corrections needed to recover from a crisis and to push the system back to "normal" is often significantly larger than the strength of the causes that led to the crisis itself.

This chapter is based on the article [*Damian Smug, Didier Sornette and Peter Ashwin.* ***"A Generalized 2D-Dynamical Mean-Field Ising Model with a Rich Set of Bifurcations (Inspired and Applied to Financial Crises)"*** *(2018). International Journal of Bifurcation and Chaos 28(4)]*.

4.1 Introduction

The Ising model and its mean-field version have a time-honored history in economics, sociology and finance, since its introduction as a mathematical model of ferromagnetism in statistical mechanics in 1920. Rather than magnetic spins related via Heisenberg interactions, the spins represent agents who have several options and decide to adopt one of them according to a combination of inputs involving their own idiosyncratic judgments (akin to thermal noise in physics), external news (similar to the external magnetic field) and social influences (analogous to the spin-spin exchange interaction). A large set of economic models can be mapped onto various versions of the Ising model to account for social influence in individual decisions. And the Ising model is one of the simplest models describing the competition between the ordering force of imitation or contagion and the disordering impact of private information or idiosyncratic noise. It is sufficiently rich to exhibit complex behaviours, such as phase transitions (bifurcations) and spontaneous symmetry breaking [86]. Since decision making and social interactions are two of the most important ingredients of social organisation, it is thus natural that the Ising model and its extensions to understand social organisation have blossomed over many decades (see e.g. [55, 87–101]).

Motivated by its applications to financial markets, we study an extended version of the dynamical mean-field equation of the Ising model in which the external (magnetic or news) field is endogenised to represent a smoothed moving average of the past state variable. This new model stands for a simplification of the interplay between instantaneous social imitation and past trends in social coordinations [102–105]. We show the existence of a rich set of bifurcations as a function of the two parameters quantifying the relative importance of immediate versus past social opinions on the formation of the next value of the state variable. Moreover, we identify where one can find chaos in the 3-D parameter space. Finally, we explore how the parameter shifts through certain bifurcation curves lead to variations in the behaviour of the system.

The chapter is organised as follows. The next section recalls the equation and main properties of the standard mean-field Ising model. Section 4.3 introduces the extended mean-field Ising model, which takes the form of two coupled discrete equations. In Sec. 4.4, we analyse bifurcations in the extended

system and, in Sec. 4.5, we compare the behaviour to the original 1-D system. Section 4.6 presents where one can find chaotic behaviour in the extended system. Section 4.7 covers certain scenarios of market passages through when parameters are change from one regime to another. Section 4.8 concludes.

4.2 Dynamical version of the standard mean-field Ising model

The standard mean-field equation of the Ising model can be written as

$$s = \tanh[\beta(s + H)]\,, \tag{4.1}$$

where s is the the average state variable (mean spin or magnetisation) of a given representative agent and H is the external influence (magnetic field). In financial applications, s can represent the traders' opinions whether to buy or sell and H is the impact of incoming news on their decisions. Parameter β quantifies the strength of the social imitation between agents (or, originally, the inverse temperature). Expression (4.1) describes the value of the average opinion s as being determined by the sum of the external influence H and of an effective impact exerted by the other surrounding agents, themselves adopting on average the same opinion s. The average state variable s is thus the solution of the implicit Equation (4.1), which has two control parameters β and H.

In a dynamical context, one can generalise Eq. (4.1) into a recurrence equation describing how the collective opinion evolves, when influenced by external news and its past state [48]:

$$s_{t+1} = \tanh[\beta(s_t + H)]\,, \tag{4.2}$$

Then, the fixed points of the map (4.2) are solutions of the implicit Equation (4.1). Fig. 4.1 presents how the fixed points of the map (4.2) vary when the parameters H and β change. In the symmetric case for $H = 0$ (Fig. 4.1A and Fig. 4.1B), there is a pitchfork bifurcation at $\beta = 1$, hence, when the system passes that point, a symmetry breaking occurs (assuming tiny noise in the system or slightly asymmetric initial conditions). However, the pitchfork bifurcation is structurally unstable with respect to the second control parameter H: for non-zero H, saddle-

node bifurcations occur instead (see Fig. 4.1C and Fig. 4.1D). The system has thus always either one or three fixed points. In the latter situation, two out of three fixed points are always stable and for $\beta = 1$ and $H = 0$ one can observe a cusp (Fig. 4.1E).

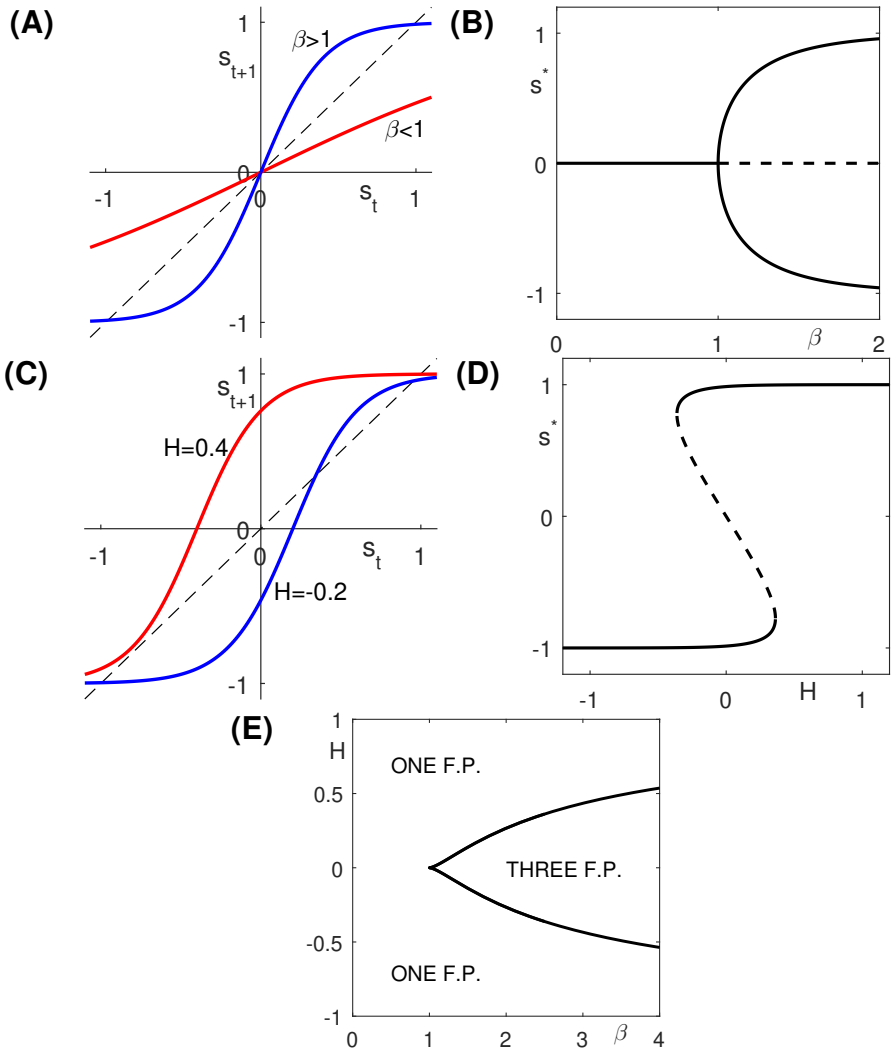

Figure 4.1: The map (4.2) $s_{t+1} = \tanh[\beta(s_t + H)]$ and its bifurcation diagrams for different values of the coupling strength β and external field H. (A) $H = 0$. Depending on β the shape of the map changes. Higher values of β increase the curvature of the map giving birth to two new fixed points at $\beta = 1$. The schematic curves are plotted for $\beta = 0.5$ (red) and $\beta = 2.5$ (blue). (B) Bifurcation diagram for $H = 0$ with a pitchfork bifurcation at $\beta = 1$. (C) $\beta = 2.5$. Depending on H the function is moved horizontally. For $\beta > 1$ such a shift can make some of the fixed points disappear in a saddle-node bifurcation. The curves are plotted for $H = -0.2$ (blue) and $H = 0.4$ (red). (D) Bifurcation diagram for $\beta = 2.5$. For a set of parameters there are three fixed points, but if the external field is too strong (in absolute value), two of the fixed points disappear in a saddle-node bifurcation. (E) Bifurcations in two-parameter plane. For $H = 0$ and $\beta = 1$ there is a cusp.

4.3 Extended mean-field Ising model

The map (4.2) is generalised by introducing a dynamics on the field H. In the standard model (4.2) H is considered to be exogenous, and is taken to represent the influence of outside news on the opinion or decision $s(t)$ of the typical agent. Motivated by models of financial price dynamics [48, 103], we propose to interpret H as a measure of momentum of the opinion dynamics. To reduce the dynamics to the arguably simplest model without the need for specifying the price evolution, one can consider that the opinion dynamics momentum is an approximate proxy for the price momentum included in the asset price dynamics of Ref. [103]. Let us recall that the logic of the initial model [103] is that so-called noise traders or technical analysts come to their investment decisions based on the information they gather from the opinion of their fellow noise traders and on their measure of the strength of the price trends. Trend-following or momentum investing is indeed a widely used class of investment strategies (see e.g. [106–108]). The influence of the decisions of other investors is captured by the term βs_t in Eq. (4.2). The momentum of the social opinion mirroring the trend of the price is embodied in the H term, which is assumed to be given by the following auto-regressive dynamics

$$H_{t+1} = \theta \cdot H_t + (1-\theta) \cdot s_t \ , \quad \text{where } \theta \in [0,1) \ . \tag{4.3}$$

Equation (4.3) defines H_t as the exponential moving average of approximately $n_\theta \simeq 1/(1-\theta)$ previous opinion states $\{s_{t-1}, s_{t-2}, ..., s_{t-n_\theta}\}$. For $\theta = 0$, Eq. (4.3) gives $H_{t+1} = s_t$, corresponding to a one-step memory. For $\theta \to 1^-$, the memory becomes infinite (with $H_{t+1} = H_t = H_0$) and the initial momentum value H_0 is always remembered.

Putting Eq. (4.3) together with Eq. (4.2) yields the dynamical system that we study in this chapter, namely

$$\begin{cases} s_{t+1} = \tanh(a \cdot s_t + b \cdot H_t) \\ H_{t+1} = \theta \cdot H_t + (1-\theta) s_t \end{cases} , \tag{4.4}$$

where s_t is the opinion (positive – buy, negative – sell) of the representative investor and H_t is its momentum. For $\theta = 0$, this system reduces to the dynamical mean-field Ising model (4.2) for $a = b = \beta$. For notational convenience, we will

refer to the 2D-map (4.4) as M, such that $\{s_{t+1}, H_{t+1}\} = M(\{s_t, H_t\})$.

In the standard mean-field equation (4.1), and by extension in the map (4.2), the parameters a and b are usually taken positive, corresponding respectively to so-called 'ferromagnetic' interactions (or positive feedback and imitation in the social context) and a positive organising effect of the external influence H. Negative values of a should not be interpreted as 'antiferromagnetic' interactions, since the later refer to a propensity to take a spin value opposite to that of the neighbour, which is different from a tendency to take the sign at the next time step that is the opposite of the sign at the previous time step. Instead, a negative value of a in Eq. (4.4) can be interpreted as a contrarian behaviour tending to correct at the next time step what can be perceived as a dangerous consensus. Such a mechanism was identified and explored by Corcos et al. [49] in a simpler 1D-map describing the proportion of 'bullish' agents in the population of investors. The rational for negative values of a is thus that investors may become worried when the consensus is too large, which may signal an exuberant unsustainable bubble. In response, these investors may decide to become contrarians and change their decision. If the representative agent adopts this stance, this will give oscillatory dynamics as well as deterministically chaotic behaviours, as we document in details below. Similarly, negative values of parameter b can be rationalised by such a contrarian response, but now built on a longer time scale according to the sensitivity to a growing trend.

4.4 Bifurcations for fixed θ

Let us explore the transitions that can be observed in the system (4.4) for certain fixed values of $0 < \theta < 1$. The Jacobian J and its eigenvalues λ_1 and λ_2 are

$$J = \begin{bmatrix} a & b \\ 1-\theta & \theta \end{bmatrix} \tag{4.5}$$

and

$$\lambda_{1,2} = \frac{a + \theta \pm \sqrt{(a-\theta)^2 + 4b(1-\theta)}}{2}. \tag{4.6}$$

4.4.1 Codimension-one bifurcations

The following bifurcations of codimension-one can be classified.

1. Bifurcations of the fixed point $(0, 0)$:

   - A pitchfork bifurcation occurs when one of the eigenvalues is equal to 1 (marked with the black solid line in the two-parameter bifurcation diagram in Fig. 4.2 and with the black surface in Fig. 4.3). The bifurcation occurs for a obeying the following dependence as a function of b and θ:

   $$a(b, \theta) = -b + 1 \,. \tag{4.7}$$

   - Period doubling (flip) occurs when one of the eigenvalues is equal to -1 (marked as the red solid line in the two-parameter bifurcation diagram in Fig. 4.2 and as the red surface in Fig. 4.3). The bifurcation occurs for a obeying the following dependence as a function of b and θ:

   $$a(b, \theta) = b\frac{1-\theta}{1+\theta} - 1 \,. \tag{4.8}$$

   - Neimark-Sacker bifurcation occurs when both eigenvalues lie on the unit circle and have equal real parts (marked as a green solid line below the black one in Fig. 4.2 and with the green surface in Fig. 4.3). The bifurcation occurs for a obeying the following dependence as a function of b and θ:

   $$a(b, \theta) = \frac{1 + b(1-\theta)}{\theta} \,. \tag{4.9}$$

2. Bifurcations of non-zero fixed points (there is no available analytical expression):

   - Period doubling (as previously; marked with light blue line in Fig. 4.2).
   - Neimark-Sacker bifurcation (as previously; marked with green solid line above the black one in Fig. 4.2).

3. Bifurcations of period-2 fixed points (no explicit analytical expression):

   - Pitchfork bifurcation occurs when the period-2 fixed point has one eigenvalue equal to 1 under the twice iterated map $M(M(\cdot))$. It is mar-

ked with the blue solid line in the two-parameter bifurcation diagrams (Fig. 4.2).

- Neimark-Sacker bifurcation (as previously but for the second iterate of the map M, namely $M(M(\cdot))$).

Figure 4.4 presents bifurcation diagrams for one value of $\theta = 0.99$ and three different values of b, namely 3, 1 and -1. In all the cases for large values of a there are stable non-trivial fixed points (black solid) and, for small values of a, there are stable period 2 points (red solid). Depending on b, the transition between those states occurs in a variety of ways. For $b = 3$ (Fig. 4.4A) while varying a, the following bifurcations occur (order from left to right): pitchfork giving rise to two new unstable fixed points; period doubling of unstable fixed points; pitchfork of period 2 fixed points; period doubling of unstable trivial fixed point. The region of bistability between flipping (jumping from one to another period 2 fixed point) and non-zero fixed points is shown in gray shade. Decreasing b to 1 (Fig. 4.4B) shifts linearly the pitchfork bifurcation to the right in terms of a (see Eq. (4.7)), whereas the flip remains practically in the same position ($\frac{1-\theta}{1+\theta} \approx 0$ in Eq. (4.8)). This leads to 'untying' the characteristic 8-shaped curve and leaves only bifurcations of the trivial fixed point. For b becoming sufficiently negative (here: $b = -1$ in Fig. 4.4C), additional phenomena occur. At $a \approx 1$, there is a Neimark-Sacker bifurcation that destabilises the trivial fixed point giving rise to stable oscillations. The oscillations disappear due to a sequence of bifurcations in a tiny region in parameter space (for more information see: Chapter 7 in [15]). Bistability can be found there as well, but the region is so narrow as to be invisible. Interestingly, the switches between attractors here can be considered as Critical Transitions, however it is not clearly visible in Fig. 4.4. This is due to the fact that the system's reaction is slower than the variation of parameter.

4.4.2 Codimension-two bifurcations

For the two-dimensional discrete system (4.4), codimension-two bifurcations occur if $|\lambda_1| = |\lambda_2| = 1$. This implies that there are three possible bifurcations and all of them can be parametrised in terms of θ:

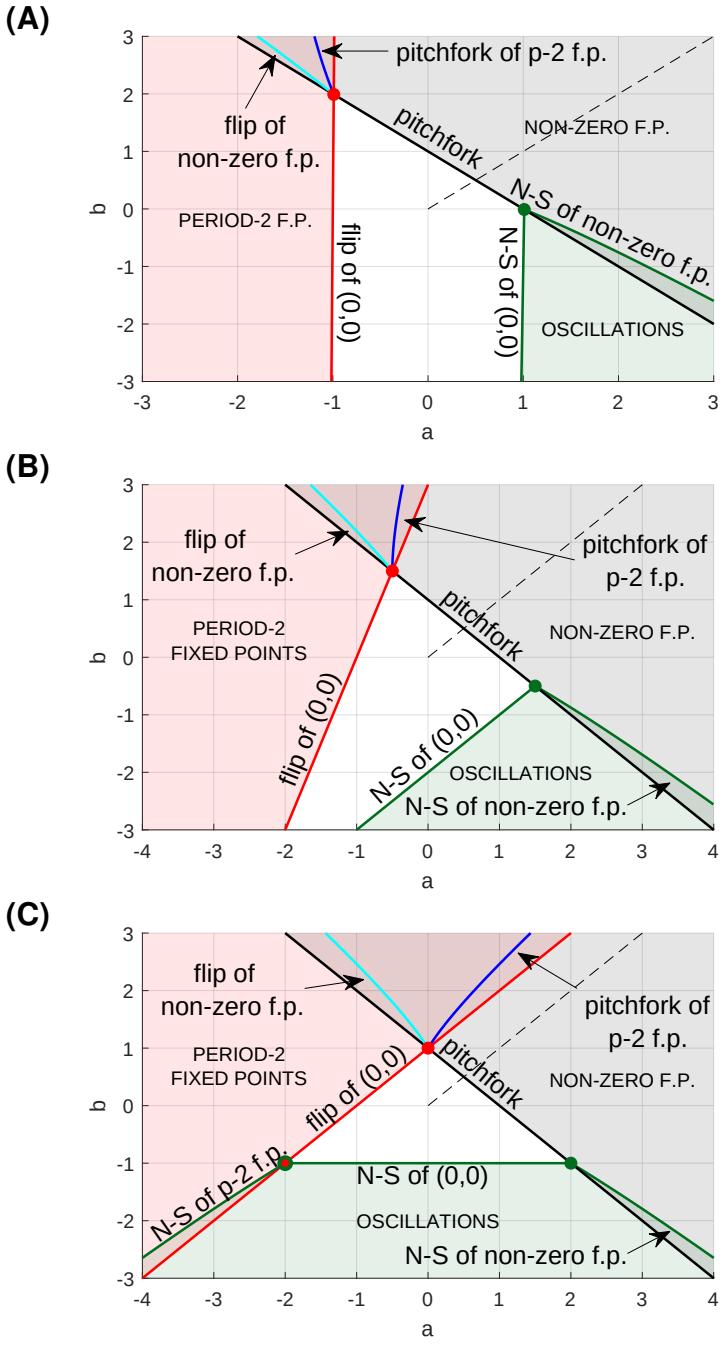

Figure 4.2: Bifurcation diagrams of system (4.4) in the two-parameter plane $\{a, b\}$ for three fixed values of θ. (A) $\theta = 0.99$, (B) $\theta = 0.50$, (C) $\theta = 0.00$. Besides all the bifurcation curves, the black dashed line represent the case $a = b = \beta \geq 0$, corresponding to the original 1D-map (4.2). Similarly to the situation shown in Fig. 4.1B, a pitchfork bifurcation also occurs here, but for $\beta = 0.5$ (instead of $\beta = 1$), due to the contribution of the momentum term in (4.4). Scanning all possible values of a and b, a variety of behaviours can be classified. All the diagrams for different values of θ are qualitatively similar. As can be deduced from Eq. (4.7), θ does not influence the position of the pitchfork bifurcations at all. The other two bifurcations (period doubling – red, Neimark-Sacker – green) of the trivial fixed points move as θ varies. For the singular case of $\theta = 1$, these bifurcation lines become parallel. The domain in white represents the existence of only one attractor, which is the trivial equilibrium.

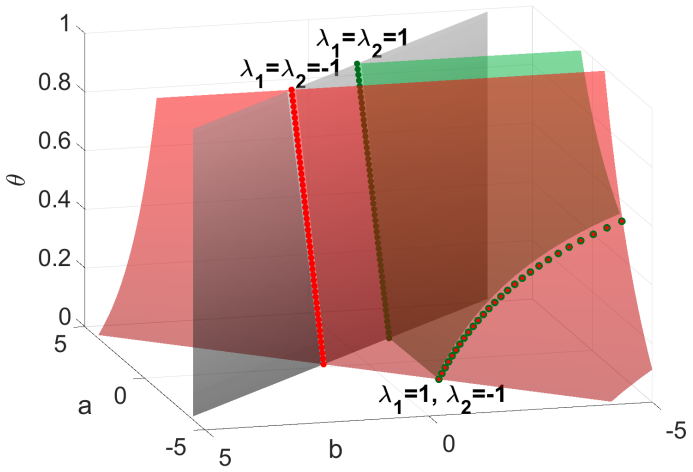

Figure 4.3: Scan of the values of θ for codimension-one and codimension-two bifurcations of the fixed point $(0, 0)$. The surfaces in black, red and green correspond to the boundaries for the pitchfork, flip and Neimark-Sacker bifurcatioins, respectively.

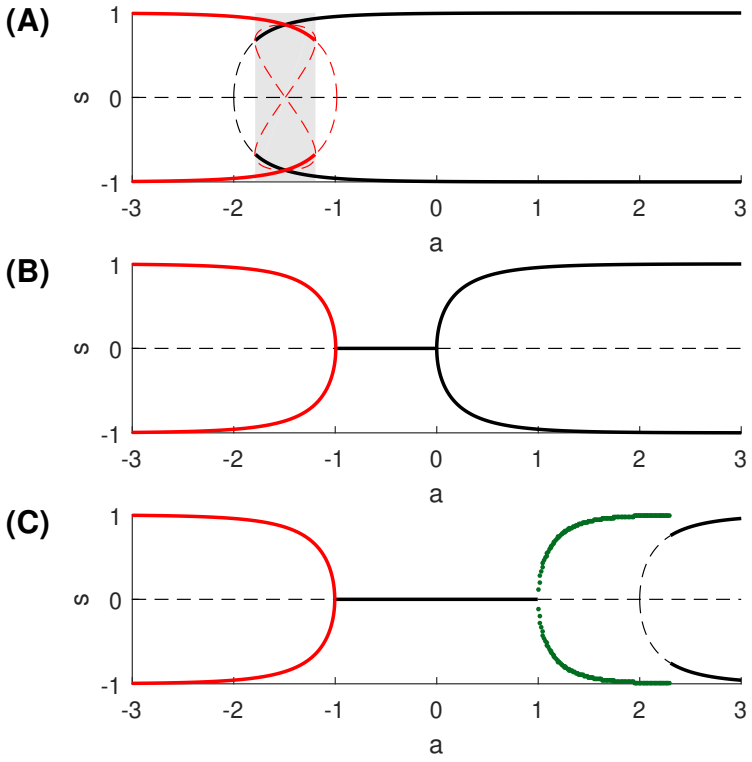

Figure 4.4: Phase-parameter bifurcation diagrams for $\theta = 0.99$. The solid lines stand for stable points and dashed for unstable. The colours black, red and green represent fixed points, period-2 fixed points and oscillatory or quasi-oscillatory behaviour, respectively. (A) $b = 3$, (B) $b = 1$ and (C) $b = -1$.

1. $\lambda_1 = \lambda_2 = 1$ (pitchfork + Neimark-Sacker; green points in Fig. 4.3):

$$a = -\theta + 2, \qquad b = \theta - 1\,. \tag{4.10}$$

2. $\lambda_1 = 1$ and $\lambda_2 = -1$ (pitchfork + flip; red points in Fig. 4.3):

$$a = -\theta, \qquad b = \theta + 1\,. \tag{4.11}$$

3. $\lambda_1 = \lambda_2 = -1$ (flip + Neimark-Sacker; green points with red face colour in Fig. 4.3):

$$a = -\theta - 2, \qquad b = \frac{(\theta+1)^2}{\theta - 1}\,. \tag{4.12}$$

We present the curves where codimension-two bifurcations occur as bold points both in Fig. 4.2 and also in the 3-dimensional plane $\{a, b, \theta\}$ in Fig. 4.3. Figure 4.3 visualises additionally codimension-one bifurcations for which the analytical form exists. One can notice that for $\theta = 0$ codimension-two bifurcations occur one close to each other, whereas for $\theta \to 1$ one of those bifurcations is shifted towards infinity.

4.5 Comparison between extended and original mean-field Ising models

The crucial question to be answered at this point is how the behaviour of the extended system actually varies from what was observed in the original Ising mean-field model. If $a = b = \beta \geq 0$ the 2-dimensional system, independently of θ, exhibits a bifurcation at $\beta = 0.5$. In contrast to the system (4.2) and its pitchfork in $\beta = 1$, adding the equation for H_{t+1} in (4.4) makes the bifurcation occur for a value β twice smaller. This is caused by the fact that, around the stable fixed point $(0, 0)$, we can use the approximation $s_t \approx H_t$ and retrieve $s_{t+1} = \tanh[2\beta(s_t + 0)]$.

If the system (4.4) is constrained to the physical interpretation of the parameters, i.e. $a > 0$ and $b > 0$, and if the memory parameter θ is less than 1, there always exists a region where the period-2 solutions arise. This follows from Eq. (4.8): $a(b, \theta) = b\frac{1-\theta}{1+\theta} - 1$, which governs the position of the flip bifurcation. Obviously, for any given positive $\theta < 1$, the term $\frac{1-\theta}{1+\theta}$ is positive as well. Therefore,

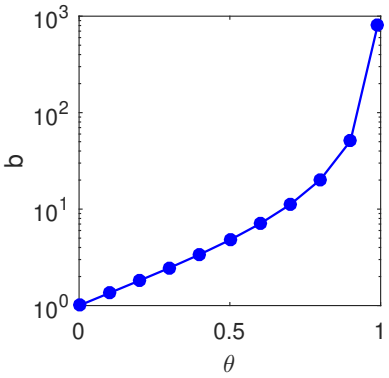

Figure 4.5: Value of b for $a = 0$ on the dark blue curve representing pitchfork bifurcations to period-2 fixed points depending on θ. The selected points represent where the bistability occurs in the regime $b > 0$. The diagram says that for every $\theta < 1$ there occurs bistability in the physically justified region $(a > 0, b > 0)$. Of course, for θ near 1, this region might not be accessible as b needs to be very large. For lower values of θ, the parameter b decreases gradually to 0. This means that the lower the memory coefficient, the lower parameter b needs to be to obtain bistability in the physical region of positive parameters a and b.

one can find a sufficiently large b such that $b\frac{1-\theta}{1+\theta} > 1$, hence there always will exist $a > 0$ where period-2 points exist. Nevertheless, this does not mean that those periodic points are directly observable as they are not stable until the pitchfork of period-2 point occurs. This bifurcation is marked with dark blue colour in Fig. 4.2 but also occurs at the right boundary of the shaded interval in Fig. 4.4A. When the period-2 points stabilise, one can observe that, for different initial conditions, the system might behave differently – it might either converge to a single fixed point (positive or negative one) or to a flipping behaviour (see Figs. 4.6A and 4.6B).

Numerical simulations show that, even for θ very close to 1, the curve of period-2 fixed point pitchfork bifurcation (dark blue line in Fig. 4.2) crosses the line $a = 0$. We present in Fig. 4.5 the values of b when a crosses 0 for certain values of θ.

To sum up what was stated above, we would like to underline that, for different values of $a > 0$ and $b > 0$, only three types of attractors are possible:

- trivial equilibrium,
- non-trivial fixed point (positive and negative),
- period-2 fixed points.

If we allow a and b to take values from the whole $\mathbb{R}^2$, the system may exhibit a much broader variety of behaviours. There is for instance a set of parameters

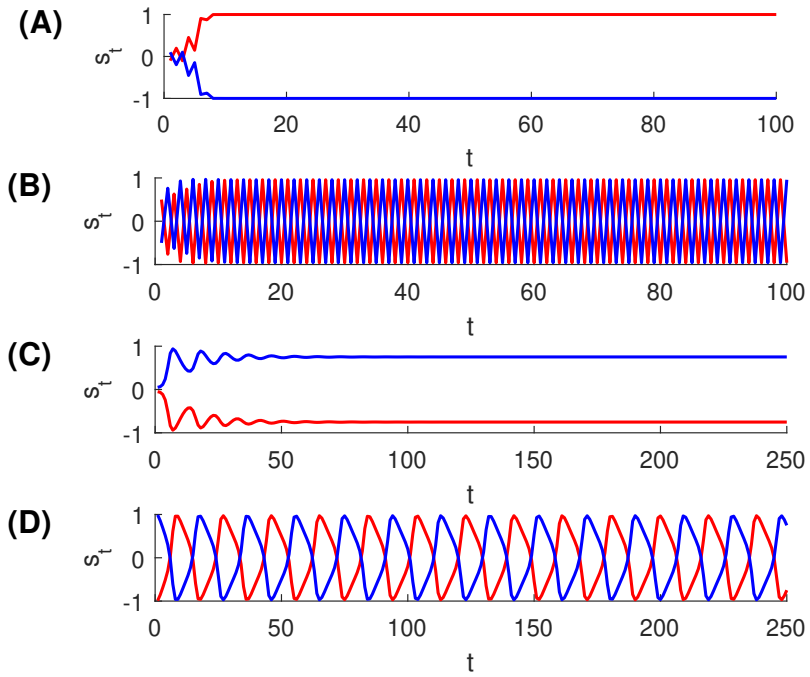

Figure 4.6: Time series for different initial conditions and $\theta = 0$. (A) and (B) $a = 1$, $b = 3$. Initial conditions: (A) in red: $s_0 = -0.1$ and $H_0 = 0.1$, in blue: $s_0 = 0.1$ and $H_0 = -0.1$, (B) in red: $s_0 = 0.5$ and $H_0 = -0.5$, in blue: $s_0 = -0.5$ and $H_0 = 0.5$. (C) and (D) $a = 3.3$, $b = -2$. Initial conditions: (C) in red: $s_0 = -0.05$ and $H_0 = -0.05$, in blue: $s_0 = 0.05$ and $H_0 = 0.05$, (D) in red: $s_0 = -0.99$ and $H_0 = -0.99$, in blue: $s_0 = 0.99$ and $H_0 = 0.99$.

for which oscillations occur (see the green filled area in Fig. 4.2). The region of existence of oscillations intersects with the region where the non-trivial stable solutions exist (see Figs. 4.6C and 4.6D). We do not explore it further here, but some of the oscillations can be quasi-periodic, while other stay strictly periodic. We have observed periodic behaviour for periods between 3 and 8 (we assume that higher periodicity is also possible), and even chaotic behaviour. The latter is analysed further in Sec. 4.6.

4.6 Chaos

This section presents several tests to show where in parameter space chaos exists and what kind of attractors can be expected in system (4.4).

In order to better understand the bifurcations present in the system, we show scans of the largest Lyapunov exponent for several values of θ, computed by examining the growth of solutions of the variational equation for a typical initial condition and perturbation vector. The result is presented in Fig. 4.7: blue denotes negative and red denotes positive exponents. For $a > 0$ and $b > 0$ we find no

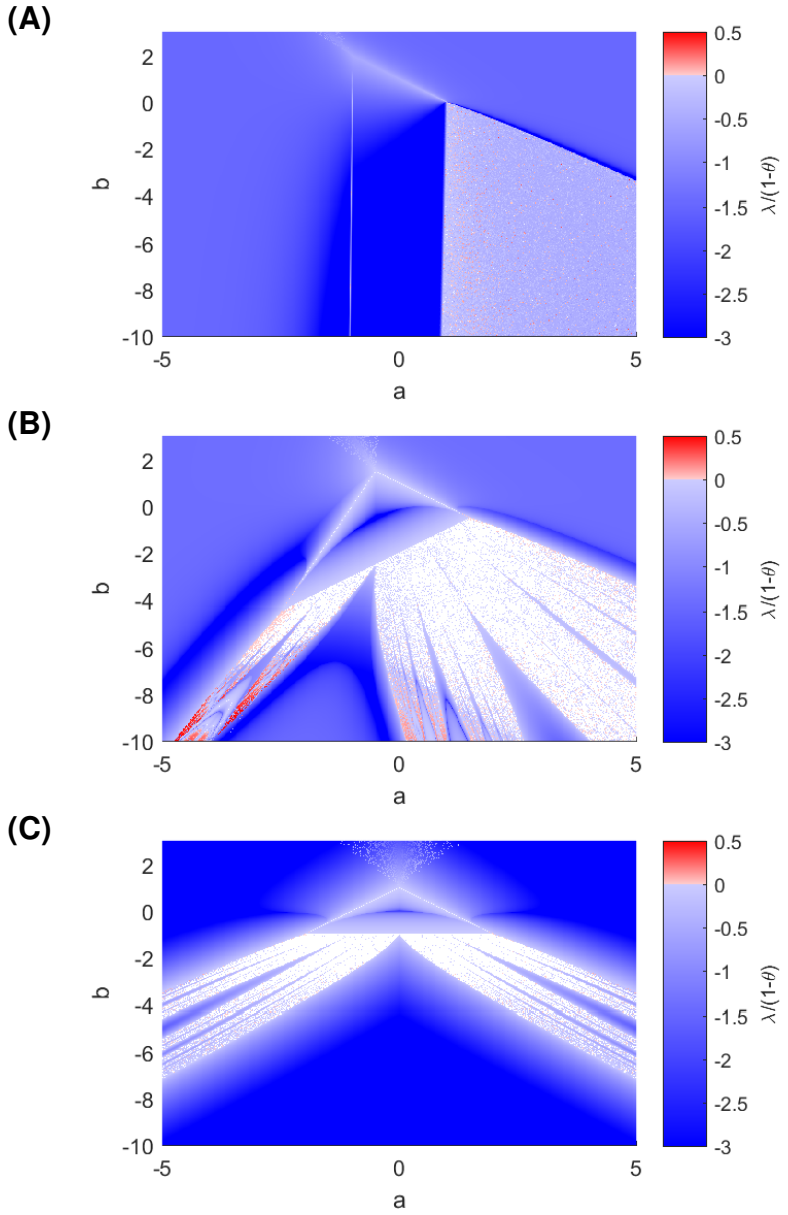

Figure 4.7: Largest Lyapunov exponent, rescaled by $\frac{1}{1-\theta}$. (A) $\theta = 0.99$, (B) $\theta = 0.50$ and (C) $\theta = 0.00$. The parameters are chosen so to correspond with Fig. 4.2. For $\theta = 0.99$ (panel (A)) there is no region with chaotic behaviour, the sporadic light red dots in the bottom right-hand side of the plot are caused by quasi-periodic behaviour and cannot be interpreted as chaos. In panel (B) one can observe a region with potentially chaotic behaviour, moreover, in panels (B) and (C) there are characteristic Arnold tongues corresponding to period locking.

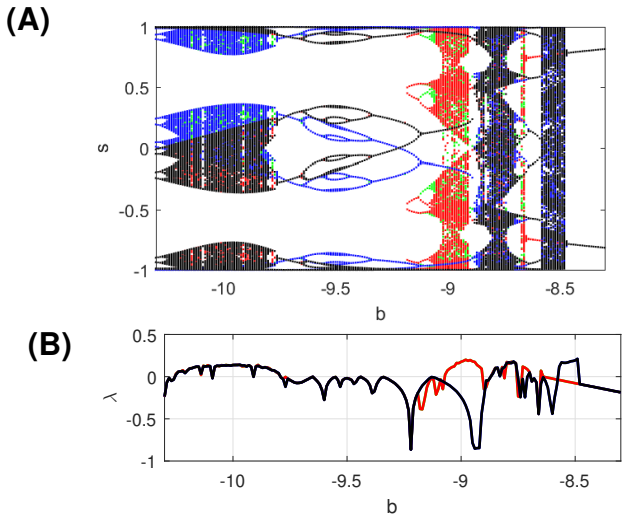

Figure 4.8: Bifurcation diagrams illustrating multistability and chaotic behaviour in the system (4.4). For both panels, the parameters are $a = -4.17$ and $\theta = 0.5$. (A) Bifurcation diagram of system (4.4). In red and blue are marked attractors to which the system converges when increasing b and initiated in $(-0.5, 0.5)$ and in $(0.5, -0.5)$ respectively. Similarly, for decreasing b, we use green and red colours. One can deduce that chaotic behaviour is possible within several intervals (b around -10, around -8.75 and around -8.55). For other values of b, the system converges to periodic or quasiperiodic oscillations. For $b = -9$, there are two period-3 orbits coexistent with a chaotic attractor, whereas for $b = -9.5$ one can observe two separated period-24 orbits. In between, there is a triple cascade of period-doubling bifurcations. (B) The largest of the two Lyapunov exponents for the blue attractor in (A). Occurences of Lyapunov exponent $\lambda > 0$ confirm that one can expect chaos for $b \approx -10$, $b \approx -9$, $b \approx -8.77$ and for $b \approx -8.53$.

chaos, but for some negative values of a or b, more interesting behaviours occur. The diagrams in Fig. 4.7 clearly show many features of the bifurcation diagrams in Fig. 4.2 – in particular the lines of bifurcation of stable attractors. The bifurcations of unstable attractors are however not visible. Note that in order to compensate for the slow dynamics as $\theta \to 1$, we normalise the exponent by $(1 - \theta)$.

In Fig. 4.7A ($\theta = 0.99$) the slightly visible light red dots scattered in the right part of the diagram correspond to quasi-periodic behaviour, much more iterations taken into computation of Lyapunov exponent will allow the dots to actually vanish. For $\theta = 0.00$ (Fig. 4.7C), we have been unable to identify any trace of chaos within the selected parameter values. Analysis of Fig. 4.7B ($\theta = 0.5$) suggests that the parameter domain $a \in (-5, -3)$ and $b \in (-10, -8)$ may be the most favorable to find chaotic behaviour. Therefore, we explore this region more thoroughly.

For example, let us fix $a = -4.17$ and $\theta = 0.5$. These parameters are chosen so as to obtain several regions of chaotic behaviour while scanning b. Figure 4.8A illustrates the attractors as the s component against parameter b. To generate this kind of diagram, we start with two initial conditions $\{-0.5, 0.5\}$ and $\{0.5, -0.5\}$

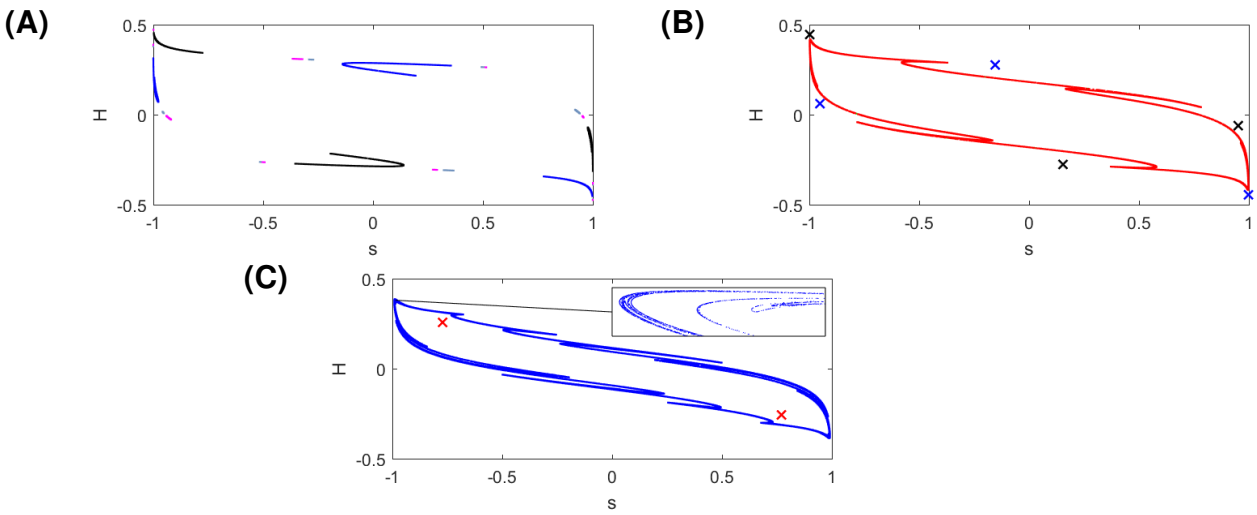

Figure 4.9: Examples of chaotic attractors for $a = -4.17$ and $\theta = 0.5$: (A) shows four stable chaotic attractors for $b = -10$, (B) shows a single chaotic attractor (red) stable with two period-three orbits (blue, black) for $b = -9$, and (C) shows bistability between a single chaotic (blue) and periodic (red) attractor for $b = -8.53$. The colours correspond to the colours in Fig. 4.8A. Observe the characteristic folding of the chaotic attractors.

for $b = -10.3$ and iterate the system 400 times. Then, we discard the first one hundred points and plot the last 300 points. For the next value of b, namely -10.29, we use as the initial condition the final state of the system after those 400 iterates. The procedure is repeated until $b = -8.3$. The attractors obtained in this scheme are plotted in black and blue. Moreover, we perform identically, starting with the same initial conditions and decreasing b from -8.3 to -10.3. The attractors are then plotted in green and red. It is visible that changing the direction of the scan helps to discover different attractors and the systems is multi-stable or at least bistable in the vast part of the diagram – up to $b \approx -8.5$.

For all the attractors, we investigate again the Lyapunov exponent to identify where exactly the chaotic attractors can be expected (see Fig. 4.8B). Indeed, there are several regions with a positive exponent. We select some of them and plot the attractors in phase space $\{s, H\}$ in Fig. 4.9. The methodology explained above obviously does not provide all the attractors, what can be instantly spotted in Fig. 4.9A, where two minor attractors are marked.

The attractors in Fig. 4.9B and Fig. 4.9C are more interesting. When zoomed-in on the tip of the attractor, we can clearly see the characteristic chaotic folding. This allows us to conclude that, indeed, chaotic behaviour is possible in the dynamics of noise traders' opinion.

To provide basic intuitions about the system's behaviour in the chaotic regi-

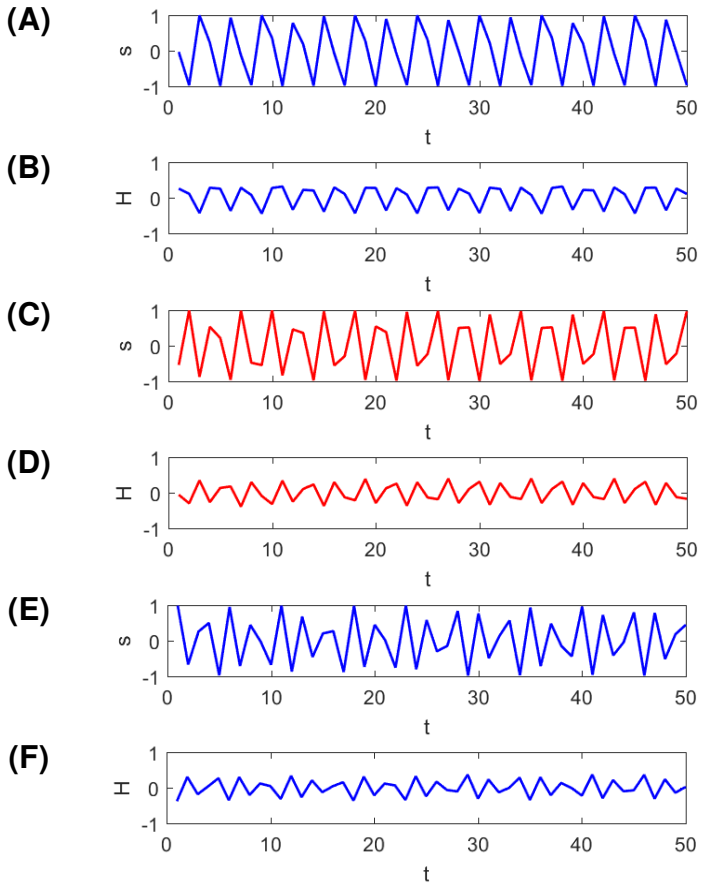

Figure 4.10: Chaotic trajectories corresponding to the attractors presented in Fig. 4.9. (A) s variable taken in the blue region in Fig. 4.9A, (B) H variable taken in the blue region in Fig. 4.9A, (C) s variable taken in the blue region in Fig. 4.9B, (D) H variable taken in the blue region in Fig. 4.9B, (E) s variable taken in the blue region in Fig. 4.9C, (F) H variable taken in the blue region in Fig. 4.9C.

mes, we include Fig. 4.10 with time series of s and H for some of the attractors presented in Fig. 4.9. The colours of the time series correspond to the colours denoting the chaotic attractors.

4.7 Market passages through a bifurcation

This section presents how parameter changes can influence the noise traders' behaviour. We analyse four scenarios of parameter shifts across certain bifurcation curves. To keep it simple, we vary only parameter a fixing b and θ. One can interpret the linearly shifted parameter as an extension of the system (4.4) taking

the form:

$$\begin{cases} s_{t+1} = \tanh(a_t \cdot s_t + b \cdot H_t) \\ H_{t+1} = \theta \cdot H_t + (1-\theta) s_t \\ a_{t+1} = a_t + k \end{cases}, \tag{4.13}$$

where k is a fixed value.

Let us analyse four scenarios:

1. **Market passage through flip and Neimark-Sacker bifurcation (Fig. 4.11A, $k = 0.04$).** This scenario begins with a situation where the traders have mixed stable opinions whose average is $s_t = 0$. Let us then pick an average memory length ($\theta = 0.5$) and contrarian attitudes ($a = -1$ and $b = -2$) representing for instance mindsets after a recent financial draw-down. This is a regime with only one stable state. If the market conditions change in terms of parameter a (for instance to a more contrarian stance – $a = -3$, or to a highly imitating behaviour – $a = 3$), the traders' opinions are destabilised and the variables start to flip or oscillate. Two important observations can be made at this point:

   - if the market conditions change because of reasons which are difficult to track, it might be not possible to determine which way the parameter a should be changed to revert to the original state;
   - a transition back to the nominal state $s_t = 0$ requires a larger shift of a than the original one. For instance, if a shift occurs from a fixed point with $a = 1$ to $a = 3$ (blue trajectory), oscillations appear. A backward transition to a state without oscillations (red trajectory) requires shifting the parameter much further than just to 1, namely as far as $a = -1$. A similar behaviour exists when decreasing a from $a = -2$ to $a = -3$ (red trajectory) and then increasing a (blue trajectory) to -1. This might be confused with a hysteresis loop, but this is actually a bifurcation delay that arises often in fast-slow dynamical systems (see for instance [109] or [110]).

2. **Market passage to a chaotic regime (Fig. 4.11B, $k = 0.04$).** When the system is in a highly contrarian flipping state ($\theta = 0.5$, $a = -4$, $b = -6$),

certain parameter changes might lead to a transition to a chaotic regime. Then, instead of switching opinions at every step, the behaviour of traders cannot be predicted, which might lead to an undesired market behaviour. Nevertheless, there is some remaining regularity in the sense that in the chaotic regime one can observe that the transition from a positive to a negative opinion state and vice versa occurs at least once per three steps. The bifurcation delay is not significant in this scenario, after 3-4 iterations when moving leftwards through bifurcation line the system retrieves its flipping behaviour.

3. **Market passage into the rapid oscillations regime (Fig. 4.11C, $k = 0.004$).** Similarly to the first scenario, the transition through a Neimark-Sacker bifurcation of the trivial fixed point exhibits a bifurcation delay. Moreover, the oscillations become very rapid and not symmetric (see Chapter 3 in [48]), which corresponds to large market price changes such as during bubbles and crashes. Decreasing parameter a can lead to accelerating oscillations (such as those described by the so-called log-periodic power law singularity (LPPLS) models presented for instance in [28, 61, 75, 76]). On the other hand, the system can pass through another Neimark-Sacker bifurcation (this time of non-zero fixed points) and stabilise on a non-trivial positive or negative fixed point. The way the system settles down on one of the fixed points is very sensitive to the current opinion value. This means that if the market opinion varies quickly it is prone to settle easily to either a bullish or a bearish market, depending not only on the parameter value a, but also on the transition time. This may lead to market unpredictability even if all of the parameters were known precisely.

4. **Switching through a bistable region (Fig. 4.11D, $k = 0.04$).** The last scenario we present is a passage across four bifurcation curves, but actually only two of them change the behaviour of the system. Those are the flip of non-zero fixed points and the pitchfork of period-2 fixed points. The region in the middle is bistable as in Fig. 4.4A. The behaviour of the system is in essence a mixture of three components: a) bifurcation delay as in scenario 1, b) sensitivity of settling down as in scenario 3, and c) hysteresis in response (see for instance the saddle-node case in [4]). Component c) is

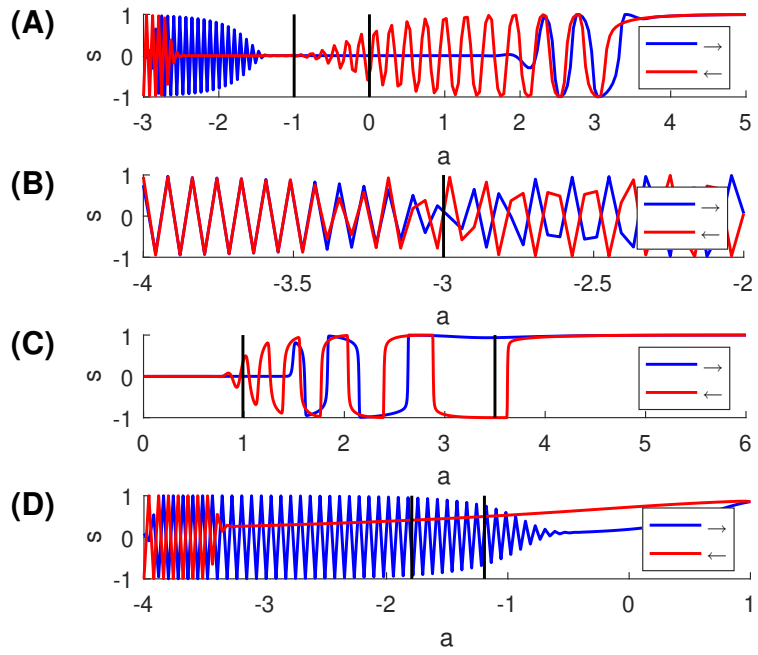

Figure 4.11: Linear passages through bifurcations as described by the system (4.13). Initial values are taken in the neighbourhood of an attractor corresponding to the parameter a given by the leftmost value in each diagram. Parameter a is increased at each time iteration by a certain fixed value k, leading to the dynamics for the order parameter represented by the blue curve. The red curve is generated by decreasing a from the rightmost value. (A) $\theta = 0.50$, $a \in [-3, 5]$, $b = -2$, $k = 0.04$, (B) $\theta = 0.50$, $a \in [-4, -2]$, $b = -6$, $k = 0.04$, (C) $\theta = 0.99$, $a \in [0, 6]$, $b = -2$, $k = 0.004$, (D) $\theta = 0.99$, $a \in [-3, 0]$, $b = 3$, $k = 0.04$. Black vertical lines represent where do the bifurcations occur.

caused by the existing bistability. Namely, for lower values of a, the system jumps up and down. After the second black line in Fig. 4.11D, it slowly converges to a fixed point. On the way back, it starts to flip very slowly when the system passes the left black line. This hysteresis in behaviour results in a much larger delay than observed in scenario 1. Also, if the system is on the fixed point in the bistable region and a is decreased far enough, in order to retrieve the fixed point, reverting the parameter to its original state might not be sufficient to suppress the flipping. This means that if there is a small change which destabilises the market, simply reverting the change might not be enough to stabilise the system again and thus much larger interventions might be needed.

4.8 Conclusions

We have introduced and analysed in details an extended two-dimensional dynamical version of the mean-field Ising model. Inspired by the dynamics of social

imitation in financial markets involving fast imitation and slower trend following, the traders' opinion dynamics is modelled as the interplay between instantaneous social imitation and past trends in social coordinations. The standard magnetic field in the Ising model is re-interpreted and endogenised as a smoothed moving average of the past state opinion variable.

We have shown the existence of a rich set of bifurcations as a function of the two parameters a and b quantifying the relative importance of instantaneous versus past social opinions on the formation of the next value of the state variable. The dependence as a function of a third parameter θ controlling the memory length over the past states has also been dissected. We have presented a thorough analysis of the existence of chaotic behaviour, present in certain parameter regimes. Finally, we have examined four scenarios in which a slow change of a control parameter induces transitions through bifurcation boundaries. These scenarios have been offered as possible simplified models of change of regimes in financial markets. One important lesson is that, due to the phenomenon of delayed bifurcations often associated with fast-slow dynamical systems as well as of possible hysteresis, the amplitude of the corrections needed to recover from a crisis and to push the system back to 'normal' may be significantly larger than the strength of the causes that led to the crisis itself. In other terms, this is a quantitative reminder that 'prevention is better than cure', at least in this conceptual model of financial market opinion dynamics.

Chapter 5

Modelling joint defaults of companies

In this chapter we present ideas on how to model the dynamics and joint collapses of companies (or financial institutions) and the contagion in financial networks through double-well potential dynamical systems with noise-induced Critical Transitions. We introduce several simple models in which the *health* of a company is described as the state of a particle in a double-well potential system. The stochastic shocks can push a company to the bankruptcy state and lead to further bankruptcy cascades. We involve the contagion between companies by adapting the shape of the potential landscape and thus making it easier to default given others defaulted shortly beforehand.

5.1 Introduction

The financial crisis of 2007-2008 highlighted the interdependence between institutions in financial networks, which can lead to shock propagation or contagion of financial problems. The crisis showed that the underlying financial network structure had not been fully understood. Institutions focused on independently minimising individual risks, however, many did not take into account that the assets which are not in their portfolios can also influence them in indirect ways [111]. For instance, if a British bank does not have any asset in the Spanish housing market, it does not mean they are resilient to a housing crisis in Spain. The cause of this susceptibility is that the assets owned by the British bank can be issued by

an agent who invests in Spanish markets. Thus, a company aiming to minimise idiosyncratic risks should not only watch if the issuers of the assets they own are diversified, but also should monitor the issuers of assets these issuers own. In short, a single player should observe a much broader part of the market than it may initially seem to be necessary and they might be susceptible to a contagion of bankruptcies which starts in a sector they do not have direct links to. Many studies showed that even though high connectedness of financial networks may enhance individual stability, at the same time it can allow quicker shock propagation making the whole system less stable – see for example [112–115].

Since the crisis of 2007-2008 the number of studies focussed on modelling the systemic risk and spread of defaults has increased dramatically. An early attempt to capture financial contagion can be traced back to Allen and Gale (2000) [116], who present a probability based model and conclude that highly connected markets are preferred from the perspective of individual robustness. Watts (2002) [117] showed that randomly induced cascades in highly connected networks are harder to predict and that sparse networks are as stable as their most connected nodes. Interestingly, during a crisis some of the nodes may become more central than they were earlier and this can make their bankruptcy unexpectedly more problematic than predicted beforehand [118]. Caccioli et al. [115] point out that in order to avoid crises there are three key objectives: understand, predict and control. The reference [115] argues that there is still not enough understanding of large financial systems.

In order to comprehend the problem of joint defaults we employ a continuous-time potential landscape model. Application of potential systems in finance has been performed for instance by Bouchaud and Cont [119], who modelled drawdowns as exponentially rare noise-induced transitions in a one-dimensional system with one stable and one unstable equilibrium. In their model the drawdowns were described by a particle escaping over the potential barrier. We try to capture companies' *health* a bit differently – by a potential system with two stable equilibria: the entirely healthy state and the bankrupt state. The general n-dimensional model is constructed as follows:

$$dx_n(t) = \left[f(x_n(t);\boldsymbol{p}) + h(x_n(t),\boldsymbol{x}(t);\boldsymbol{\beta})\right]dt + \sigma_n dW_n(t), \tag{5.1}$$

where x_n denotes the health of n-th agent and $f(x,p) = -\frac{\partial V(x,p)}{\partial x}$ stands for the dynamics in a quartic potential landscape V when no other agent is involved. Function h couples the state variables given the full variables vector $\boldsymbol{x} = (x_1, ..., x_n)$ and a coupling matrix $\boldsymbol{\beta} \in \mathbb{R}^{n\times n}$. The parameter vector $\boldsymbol{p}$ describes the curvature of the potential landscape as well as the height of the barrier that one needs to cross in order to default. In this framework the height of the barrier can be understood as the rating of a company – the lower it is, the easier to go bankrupt. For the sake of simplicity we keep the barrier height fixed in time and identical for all agents, however, it could follow a random discrete process – see an example of a discrete model of ratings during bankruptcy cascades in [120].

Ashwin et al. [121, 122] analysed a simple two-dimensional model which belongs to the family (5.1) with $h(x_1, \boldsymbol{x}, \boldsymbol{\beta}) = \beta(x_2 - x_1)$ and vice versa for x_2. In their model the two stable equilibria are described as the *quiescent* state (in our case: healthy state) and the *active* state (in our case: bankrupt state). In such a model with positive coupling ($\beta > 0$) if one of the particles tips from the quiescent to the active state, the other particle becomes more vulnerable to random shocks and thus it is more likely to tip as well. Depending on β there are three possible regimes of coupling: weak coupling, slow domino and fast domino. We explain what are the characteristics of these three regimes in Sec. 5.3.1. In all of the models we suggest the weak coupling and slow domino effect can be observed – see the phase portraits for the model given by Eq. (5.11) where we describe graphically the three regimes. In the models introduced in Sec. 5.3 fast domino can also occur.

A different approach to model joint defaults was presented in [123], where the company's default intensity follows a CIR process and can be identified with a mean-reversing particle in a single-well potential. The default occurs when the intensity integrated over time exceeds threshold that is exponentially distributed and different for each agent. At the time of default other (not defaulted) agents undergo a shock that increases their default intensity by certain fixed value. The mean reversal property forces a gradual decrease of the default intensity to the mean. We will formulate this model in Sec. 5.5 and treat it as a benchmark for our studies.

In this chapter we present a study of several models which are meant to capture joint collapses of coupled agents. We begin in Sec. 5.2 by formulating the

double-well system for a single company. Then, in Sec. 5.3 we introduce two simple models with linear and quadratic coupling. The drawback of these models is that an occurrence of a default affects others thereafter. This is not a realistic scenario, thus, in Sec. 5.4, we introduce a model where the contagion delay is captured by an additional response variable that allows recovery to a background default rate. In Sec. 5.5 we revisit a model by Giesecke et al. [123] and use it to benchmark our results. Finally, we summarise our results in Sec. 5.6.

5.2 Dynamics of a single company in the potential landscape

We model the behaviour of companies using an intuitive mathematical description of a potential landscape. In the uncoupled case we start from the following SDE:

$$dx(t) = f\left(x(t); \boldsymbol{p}\right) dt + F\left(x(t)\right) dW_t = -V'\left(x(t); \boldsymbol{p}\right) dt + \sigma dW_t\,, \tag{5.2}$$

where:

- $x(t)$ is the health of a company (can for instance be understood as $\frac{\text{Equity}}{\text{Assets}}$);
- σ is the noise strength;
- V stands for the function describing the potential landscape, which can be understood as summarising market conditions. We require two stable equilibria: the right-hand side well represents the *healthy state* whereas the left-hand side well denotes the *defaulted state* – see Fig. 5.1. The unstable equilibrium is called the *risky state*. In this formulation the transition to the left well can occur because of noise increments or due to the change of conditions **p** (i.e. after a saddle-node bifurcation of healthy state and risky state).

An exact form of the potential landscape parametrised with $\boldsymbol{p} = [H, \omega_r, \omega_h]$ is obtained assuming four conditions:

1. Without loss of generality, the defaulted state is assumed to be $x_d = 0$ and $V(x)$ has there a stationary point: $V(x_d) = V'(x_d) = 0$.

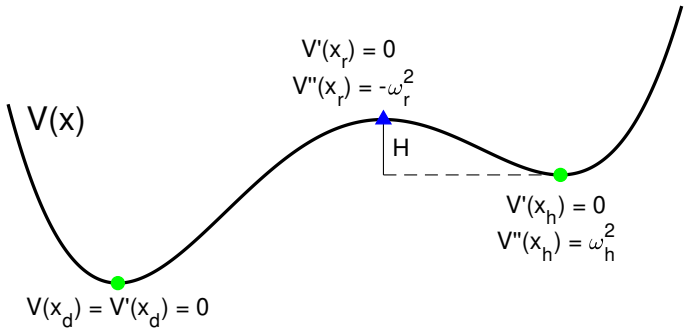

Figure 5.1: The potential landscape for a single company describing the four presupposed conditions. The healthy state is denoted by the residence in the right-hand side well whereas defaulting is equivalent to falling down to $x_d = 0$.

2. Two other equilibria (unstable risky state x_r and stable healthy state x_h) are parametrised by the curvatures $\omega_r^2 := -V''(x_r) > 0$ and $\omega_h^2 := V''(x_h) > 0$.

3. The barrier height between the risky and the healthy equilibria is given by the parameter $H := V(x_r) - V(x_h) > 0$.

4. The potential is polynomial of lowest possible order.

We assume that $x_d = 0$ is an absorbing boundary, i.e. if the health of a company decreases to x_d, it is treated as defaulted and will stay in x_d there forever.

The curvature ω_h^2 is interpreted as the rigidity of the economy which causes the business cycles to last on average 4 years, whereas ω_r^2 quantifies the resilience of a healthy company to perturbations. Barrier height H can be understood as quantification of rating category. In a multi-dimensional model the heterogeneous agents can be distinguished primarily by their rating and thus have different values of H.

In this chapter we analyse the phenomena that occur in the suggested models, we do not perform any parameter tuning. Nevertheless, the construction of V allows to find the parameter values given the frequencies of defaults observed in real data. A comprehensive report of occurrences of defaults grouped by companies' rating is prepared yearly by S&P [124]. The probabilities of defaults we obtain in the system (5.2) can be calculated using the Kramer's formula for escape rates [125]:

$$r \approx \frac{\omega_h \omega_r}{2\pi} \exp\left(-\frac{2H}{\sigma^2}\right). \tag{5.3}$$

The conditions 1–4 uniquely determine all the coefficients of the quartic po-

tential form:

$$V(x) = a_4\frac{x^4}{4} + a_3\frac{x^3}{3} + a_2\frac{x^2}{2} + a_1 x + a_0\,, \tag{5.4}$$

and its derivative

$$f(x) := -V'(x) = -(a_4x^3 + a_3x^2 + a_2x + a_1)\,. \tag{5.5}$$

Condition 1 sets $V(0) = 0$ and $V'(0) = 0$, thus $a_1 = 0$ and $a_0 = 0$. The parametrisation in Conditions 2 and 3 is enough to determine a_4, a_3 and a_2 explicitly in terms of ω_r^2, ω_h^2 and H. The correspondence is the following:

$$\begin{cases} a_4 = \frac{1}{12H}(\omega_h^2 - \omega_r^2)(\omega_h^2 + \omega_r^2) \\ a_3 = -\frac{1}{2\sqrt{3H}}(\omega_h^2 + \omega_r^2)^{3/2} \\ a_2 = \frac{\omega_h^2\omega_r^2}{\omega_h^2 - \omega_r^2} \end{cases}. \tag{5.6}$$

In order to observe V with two stable equilibria, the coefficient a_4 needs to be larger than 0, hence $\omega_h > \omega_r$ and thus $a_3 < 0$ and $a_2 > 0$.

Finally, the three equilibria can be written explicitly in terms of H, ω_h^2 and ω_r^2:

- trivial stable equilibrium (default state):

$$x_d = 0\,, \tag{5.7}$$

- the unstable equilibrium (risky state):

$$x_r(H, \omega_h, \omega_r) = \frac{2\sqrt{3H}\omega_r^2}{(\omega_h^2 - \omega_r^2)\sqrt{\omega_h^2 + \omega_r^2}}\,, \tag{5.8}$$

- the stable non-trivial equilibrium (healthy state):

$$x_h(H, \omega_h, \omega_r) = \frac{2\sqrt{3H}\omega_h^2}{(\omega_h^2 - \omega_r^2)\sqrt{\omega_h^2 + \omega_r^2}}\,. \tag{5.9}$$

5.3 Simple models with coupling

In this section we introduce two simple coupled models to understand some basic effects of default contagion. The suggested models come from the family (5.1),

which, given the form of the potential landscape from the previous section, is transformed into:

$$\begin{cases} dx_1 = \left[-V'(x_1;\boldsymbol{p}) - \beta x_1 h(x_2)\right] dt + \sigma dW_1 \\ dx_2 = \left[-V'(x_2;\boldsymbol{p}) - \beta x_2 h(x_1)\right] dt + \sigma dW_2 \end{cases}, \tag{5.10}$$

where β denotes the strength of coupling and $\boldsymbol{p} = (H, \omega_h^2, \omega_r^2)$. The positive impact ($\beta > 0$) means that the companies cooperate and if one defaults, the other is negatively affected. Conversely, $\beta < 0$ means competition – if for instance two companies work in the same area, one can take over the market after the other has defaulted. If we consider two layers of firms (for instance suppliers and receivers) in a multi-dimensional model, it is straightforward to introduce intralayer competition and interlayer cooperation. In this thesis we will assume the reaction function h is a nonincreasing function of x_i. However, to address positive aspects of competition one could allow the reaction function to increase for values between x_r and x_h. This construction would mean that in the world of competing firms the reaction would be positive either during a default or while being healthy, whereas the least influence would be transferred around the risky state. The model given by Eq. (5.10) assumes that the more healthy a company is, the more impacted by other's actions it gets, i.e. the more one has, the easier it is to lose a certain part of it.

Note that we do not include any kind of systemic risk common to all the companies although this can be achieved through correlating the Brownian increments.

5.3.1 Linear coupling

In the easiest version of the model we can consider a system where the response of one company to another's behaviour is linear. It can be obtained by simply setting in Eq. (5.10) $h(x) = -x$:

$$\begin{cases} dx_1 = \left[-V'(x_1;\boldsymbol{p}) + \beta x_1 x_2\right] dt + \sigma dW_1 \\ dx_2 = \left[-V'(x_2;\boldsymbol{p}) + \beta x_2 x_1\right] dt + \sigma dW_2 \end{cases}. \tag{5.11}$$

In this model for different values of coupling parameter β different routes of joint escapes can be observed. Following [121], we can distinguish three regimes

how the first escape (i.e. the first transition from healthy to default state) can influence the route of the second escape:

1. *weak coupling*: the escape of company A skews slightly the potential for the company B, however the company B can stay for an exponentially long time in a stable state that is lower than the initial healthy state x_h. Noisy increments are the only factor that can cause the second escape;

2. *slow domino*: the escape of company A skews the potential for the company B strongly enough that the escape of B will occur even with no further noise. In the joint potential it means that the state where one company is in the healthy state and the other in a defaulted state does not exist any more due to a saddle-node bifurcation. There is one saddle close to x_1-axis and one close to x_2-axis and the most probable route between (healthy,healthy) state and (defaulted,defaulted) state leads through those saddles with a symmetric hilltop between them. The asymmetric detour through the saddle causes the delay between escapes. Hence the name *slow domino*;

3. *fast domino*: for β large enough the two saddles collide with a source in a pitchfork bifurcation (*hilltop*) leaving only a symmetrically located saddle and two sinks. The preferred escape from (healthy,healthy) state to (defaulted,defaulted) state leads through the remaining saddle, what means that the escapes are happening almost at the same time. Hence the term *fast domino* is used.

In Fig. 5.2 we present the bifurcation diagram β vs. x_1^* (the equilibria of the first variable) and in Fig. 5.3 the phase portraits for the deterministic version of the model (5.11). If we assume that the particles are pushed around by small amplitude Brownian increments then noise-induced transitions can occur. Most likely, this kind of transition occurs through a saddle [121]. From this set of diagrams one can deduce, that:

- strong negative coupling (strong competition) can lead to only one company surviving for exponentially long time whereas the second one most likely defaults immediately;

- positive coupling shifts the stable equilibrium further from the origin, which

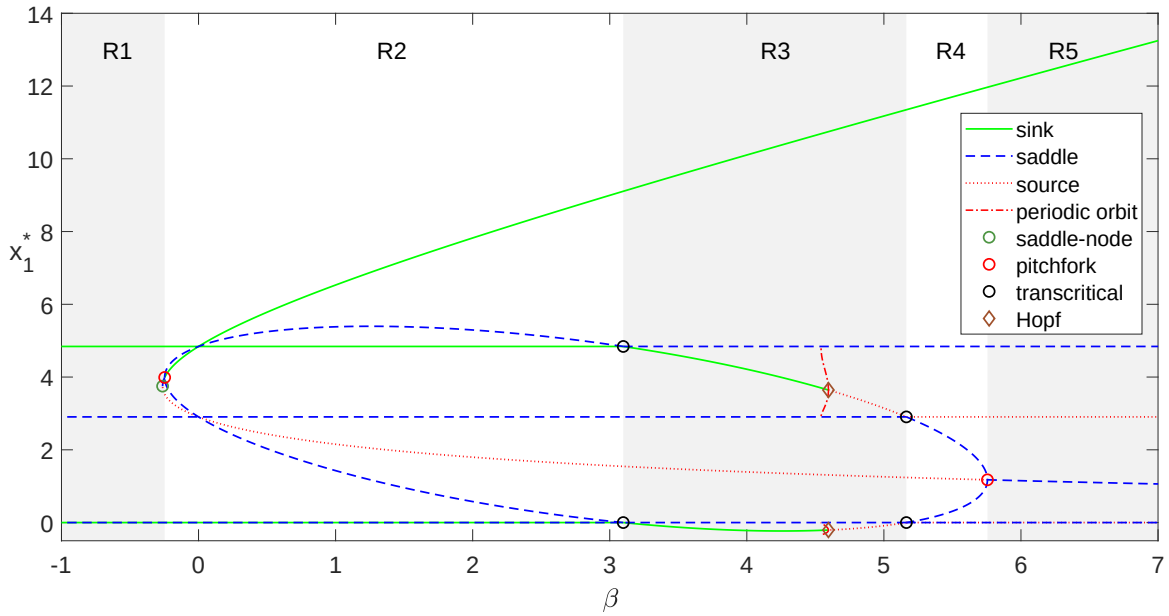

Figure 5.2: Bifurcation diagram for the model (5.11). Note that there is one more region between R1 and R2. In there a saddle-(stable)node bifurcation is immediately followed by a pitchfork of the saddle into two saddles and one source, however, for clarity, as the region is very narrow, we do not mark it here. Parameters of V are: $H = 5$, $\omega_h^2 = 10$ and $\omega_r^2 = 6$.

means that the waiting time for a noise-induced transition increases compared to the uncoupled case;

- in the weak coupling regime (R2), after the first company defaults the other is likely stay in the sink on an axis OX or OY for some additional time;
- when the coupling becomes stronger (regions R3 and R4), we can observe slow domino effects;
- for even stronger coupling (R5), the saddles close to the origin merge with a source in a pitchfork bifurcation and only one symmetric saddle remains. The companies will very likely default simultaneously (fast domino).

The simplicity of the model (5.11) allows for complete understanding of the dynamics governing the trajectories and gives good ideas and intuitions of what behaviour one can expect from companies moving in a coupled potential. However, the model has three very big disadvantages. As the coupling is active all the time, in the strong competition regime the model does not allow for existence of two players (see the phase portrait in Fig. 5.3A). Moreover, for positive coupling term, the (healthy,healthy) equilibrium can be shifted very far away from the origin

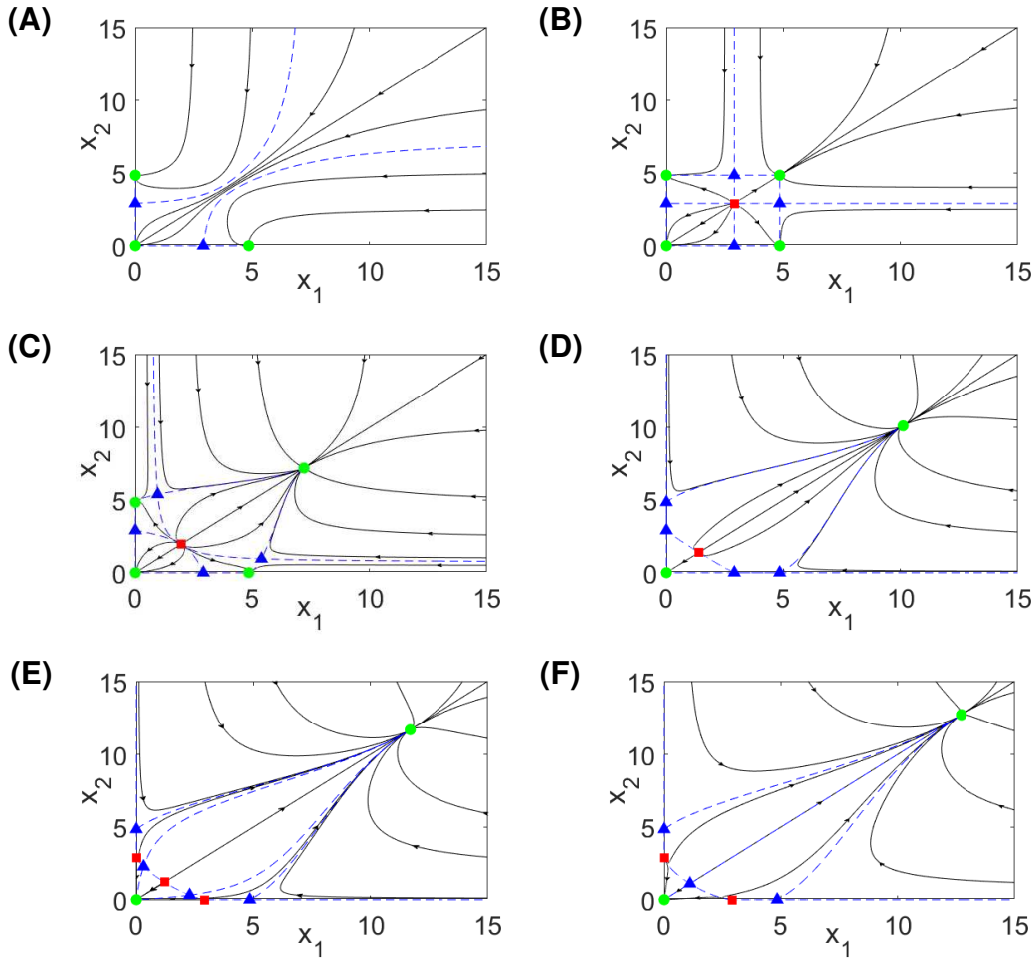

Figure 5.3: Phase portraits for the model (5.11). The regions mentioned below as R1-R5 correspond to the areas in Fig. 5.2. Note that we include two different portraits in R2. Green dots represent sinks, blue triangles saddles and red squares sources. (A) R1, $\beta = -0.6$: high competition, at least one of the companies is forced by deterministic dynamics to default; (B) R2, $\beta = 0$: no coupling (weak coupling regime), defaults are independent; (C) R2, $\beta = 1.5$: weak coupling, default of one increases the default rate of the other; (D) R3, $\beta = 4$: slow domino effect – joint escape most likely through saddles on OX or OY; (E) R4, $\beta = 5.5$: slow domino effect – joint escape most likely through saddles with both positive variables; (F) R5, $\beta = 6.5$: fast domino effect – joint escape through a symmetrically positioned saddle. Parameters of V are: $H = 5$, $\omega_h^2 = 10$ and $\omega_r^2 = 6$.

meaning a significant (exponential) decrease of the probability of default. Finally, for positive coupling the positive feedback loops bring the system even further from the origin. To prevent this kind of behaviour, the next iteration of the model will suppress the influence from company A to B if the company A is in a healthy state.

5.3.2 Quadratic coupling with an activation threshold

The second model we introduce manages the main problem observed in the previous model, i.e. that in the healthy state highly cooperating companies are very resilient to any shocks. In order to address this we introduce an activation threshold of the coupling in the critical point x_c, such that if the state variable x is greater than x_c, the coupling function $h(x) = 0$. Moreover, we alter the coupling from linear to quadratic, so that the obtained deterministic system is a gradient system in some regions of the (x_1, x_2)-plane, namely in $\{(x_1, x_2) : (x_1 \geq x_c \wedge x_2 \geq x_c) \vee (x_1 \leq x_c \wedge x_2 \leq x_c) \vee x_1 \equiv 0 \vee x_2 \equiv 0\}$ and symmetric outside of these regions. This is enough to be sure that the system will not exhibit any unwanted deterministic oscillatory behaviour, as for instance default-healthy oscillations.

Moreover, for the quadratic coupling, when one company passes the critical state x_c, it becomes quickly problematic for the other. The function h is of the form $h(x; x_c) = \max\left(0, 1 - \left(\frac{x}{x_c}\right)^2\right)$ – see Fig. 5.4 for a graphical representation of coupling in this model. The final form of this model is the following:

$$\begin{cases} dx_1 = \left[-V'(x_1; \boldsymbol{p}) - \beta x_1 \max\left(0, 1 - \left(\frac{x_2}{x_c}\right)^2\right)\right] dt + \sigma dW_1 \\ dx_2 = \left[-V'(x_2; \boldsymbol{p}) - \beta x_2 \max\left(0, 1 - \left(\frac{x_1}{x_c}\right)^2\right)\right] dt + \sigma dW_2 \end{cases} . \tag{5.12}$$

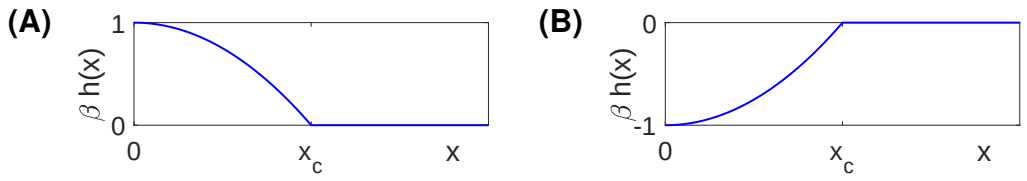

Figure 5.4: Quadratic coupling with the activation threshold in model (5.12). (A) $\beta > 0$, (B) $\beta < 0$.

We explore what kind of behaviour one can observe in this formulae through bifurcation diagrams presented in Fig. 5.5. For the sake of simplicity we fix $\omega_r^2 = 6$,

$\omega_h^2 = 10$ and $H = 5$, nevertheless we expect very similar bifurcation diagrams for any combination of ω_r^2, ω_h^2 and H assuming that $H > 0$ and $\omega_h^2 > \omega_r^2$.

It turns out that for any value of x_c we can observe a Critical Transition (saddle-node bifurcation) at $\beta = 1$. Thus, $\beta < 1$ denotes the weak coupling regime and domino effects are possible only for $\beta > 1$. Depending on the critical value x_c the system can undergo a smooth pitchfork bifurcation leading from the slow-domino regime to the fast-domino regime. This transition is not a Critical Transition though. If $x_c < x_r$, i.e. the coupling is activated below the hilltop of the potential, there will always exist a sink and two neighbouring saddles and hence only slow domino is possible. For larger values of of x_c, fast domino can happen depending on the value of β.

Interestingly, because the map $h(x)$ is not smooth, for β large enough there can be observed an immediate change in the system under the variation of parameter x_c. Just before the bifurcation ($x_c \leq x_r$) there exist two saddles and a source in the configuration identical to the uncoupled case, marked by the big blue triangle in Fig. 5.5A. However, for an infinitesimally small increase of x_c over x_r the three equilibria disappear in a non-smooth pitchfork bifurcation with no earlier shift of equilibria towards each other. The instantaneous nature of this process induces that this bifurcation can be classified as a Critical Transition between slow and fast domino regimes despite that the smooth pitchfork is not a CT. Presumably, incorporating a smooth coupling instead of the suggested one would solve the problem, nevertheless, the obtained system probably would not be a gradient one.

The largest drawback of the suggested model is that one companies' health is deteriorated forever after the other company defaults and that we can observe non-smooth transitions when varying some of the parameters. A study of an extended model which does not exhibit these features is presented in the next section.

5.4 An improved model with adaptation

In the previous section we suggested two simple models of health of coupled companies. The system (5.11) has an undesired property that even for slightly

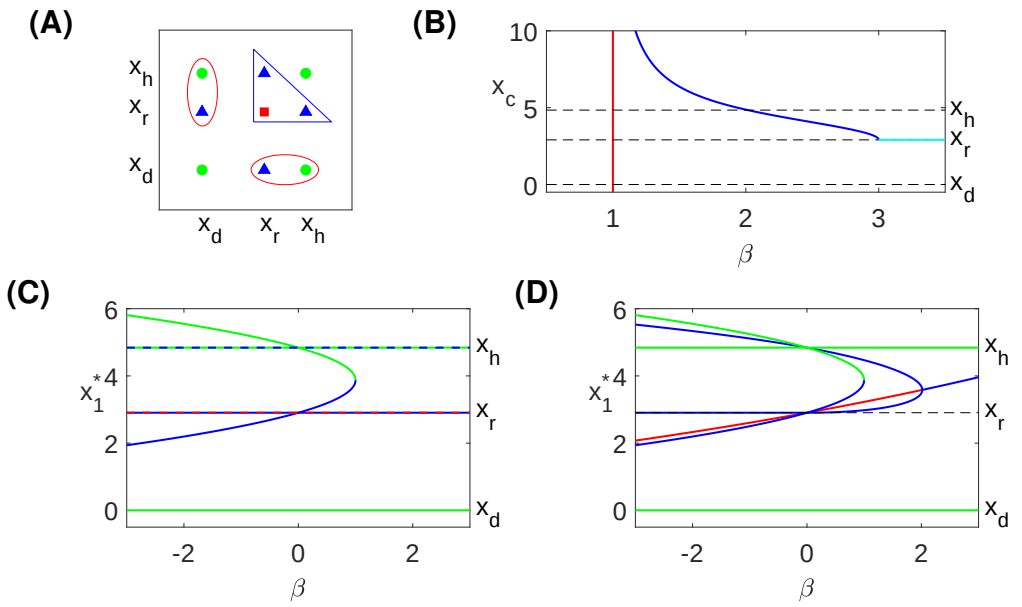

Figure 5.5: Diagrams for the model (5.12). (A) A schematic phase portrait of the uncoupled model ($\beta = 0$). Red ellipses denote the points which undergo a saddle-node bifurcation (green circle – sink, blue triangle – saddle) and the big blue triangle marks the points which undergo a pitchfork bifurcation (two saddles and a source). (B) Two-parameter bifurcation diagram, the red line denotes the saddle-node bifurcation, whereas the blue line denotes the pitchfork bifurcation. Because the coupling function $h(x)$ is not smooth there is a non-smooth pitchfork bifurcation at $x_c = x_r$ for $\beta > 3$ – marked with cyan line. (C) Phase-parameter bifurcation diagram for $x_c = x_r$, (D) phase-parameter bifurcation diagram for $x_c = x_h$. Parameters of V are: $H = 5$, $\omega_h^2 = 10$ and $\omega_r^2 = 6$.

positive coupling the default times are increasing exponentially in comparison to the uncoupled case. We removed this feature by introducing the coupling activation threshold in the model (5.12), however, the suggested coupling function induced a non-smooth transition between the slow and fast domino regimes. Nevertheless, the drawback of both models is the fixed and infinite dependence of the health of a company on a previous default. Half-life time a default exhibits an impact on default rate is estimated to be around three months [126], hence the observed drawback cannot be removed by simply adding a threshold where the coupling switches off.

This section introduces a model which addresses the aforementioned problems. We extend the application of the potential landscape from the previous models by adding an *adaptation* variable for each company. This variable expresses an adaptive response of a company to other players behaviour. We start from a two-player, and thus four-dimensional, model.

5.4.1 Two-player model

The suggested model is the following:

$$\begin{cases} dx_1 = (-V'(x_1;\boldsymbol{p}) - c_1 x_1)\,dt + \sigma dW_1 \\ dx_2 = (-V'(x_2;\boldsymbol{p}) - c_2 x_2)\,dt + \sigma dW_2 \\ dc_1 = \left(\frac{1}{\tau}\left(\beta g(x_2;\boldsymbol{p}) - c_1\right)\right)dt \\ dc_2 = \left(\frac{1}{\tau}\left(\beta g(x_1;\boldsymbol{p}) - c_2\right)\right)dt \end{cases}. \tag{5.13}$$

The variables c_i express the adaptation of company i through a response function $g(x,\cdot)$, which we require to be continuous, $g(x_d) = g(x_h) = 0$. The parameter τ_i specifies the response time to the current market situation. It means that for a lower value of τ a company is strongly affected by another's default, however, after a default it recovers faster to the pre-default state.

The simplest form of the function g which fulfils the above prerequisites is the following:

$$g(x;\boldsymbol{p}) = \begin{cases} 0 & \text{for } x \le x_{dr} \text{ or } x \ge x_{rh}\,, \\ 2\frac{x - x_{dr}}{x_{rh} - x_{dr}} & \text{for } x \in \left(x_{dr}, \frac{x_{dr}+x_{rh}}{2}\right), \\ -2\frac{x - x_{rh}}{x_{rh} - x_{dr}} & \text{for } x \in \left(\frac{x_{dr}+x_{rh}}{2}, x_{rh}\right), \end{cases} \tag{5.14}$$

where x_{dr} is the location between x_d and x_r where the response switches off and a company is treated by other as defaulted. Analogously, x_{rh} is a value between x_r and x_h that indicates the state where one is assumed to be in trouble and affects the other company. Interestingly, if we fix $x_{rh} = x_r$ the function g causes the lowest lag in transmission of negative influence between a defaulting company and the remaining one for $x_{dr} = \frac{1}{2}x_d + \frac{1}{2}x_r$. We presume that this is caused by an interplay between the relatively small distance of the maximum of the function g to x_r and the relatively wide activation zone. However, in order to avoid the non-smooth transitions observed in the model (5.12), we fix x_{rh} slightly above x_r, namely we set $x_{rh} = \frac{9}{10}x_r + \frac{1}{10}x_h$. This accounts for speculations about a company which is not in the defaulting stage yet, but is close to the risky state. Because the location of the three equilibria depends on the potential V, the function g depends on the parameters of the potential $\boldsymbol{p} = (H, \omega_h^2, \omega_r^2)$ as well. We will call *activation zone* the interval where the function g is positive. We present the function g in terms of the

location of activation zone compared to the potential in Fig. 5.6.

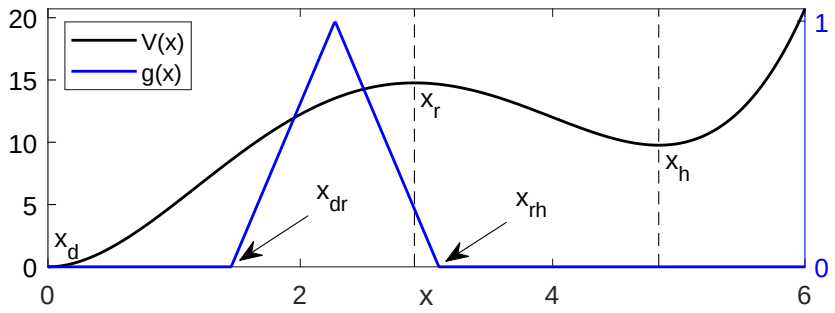

Figure 5.6: Coupling function $g(x)$ compared to the potential landscape $V(x)$. The influence of the function g is the strongest if x_{dr} is around the middle between x_d and x_r. On the other hand, obviously, the larger x_{rh}, the earlier the coupling is switched on and hence the greater influence. We decided to take x_{dr} as the midpoint of the interval $[x_d, x_r]$ and x_{rh} in the 10% of the interval $[x_r, x_h]$. Parameters of V are: $H = 5$, $\omega_h^2 = 10$ and $\omega_r^2 = 6$.

In the deterministic case we have $\dot{x}_i = -V'(x_i; \boldsymbol{p}) - c_i x_i$, thus the *effective potential* (i.e. the potential modified by the coupling) is the following:

$$\widetilde{V}(x_i; \boldsymbol{p}) = V(x_i; \boldsymbol{p}) + \frac{1}{2} c_i x_i^2. \tag{5.15}$$

The effective potential $\widetilde{V}$ can be described analogously to the original one V by the parameters $\widetilde{H}$, $\widetilde{\omega}_h^2$ and $\widetilde{\omega}_r^2$, and thus by the location of equilibria $\tilde{x}_r$ and $\tilde{x}_h$. Note that the effective potential has an equilibrium in x_d. Increasing c_i shifts the positive equilibria $\tilde{x}_r$ and $\tilde{x}_h$ towards each other making it easier to observe noise-induced transitions. In some cases (for coupling parameter β large enough or for x_i residing for a long time in the zone where the function g is positive) $\widetilde{x}_r$ and $\widetilde{x}_h$ collide and disappear in a saddle-node bifurcation, which implies that a company should follow a (slow-)domino route to a default. On the one hand, after some time this bifurcation can be reversed and two equilibria reappear, and thus, if the gap between the two bifurcations is (time-wise) short enough, the tipping might not occur and the variable can track $\tilde{x}_h$ again. On the other hand, if the gap is large enough, the trajectory is likely to tip. We have presented these three scenarios in Fig. 5.7 together with the values of c_i assuming that one variable has no stochastic input (i.e. $\sigma_2 = 0$). It shows how the coupling actually modifies the effective potential. When the attractors vanish and before they reappear the Kramer's rate of escape given by Eq. (5.3) does not exist (is infinite), however there might be no tipping observed.

If we assume the noisy input in the red trajectory ($\sigma_2 = \sigma_1$), the second com-

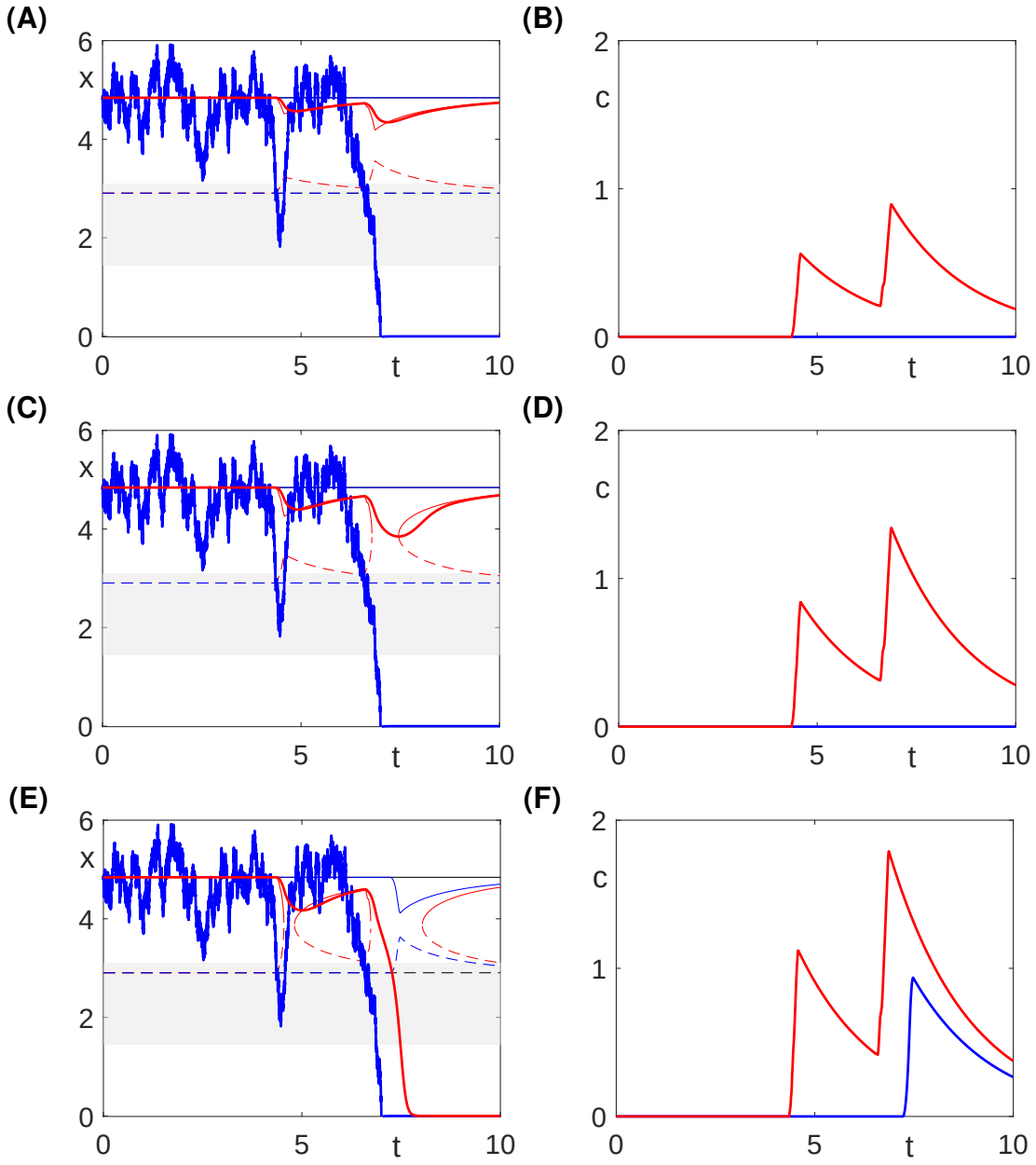

Figure 5.7: Different modes showing the behaviour of the effective equilibrium in the model with adaptation (5.13). The left panels (A), (C) and (E) present the behaviour of the two main variables x_1 (noisy, thick blue) and x_2 (noiseless, thick red) in the varying potential. The thinner lines represent the healthy (solid lines) and the risky state (dashed lines) for the uncoupled potential (black), and effective potential $\widetilde{V}$ (blue and red for x_1 and x_2, respectively). The panels (B), (D) and (F) show the values of variables c_1 (blue) and c_2 (red). The parameters are: $\omega_r^2 = 6$, $\omega_h^2 = 10$, $H = 5$, $\tau = 2$, $\sigma_1 = 2$, $\sigma_2 = 0$, (A) and (B) $\beta = 8$, (C) and (D) $\beta = 12$, (E) and (F) $\beta = 16$.

pany will default in finite time. Following [18], we classify the causes of such a default as:

- diffusion-dominated escape (possible in Fig. 5.7A),
- noise-drift balanced regime (possible in Fig. 5.7C),
- drift-dominated escape (Fig. 5.7E).

5.4.2 N-player model

The N-dimensional model we introduce in this section is an extension of the 2-dimensional model given by Eq. (5.13). We analyse a homogeneous model, i.e. we assume that the companies affect each other in the same way and all the parameters of the potential, noise strength and the response τ are equal for all the companies. The mathematical formulation is the following:

$$\begin{cases} dx_i = (-V'(x_i; \boldsymbol{p}) - c_i x_i)\, dt + \sigma dW_i \\ dc_i = \frac{1}{\tau}\left(\frac{\beta}{N-1}\sum_{j\neq i} g(x_j; \boldsymbol{p}) - c_i\right) dt \end{cases} . \tag{5.16}$$

The only difference from the model (5.13) is in the term $\frac{g(\cdot)}{N-1}$ which stands for the influence $g(x_j; \boldsymbol{p})$ coming from the company j that is distributed evenly among all the other companies.

In this chapter we treat β as a single value. However, by replacing $\beta \sum_{j\neq i} g(x_j; \boldsymbol{p})$ with $\sum_{j\neq i} B_{j,i} g(x_j; \boldsymbol{p})$ one can study a network defined by coupling weight matrix B. For instance, this formulation would allow modelling of supply chains where some companies cooperate with their suppliers/receivers and compete against others with similar products.

The N-dimensional model exhibits the same behaviour from a single company perspective as the 2-dimensional version. However, this extension allows to observe how the contagion between the players propagates. In Fig. 5.8 we present a sample diagram for 10 companies where one can see how the coupling changes the potential and how c_i varies during cumulation of default events.

In Fig. 5.8A and 5.8B there are shown the paths obtained from exactly the same process (with the same noise realisations) differed by the values of β ($\beta = 0$

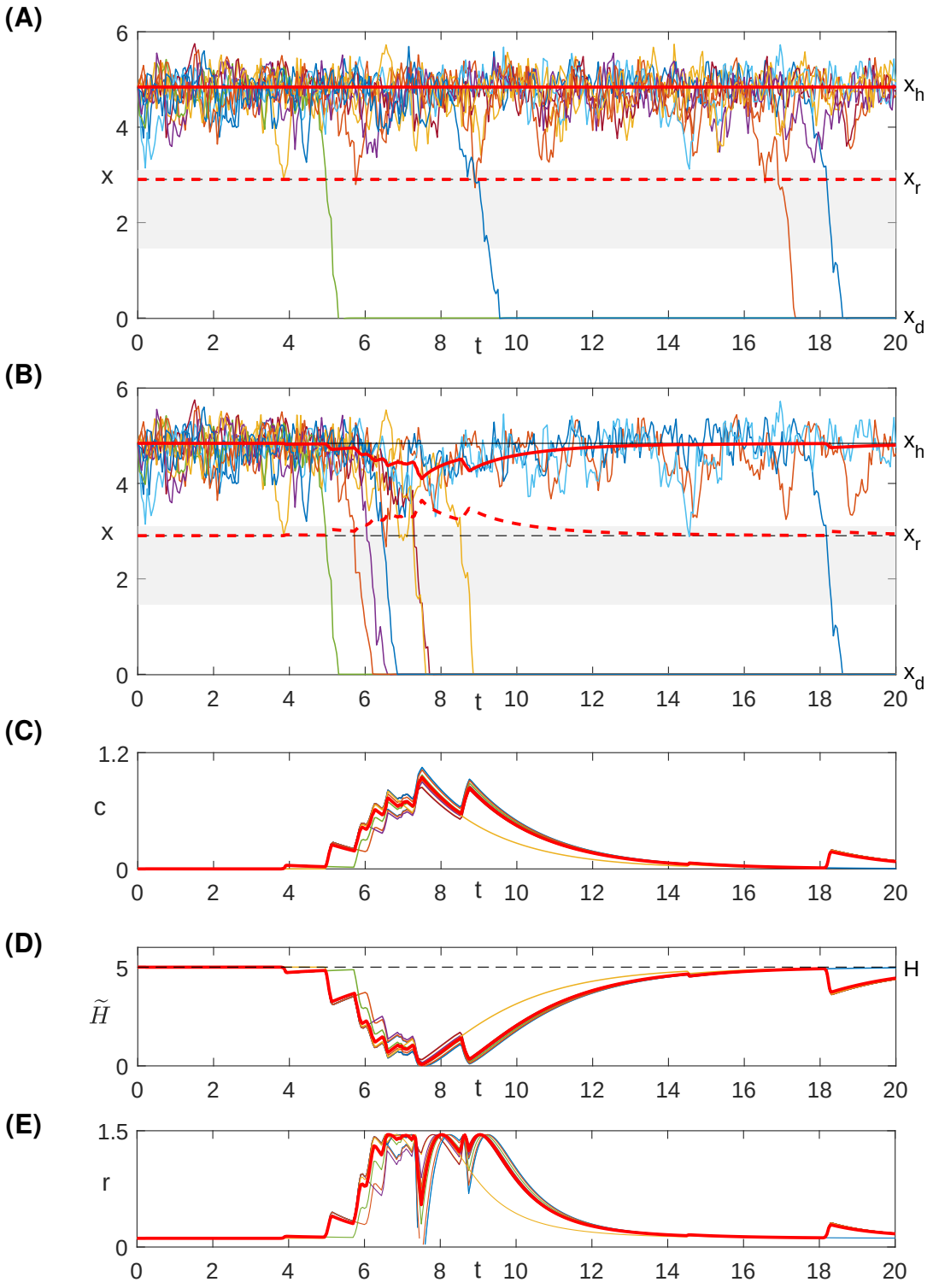

Figure 5.8: A single realisation of the model with adaptation (5.16) with $N = 10$ players. (A) and (B) are the sample paths in the uncoupled ($\beta = 0$) and coupled ($\beta = 40$) cases, respectively. In red we mark the equilibria x_h and x_r of the effective potential given the average $\bar{c} = \frac{1}{N}\sum c_i$. (C) values of c_i and an average $\bar{c}$ (marked in bold red) for $\beta = 40$, (D) barrier height $\widetilde{H}$ in the averaged potential $\widetilde{V} = V(x) + \frac{1}{2}\bar{c}x^2$ for $\beta = 40$. (E) Kramer's escape rate given by Eq. (5.3) with the red one being based on $\bar{c}$ for $\beta = 40$. The sudden fall of the rate for very small values of $\widetilde{H}$ is caused by the significant flattening of the potential and thus the curvatures in the nominator of the Kramer's escape rate (5.3) become tiny. It does not mean though that the true rate of escape is small there, the Kramer's rate is not valid for such small $\widetilde{H}$ any more. Parameters of V are: $H = 5$, $\omega_h^2 = 10$ and $\omega_r^2 = 6$.

in the first one and $\beta = 40$ in the second one). It is clearly visible that the trajectories jump through the barrier much easier around time $t = 8$ when the equilibria approach each other. The cascade begins when the first trajectory enters deeply the activation zone of the function g and the coupling switches on making it easier to tip.

In Fig. 5.8C we present the time series of the variables c_i. There is a rise of c_i starting just after the first trajectory enters the grey zone and cumulating up until time around 8 when the rate of escape is the largest. Then, c_i decrease gradually together. By bold red we present the average $\bar{c}$ which is further used to find the mean escape height $\widetilde{H}$.

In Fig. 5.8D we show the barrier height of the potential and $\widetilde{H}$ for the effective 'mean' potential $\widetilde{V} = V(x) + \frac{1}{2}\bar{c}x^2$. What can be misleading, around time $t = 7.5$ the equilibria in Fig. 5.8B are quite far away, however the components used to compute the mean Kramer's escape rate given by Eq. (5.3) – height $\widetilde{H}$ and the curvatures $\widetilde{\omega}_h^2$ and $\widetilde{\omega}_r^2$ – are almost equal to zero. Note that for very small values of $\widetilde{H}$ the actual rate of escape in Fig. 5.8E actually drops. It is caused by the significantly flat potential so that the curvatures in the nominator of the fraction in Kramer's escape rate become tiny. Obviously, it is easy to default there, but this fact is not captured by the escape rate – the Kramer's approximation formula is not valid in the regime where the noise level is small in comparison to the potential barrier H [127, Sec. XIII.6].

5.5 Benchmarking our results

In this section we benchmark the model with adaptation (5.13) against a different model presented in the literature. We have decided on the doubly-stochastic dynamical model introduced in 2013 by Giesecke et al. [123].

5.5.1 A doubly-stochastic model of intensity of defaults

This model describes the *intensity* (i.e. rate) of defaults of companies. If the accumulated intensity is larger than some randomly distributed value, the company is assumed to be defaulted. The companies are interconnected through two components: common risk factor and influence of previous defaults. The intensity

$\lambda_n(t)$ is governed by the following N-dimensional SDE with $n \in \{1, ..., N\}$:

$$d\lambda_n(t) = -\alpha_n \left(\lambda_n(t) - \bar{\lambda}_n\right) dt + \sigma_n \sqrt{\lambda_n(t)} dW_n(t) + \beta_n^S \lambda_n(t) dX(t) + \beta_n^C dL(t) \tag{5.17}$$

with some initial condition $\lambda_n(0) = \lambda_{o,n}$.

The components of the system (5.17) are as follows:

- independent dynamics governed by a Cox-Ingersoll-Ross process

$$- \alpha_n \left(\lambda_n(t) - \bar{\lambda}_n\right) dt + \sigma_n \sqrt{\lambda_n(t)} dW_n(t) \tag{5.18}$$

  with a collection of independent Brownian motions $W_n(t)$ and parameters α_n, $\bar{\lambda}_n$ and σ_n;

- systematic risk factor

$$\beta_n^S \lambda_n(t) dX(t) \tag{5.19}$$

  where β_n^S is a parameter and X_t is described by a general SDE

$$dX(t) = b_0 \left(X(t)\right) dt + \sigma_0 \left(X(t)\right) dV(t) \tag{5.20}$$

  with some initial condition $X_0 = x_o$ and Brownian motion $V(t)$ independent of $W_n(t)$. Dynamics of $X(t)$ could be governed for instance by Ornstein-Uhlenbeck process;

- contagion term

$$\beta_n^C dL(t) \tag{5.21}$$

  with a parameter β_n^C and

$$L(t) = \frac{1}{N} \sum_{n=1}^{N} \mathbb{1}_{\{\tau_n \leq t\}} \tag{5.22}$$

  being a counting process with an increment equal to $1/N$ at the moment τ_n of a default. Formally,

$$\tau_n = \inf \left\{ t \geq 0 : \int_0^t \lambda_n(s) ds \geq \epsilon_n \right\} \tag{5.23}$$

  with ϵ_n being i.i.d. from a standard exponential distribution. The formula describes the default as a first moment when the accumulated over time

intensity reaches the value of ϵ_n.

We present a sample four-dimensional realisation of the process of intensity given by Eq. (5.17) in Fig. 5.9.

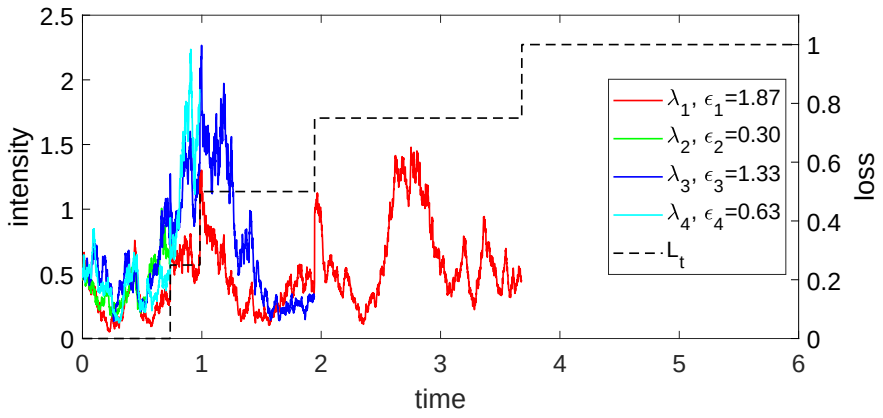

Figure 5.9: Example of time series generated with the (homogeneous) model of default intensity (5.17) with 4 companies. The parameters are as in Fig. 1 in [128]: $\sigma_n = 0.9$, $\alpha_n = 4$, $\lambda_n(0) = \bar{\lambda}_n = 0.5$, $\beta_n^C = 2$, $\beta_n^S = 1$. The systematic risk's dynamics are governed by $dX(t) = 2(1 - X(t))dt + dW(t)$ with initial condition $X(0) = 1$.

Because ϵ_n are distributed independently, the domino effects might not be present in a low dimensional version of this model at all – the distribution of default times for small N is close to the exponential distribution. For instance, if in 2-dimensional system $\epsilon_1 = 0.1$ and $\epsilon_2 = 2$, there is expected a long delay between the two defaults. On the other hand, if $\epsilon_1 = \epsilon_2$, the defaults are expected to happen one by another, and this feature is caused mainly not due to the contagion. Of course, the coupling parameter β_n^C can be used to intensify the feedback between companies and thus to trigger the default clustering in large portfolios [123].

The important property of the model of intensity (5.17) is that in the absence of noise and lack of coupling every company will default after an exponentially long waiting time. The same distribution of defaults is expected in the uncoupled model with adaptation variable (5.16). However, in the model with adaptation the escapes are noise-induced. Let us compare these two models starting with a simple analysis of the default times.

5.5.2 Comparison of models

Firstly, we compare the models with adaptation (5.13) and the model of intensity (5.17) by the distributions of escapes. For this purpose, we examine the first

and the second default in a two-dimensional system. Following [121], τ^i denotes the i-th default observed in the system.

We examine the models with no coupling as well as three cases with positive coupling. We found out that for $\beta = 5$ in (5.13) and $\beta^C = 2$ in (5.17) the models have similar ratio of the mean of the second escape to the mean of the first escape (i.e. $\overline{\tau^2}/\overline{\tau^1}$), namely 1.68 and 1.57, respectively. Hence, we will compare the histograms for these values of coupling, twice as low and twice as large coupling strength, however, we are aware that the correspondence β^C in (5.17) to β in (5.13) is not necessarily linear. The histograms of escapes are presented in Fig. 5.10.

The histograms suggest that the two models are qualitatively similar for some values of β and β^C. In the regimes with no coupling (Fig. 5.10A and Fig. 5.10B) or low coupling (Fig. 5.10C and Fig. 5.10D) there is much higher concentration of first escapes (τ_1) close to 0 in the model of intensity. Although the two models exhibit different timescales, it does not change the qualitative behaviour. In the medium coupling regime (Fig. 5.10E and Fig. 5.10F) the two corresponding histograms are indeed very similar, however this is not the case for even higher coupling (Fig. 5.10G and Fig. 5.10H).

Examining all the histograms implies that the models can exhibit similar statistics of escapes, however the correspondence β^C to β is indeed not linear. Adjusting the parameters of the models, especially decreasing the parameter $\bar{\lambda}_n$, would cause the models to be quantitatively comparable, nevertheless at this point we do not perform such a study. Because the diagrams for $\beta = 5$ and $\beta^C = 2$ are alike, we will use this strengths of coupling and fix all the other parameters as in Fig. 5.10 to compare the joint defaults in these models through copulas.

5.5.3 Escape time dependency copulas

As the second comparison measure we decided to use a more sophisticated approach. Instead of looking at the escape times separately, we explore their joint distributions. For this task we employ multivariate probability distribution framework know as copulas. For an introduction to copulas see for instance [129–131].

The main reason to use copulas in financial modelling is to capture the dependence between financial assets to provide risk management and hedging stra-

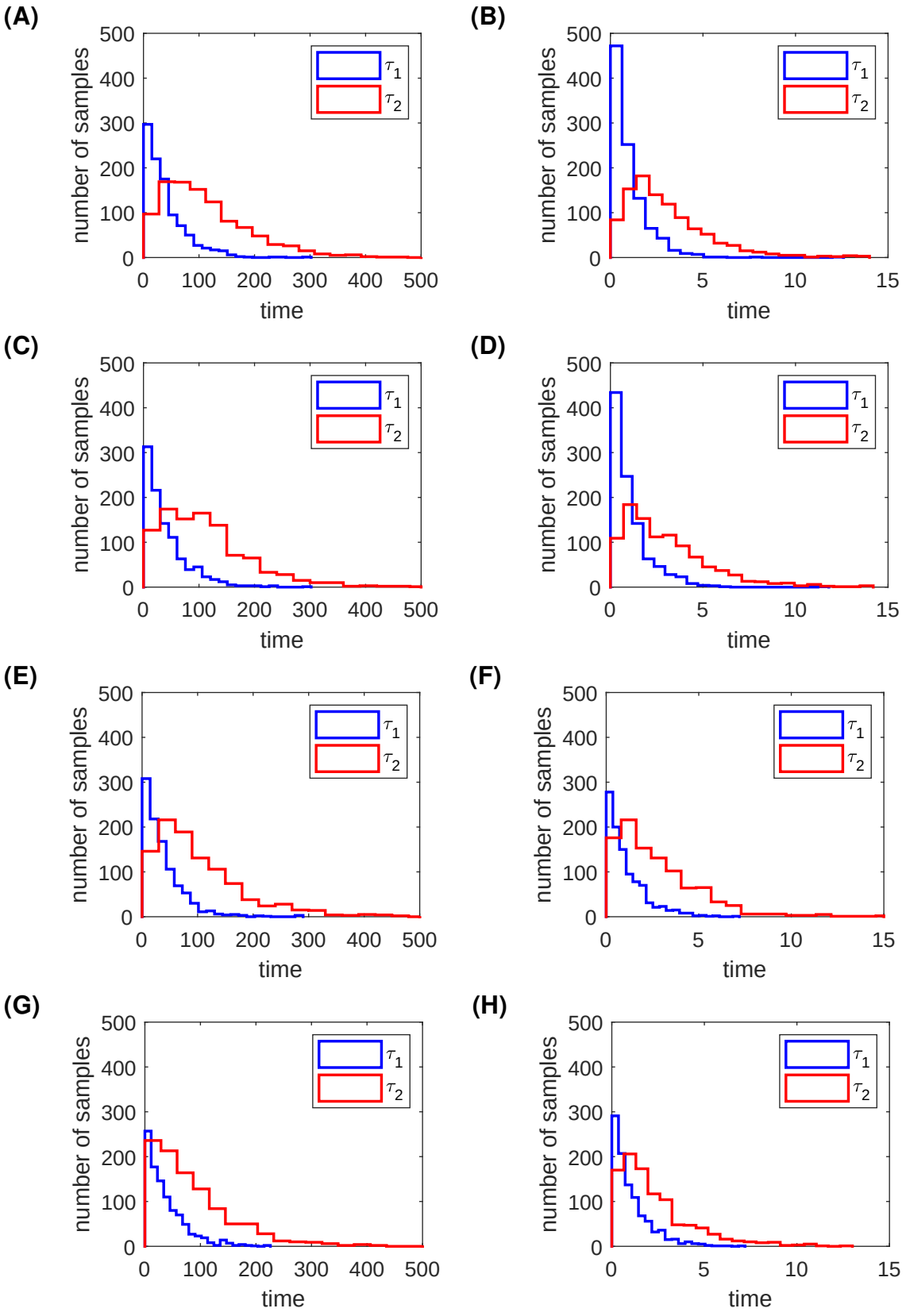

Figure 5.10: Histograms of escape times in 1000 simulated series from the model with adaptation (5.13) (left-hand side panels) against the model of intensity (5.17) (right-hand side panels) for corresponding coupling strength. (A) $\beta = 0$, (B) $\beta^C = 0$, (C) $\beta = 2.5$, (D) $\beta^C = 1$, (E) $\beta = 5$, (F) $\beta^C = 2$, (G) $\beta = 10$, (H) $\beta^C = 4$. The parameters of the model (5.13) are: $H = 5$, $\omega_h^2 = 10$, $\omega_r^2 = 6$, $x_{dr} = \frac{1}{2}(x_d, x_r)$, $x_{rh} = \frac{9}{10}x_r + \frac{1}{10}x_h$, $\tau = 2$, $\sigma = 1.5$. The parameters of the model (5.17) are the same as in Fig. 5.9 except the coupling parameter β^C.

tegies. Copulas offer a 'complete and unique description of the dependence structure' between assets with no need to compute marginal distributions [132, Chapter 3] and they quantify the relation between variables not only with a single-numbered measure (as for instance the correlation coefficient does), but with a distribution which describes such a relation in a much higher detail. The main focus of application of copulas in finance was put on measuring the relation of return rates of assets [132], nevertheless, there have been attempts to apply the copulas to model the statistics of financial defaults [133].

The most commonly applied copulas are Gaussian and Student's copula [132], however, as we do not have any preassumptions on the dependence of the escapes in the models (5.13) and (5.17), we perform numerical studies of a wide selection of copulas with their survival versions. This is carried out in `R` [134] using the package `copula` (version 0.999-18) [135]. The fitting method we use is based on maximum pseudo-likelihood estimator, whereas the optimisation method of our choice is Neldear-Mead. We do not provide the formulas for each copula as they can be found either in the functions included in the package or in the aforementioned literature. The p-values of the fits of these copulas are presented in Table 5.1.

Contrary to the previous study we do not analyse the i-th escapes, but the escapes of i-th player, which, following [121], we denote by $\tau^{(i)}$. Because in the previous section the two histograms were qualitatively similar for $\beta = 5$ in (5.13) and $\beta^C = 2$ in (5.17), we use these strengths of coupling further in this section. The other parameters are kept the same as for the study presented in Fig. 5.10

For the model (5.13) we have found one copula (i.e. Tawn survival copula with p-value over 9%) which can model well the interdependence of simulated escapes – that copula could possibly mimic our model in terms of escape distributions. The survival modification is used in applications where one studies lifetimes of objects in some populations [130]. For the model (5.17) none of the copulas we tried match the simulations. Interestingly, for the model of intensity the second largest p-value is observed for the Tawn survival copula, however it is much less than 5%. The fits of Tawn (standard and survival) copula to the simulated data coming from the two models are shown in Fig. 5.11. The way of finding the distribution of the data given the Tawn copula is presented below.

The escape times in the uncoupled double-well potential system are distri-

		Model (5.13)		Model (5.17)	
Copula	Survival	Dep. par.	p-value [%]	Dep. par.	p-value [%]
A-M-H	NO	0.42	0.05	0.51	0.05
Clayton	NO	0.17	0.35	0.22	0.05
Frank	NO	0.86	0.15	1.12	0.05
Gumbel	NO	1.06	0.05	1.11	0.05
Joe	NO	1.04	0.05	1.12	0.05
Normal	NO	0.13	0.05	0.17	0.05
t	NO	0.14	0.05	0.18	0.05
Galambos	NO	0.25	0.05	0.32	0.05
Tawn	NO	0.18	0.05	0.30	0.05
F-G-M	NO	0.40	0.05	0.47	0.05
Plackett	NO	1.56	0.05	1.84	0.05
A-M-H	YES	0.34	0.05	0.43	0.05
Clayton	YES	0.08	0.05	0.15	0.65
Frank	YES	0.86	0.05	1.12	0.05
Gumbel	YES	1.10	1.65	1.13	0.05
Joe	YES	1.14	0.25	1.18	0.05
Normal	YES	0.13	0.05	0.17	0.05
t	YES	0.14	0.05	0.18	0.05
Galambos	YES	0.31	0.05	0.35	0.05
Tawn	YES	0.28	**9.24**	0.33	0.25
F-G-M	YES	0.40	0.05	0.47	0.05
Plackett	YES	1.56	0.05	1.84	0.05

Table 5.1: Dependence parameters and the p-values of the fitted copulas. The copulas were fitted to the simulated data from the model with adaptation (5.13) and the model of intensity (5.17). Green colour denotes the p-value that is above 5%. There is only one case where the hypothesis that the data can be simulated using a certain copula cannot be rejected.

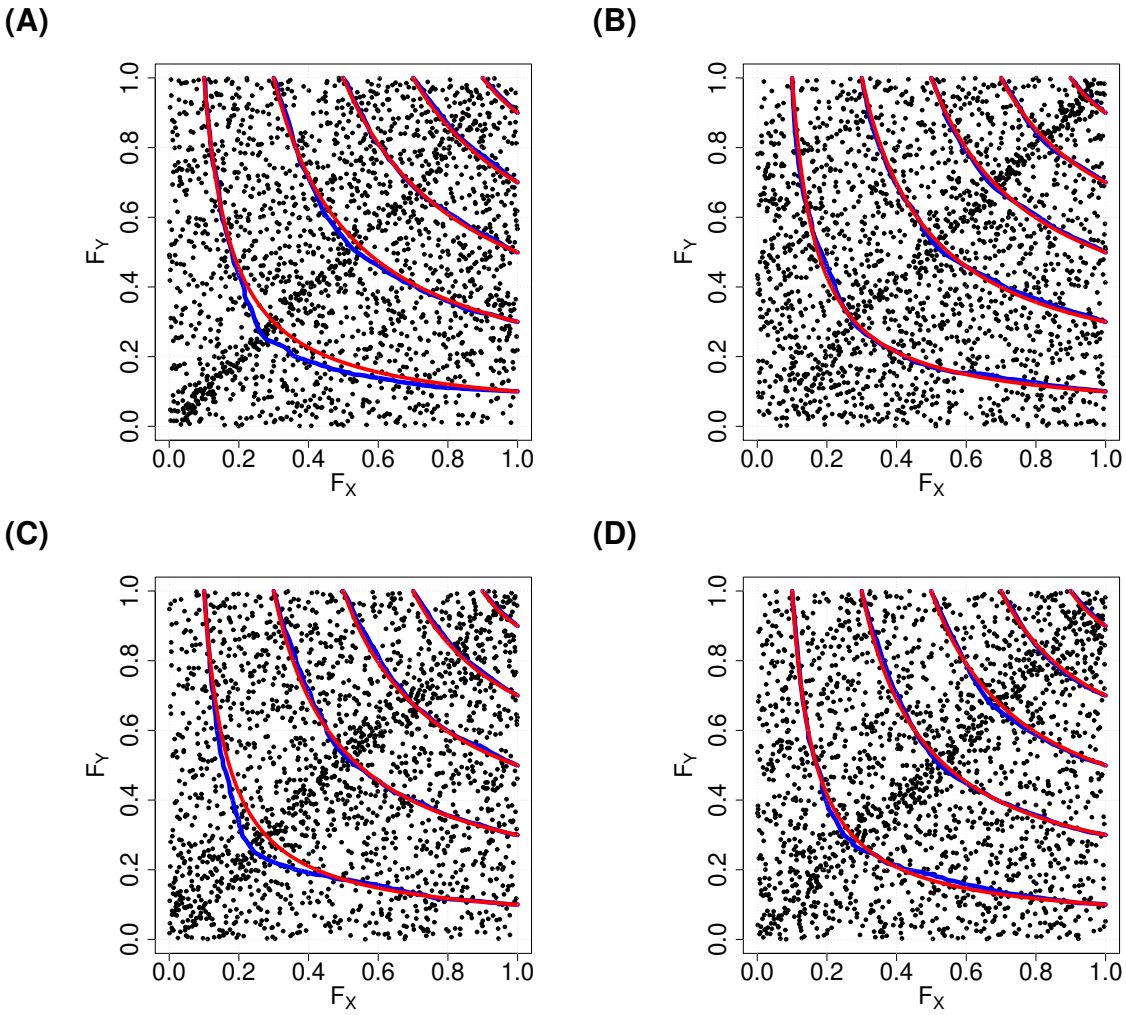

Figure 5.11: Tawn copula fitted to the ranked simulated data. The blue lines mark the quantile lines at levels 0.1, 0.3, 0.5, 0.7 and 0.9 for the empirical copula, whereas the red lines stand for the respective level lines of the fitted copula. (A) Tawn copula fitted to the simulated data from the model (5.13). The copula is far from matching the data, p-value $= 0.0005$. (B) Tawn survival copula fitted to the simulated data from the model (5.13). The copula well matches the data, the p-value $= 0.0924$ and the dependence parameter $\alpha = 0.28$. (C) Tawn copula fitted to the simulated data from the model (5.17). The copula is far from matching the data, p-value $= 0.0005$. (D) Tawn survival copula fitted to the simulated data from the model (5.17). The copula well matches the data visually, however p-value $= 0.0025$.

buted exponentially, hence we assume that the marginal cumulative distribution functions are exponential as well. Although we are aware that the data might not be strictly exponential, we treat this distribution as the first approximation. The assumed distribution of escapes is thus the following:

$$F_X\left(\tau^{(1)}\right) = 1 - e^{-\lambda\tau^{(1)}} \quad \text{and} \quad F_Y\left(\tau^{(2)}\right) = 1 - e^{-\lambda\tau^{(2)}}, \tag{5.24}$$

whilst the survival functions ($\bar{F}_X(x) = 1 - F_X(x)$) are:

$$\bar{F}_X\left(\tau^{(1)}\right) = e^{-\lambda\tau^{(1)}} \quad \text{and} \quad \bar{F}_Y\left(\tau^{(2)}\right) = e^{-\lambda\tau^{(2)}}. \tag{5.25}$$

The Tawn copula is the function linking the pseudo-observations $u \in [0,1]$ and $v \in [0,1]$ (outputs from F_X and F_Y) as

$$C(u,v) = uv \cdot \exp\left(-\frac{\alpha \log(u)\log(v)}{\log(uv)}\right) \tag{5.26}$$

with the dependence parameter $\alpha \in [0,1]$ where $\alpha = 0$ means independence. Furthermore, the joint distribution in terms of copula function is given by

$$H(x,y) = C(F_X(x), F_Y(y)). \tag{5.27}$$

As the copula of our choice is the survival modification, we need to consider the Tawn survival copula function $\hat{C}(\cdot,\cdot)$:

$$\hat{C}(u,v) = u+v-1+C(1-u,1-v) = u+v-1+(1-u)(1-v)\exp\left(-\frac{\alpha\log(1-u)\log(1-v)}{\log\left((1-u)(1-v)\right)}\right) \tag{5.28}$$

and the joint distribution of escapes is not given by Eq. (5.27), but by:

$$\begin{aligned} H\left(\tau^{(1)},\tau^{(2)}\right) &= \hat{C}\left(F_X(\tau^{(1)}), F_Y(\tau^{(2)})\right) = F_X(\tau^{(1)}) + F_Y(\tau^{(2)}) - 1 + \\ &+ \left(1 - F_X(\tau^{(1)})\right)\left(1 - F_Y(\tau^{(2)})\right)\exp\left(\frac{-\alpha\log(1-F_X(\tau^{(1)}))\log(1-F_Y(\tau^{(2)}))}{\log\left((1-F_X(\tau^{(1)}))(1-F_Y(\tau^{(2)}))\right)}\right) = \\ &= 1 - \bar{F}_X(\tau^{(1)}) - \bar{F}_Y(\tau^{(2)}) + \bar{F}_X(\tau^{(1)})\bar{F}_Y(\tau^{(2)})\exp\left(\frac{-\alpha\log(\bar{F}_X(\tau^{(1)}))\log(\bar{F}_Y(\tau^{(2)}))}{\log(\bar{F}_X(\tau^{(1)})\bar{F}_Y(\tau^{(2)}))}\right) = \end{aligned}$$

$$
\begin{aligned}
&= 1 - e^{-\lambda\tau^{(1)}} - e^{-\lambda\tau^{(2)}} + e^{-\lambda\tau^{(1)}} e^{-\lambda\tau^{(2)}} \exp\left(\frac{-\alpha \log(e^{-\lambda\tau^{(1)}}) \log(e^{-\lambda\tau^{(2)}})}{\log(e^{-\lambda\tau^{(1)}} e^{-\lambda\tau^{(2)}})}\right) = \\
&= 1 - e^{-\lambda\tau^{(1)}} - e^{-\lambda\tau^{(2)}} + e^{-\lambda\tau^{(1)}} e^{-\lambda\tau^{(2)}} \exp\left(\frac{\alpha\lambda\tau^{(1)}\tau^{(2)}}{\tau^{(1)} + \tau^{(2)}}\right).
\end{aligned}
\tag{5.29}
$$

Knowing the joint distribution there are two ways to reproduce the data, namely to simulate the data with no need to integrate the ODEs (5.13):

1. generate the dependent pseudo-observations from the given copula and map them into $\mathbb{R}_+$ through inverse functions of (5.24),

2. generate $\tau^{(2)}$ from the distribution (5.24) and then simulate $\tau^{(1)}$ given $\tau^{(2)}$ from the conditional distribution $H\left(\tau^{(1)}\middle|\tau^{(2)}\right)$.

Describing β in terms of copula dependence parameter can make it easier to calibrate the model given the real data. From Fig. 5.12 we can conclude that the Tawn survival copula parameter α depends linearly on the coupling strength β.

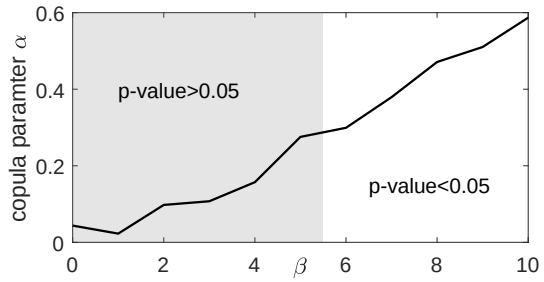

Figure 5.12: Tawn survival copula parameter α in terms of the coupling strength β.

5.6 Conclusions

In this chapter we introduced three different models of joint defaults of companies with systems based on the potential landscape. In this framework we identify the right-hand side well with the healthy state of a company, whereas the left-hand side well denotes the bankrupt state. In the suggested models the defaults occur primarily as noise-induced transitions, however, due to the saddle-node collision caused by the coupling, the deterministic forcing can drive the defaults as well.

We found that the two simple models exhibit several drawbacks. In the first model the coupling was affecting the other company all the time and hence for

the positive coupling the defaults were happening very rarely in comparison to the uncoupled case. In order to address this issue we introduced an activation threshold in a way that one company would affect the others only while residing in the left-hand side well and thus defaulting. Although the second model did not exhibit the problem with extremely rare defaults, it turned out that in this system the transitions between slow and fast domino regimes could appear in a non-smooth pitchfork bifurcation. Furthermore, in both of these simple models the influence of a defaulted company affects every other company for all future times. In order to make the model more realistic we address the aforementioned problems by adding an adaptation variable for each company. The adaptation variable is used to transfer smoothly the influence of a company while it is defaulting and then to decrease the influence gradually once the company has reached its default state. The effect of the coupling during a default is to skew the potential landscape such that the two positive equilibria (the risky state and the healthy state) move towards each other making it more likely for others to tip. Interestingly, in this model the defaults are a mixture of noise-, bifurcation- and rate-induced transitions.

In order to test if the outcome of the model with adaptation is reasonable we compare it to a model already existing in the literature and introduced in [123]. Based on the histograms of escape times we conclude that these two models can exhibit similar marginal statistics of escapes, however, the correspondence of the coupling strength is presumably not linear. Finally, it turns out that even though the histograms for selected strength of coupling look qualitatively similar, this does not imply that the joint distributions of escapes for the two models also agree. We analysed if any common copula would fit the escapes in the two-dimensional models. The copula that well matches the data simulated from model with adaptation is the Tawn survival copula, however, we did not find any copula which would fit the escapes simulated by the model of intensity introduced in [123].

We conclude that these two models are qualitatively similar when it comes to the marginal distribution of defaults, while the joint distributions of the first and the second escape in these models are different.

Chapter 6

General discussion

In this thesis we analysed several dynamical models applied to finance and economy. The models span a variety of financial sectors: stock and bond prices, traders' opinion dynamics and contagion within defaulting companies. It was shown that the Critical Transitions can be present in all examples investigated and we should be aware that a small change in conditions can lead to a rapid and difficult to reverse change in the output no matter if it concerns prices or defaults.

In Chapter 2 we studied a dynamical model of stock and bond prices introduced in [1]. We analysed scaling laws of the amplitude and the period of collapsing bubbles for certain limiting cases. Moreover, we gave a phase space description of how exactly a bubble is born and how foreshocks and aftershocks can arise. We showed that this model can exhibit noise-driven log-periodic oscillations for some parameter values. It might be a valuable experiment to see if the log-periodic oscillations are present not only for a small set of parameters, but for all cases where a deterministically driven bubble is possible. Furthermore, for the selected choice of parameters the frequencies observed in reality do not match exactly the frequencies in the model and we expect that varying the sensitivity of stock price and the noise strength could let us tune the model to the data analysed in [78].

The noise smooths the bifurcation curves, hence the oscillations in a stochastic system are observed even if no oscillations exist in the deterministic system. Thus, a different study could examine if this model can simulate intrinsic and extrinsic crashes. Namely, the externally caused crashes could depend just on the multiplicative noise, whereas the internally caused crashes are a result of the de-

terministic dynamics only. One could explore if such crashes differ in nature, for instance to see what the slope of an arising bubble and the speed of a crash would be for the different causes.

Chapter 3 looks at the model studied in Chapter 2 from a different perspective. We assume that the stochastic system is close to the saddle-node bifurcation and look for a way to predict when a crash will happen. By analysis of solutions on the centre manifold we find the approximate function of an inflating bubble. This approximation features finite-time singularities and the time of the singularity is used as a predictor of when a bubble explodes. The observed explosion of a bubble is treated as a *ghost* of the *real* finite-time singularity present only in the approximation.

This model is relatively simple as it idealises the economy to only two objects: stocks and bonds. In order to make it more realistic we could consider expanding the dimensions of the stock variable x to represent a market with several different risky assets. The risky assets can be coupled for instance by correlating the noisy increments W_t. It would be interesting to examine if any patterns of cascading downfalls of stocks can resemble the output of that model.

In an extended version, as well as in these basic two-dimensional models there is one big step needed to be done to make it more applicable, namely, finding the realistic values of parameters. They represent sensitivities of assets on past prices, which is not directly observable. Hence, it might be worthwhile to find the values of parameters based on data, for instance by the method of Kalman filtering taking x as a certain major stock index and y as a bond price from the same market. The stock price needs to be detrended in order to obtain a stationary process, whereas the bond price z should be rescaled, as the variation of z is much higher in the model than in reality – for instance, in Fig. 2.8 z oscillates between 0.1 and 0.9.

On the other hand, without any prior knowledge of sensitivities, the method of ghosts of finite-time singularities could be applied by simple curve fitting of all four parameters of the tangent function. In both of the scenarios (with and without any information on sensitivities) the approximated time to the jump can be understood as a measure of intrinsic risk.

Another issue, which is of high concern, is not only to predict but also to control

bubbles [136], for instance a market maker may wish to control the risks by taking certain actions. Without a reliable prediction of the sudden end of a bubble the control might be very expensive or even impossible. According to [37] not every bubble is of the same type. For some types of bubbles even if we predict a fall of prices in advance, it might not be possible to suppress the bubble early enough and avoid a crash anyway.

In Chapter 4 we analysed an extended two-dimensional dynamical version of the mean-field Ising model. This model presented in [48] is loosely based on social imitation in financial markets involving fast imitation and slower trend following. The main variable represents traders' opinions on an asset, whereas the other variable is incorporated as a moving average of past opinions and reinjected into the main variable.

The model was used to describe several market scenarios which are obtained when a parameter passes a bifurcation curve. It would be an interesting experiment to see if this model could be used to predict real market changes by confronting it with data about traders' decisions. Interestingly, for some parameter values chaotic behaviour was observed. We find it unlikely that the chaos in the low dimensional model is reproduced in detail by any market data, however it does hint that some apparent stochasticity may be due to nonlinear imitation behaviour.

In Chapter 5 we tried to capture contagion of defaults among companies by development of some new models of different complexity. All of the introduced models were based on a double-well potential system, where the wells represent healthy and default states. In order to reproduce a key property of mean reversion of the default rate after another company defaults we introduce a variable which stands for the adaptive response towards others' problems.

We explored different escape scenarios and found that the defaults can be a mixture of bifurcation-, noise- and rate-induced transitions. Furthermore, we compared statistics of defaults with a doubly-stochastic model of default intensity introduced in [123]. We found that even though the marginal distributions of the first and the second escape are qualitatively similar, fitting copulas to the simulated data suggests that the joint distributions of the two models are different. We showed that for coupling parameter small enough Tawn survival copula can well

match the data coming from our model, whereas for the data simulated with the model of intensity we did not fit well any common copula.

When discussing the joint probabilities of escapes in the two-dimensional model we assumed that the marginal distributions are exponential. This is only an approximation and might not be the case for higher dimensional processes. Moreover, even if in an uncoupled case the time of the first escape (which is equal to the minimum of the times of escape) is distributed exponentially, then in a coupled system it does not need to be distributed so. This is caused by the fact that one player can be influenced negatively by another one, even if the other one does not default, but only undergoes temporary problems. This phenomenon should slightly accelerate the first escape making it not necessarily distributed exponentially.

An extension of the suggested model (5.16) could be made by introducing heterogeneous coupling within an ecosystem of companies. This would involve the creation of a layered network where different layers of producers and consumers positively or negatively affect each other depending on whether they cooperate or compete. For example, producers within the same market would compete with each other, but cooperate with consumers. Such a modification would allow tracking of shock propagation in a heterogeneous network similar to [137], however in a continuous-time framework.

The final aim of the models in Chapter 5 could be to explore how a policy or a regulatory scheme could control the systemic risk within an economy, and, for example, to use this approach to understand precisely which interactions most affect the systemic risk and how to regulate this. Although more and stronger connections between companies lead to higher stability of single nodes, the entire network becomes more fragile. Hence, it would be crucial to look for some optimal interdependence of nodes to account both for the systemic as well as individual stability.

When it comes to the broader scope of applications of dynamical systems, an interesting concept to study is to determine dynamically how a crash happens to be often more dramatic than a long drawdown. Using dynamical systems formalism, it may be possible to model crashes affecting single stocks, companies or agents as rate-induced transitions. The conditions during a crash change quickly

enough that the agents that are not secured well enough are defaulting, whereas some of them would possibly survive if a global change was not as quick.

Finally, given the emergence of high frequency trading methods it would be interesting to apply fast-slow dynamical systems to understand the effects of timescale separation between manually requested transactions and the transactions initiated automatically by computer algorithms.

It is impossible to altogether avoid crashes caused by major external events, however, if they are caused by minor external events this comes into the remit of Critical Transitions. In this thesis we investigated several dynamical systems where the rapid market movements are indeed caused by Critical Transitions and thus can be interpreted as a result of intrinsic dynamics. Such dynamical models can help understand, and potentially provide tools to minimise, any negative influence of Critical Transitions, for instance by providing a better understanding of systemic risk.

References

[1] V. I. Yukalov, E. P. Yukalova, and D. Sornette, “Dynamical system theory of periodically collapsing bubbles,” *Eur. Phys. J. B*, vol. 88, no. 7, pp. 179–213, 2015.

[2] M. Scheffer, *Critical Transitions in Nature and Society*. Princeton and Oxford: Princeton University Press, 2009.

[3] V. I. Arnold, *Catastrophe theory*. Berlin Heidelberg: Springer-Verlag, 2nd ed., 1986.

[4] Y. A. Kuznetsov, *Elements of Applied Bifurcation Theory*. New York: Springer, 1998.

[5] P. Ashwin, S. Wieczorek, R. Vitolo, and P. Cox, “Tipping points in open systems: bifurcation, noise-induced and rate-dependent examples in the climate system,” *Philos Trans A Math Phys Eng Sci.*, vol. 370, 2012.

[6] S. Wieczorek, P. Ashwin, C. M. Luke, and P. M. Cox, “Excitability in ramped systems: The compost-bomb instability,” *Proc. R. Soc. A*, vol. 467, pp. 1243–1269, 2011.

[7] T. M. Lenton, H. Held, E. Kriegler, J. W. Hall, W. Lucht, S. Rahmstorf, and H. J. Schellnhuber, “Tipping elements in the Earth’s climate system,” *Proceedings of the National Academy of Sciences*, vol. 105, no. 6, pp. 1786–1793, 2008.

[8] K. J. Arrow, “General Economic Equilibrum: Purpose, Analytic Techniques, Collective Choice,” *The American Economic Review*, vol. 64, no. 3, pp. 253–272, 1974.

[9] D. A. Walker and J. Van Daal, eds., *Leon Walras, Elements of Theorical Economics or The Theory of Social Wealth*. Cambridge, UK: Cambridge University Press, 2014.

[10] J. D. Farmer and D. Foley, “The economy needs agent-based modelling,” *Nature*, vol. 460, no. 7256, pp. 685–686, 2009.

[11] S. H. Strogatz, *Nonlinear Dynamics and Chaos With Applications to Physics, Biology, Chemistry, and Engineering*. Cambridge: Westview Press, 2000.

[12] P. Glendinning, *Stability, instability and chaos: an introduction to the theory of nonlinear differential equations*. Cambridge: Cambridge University Press, 1994.

[13] S. Wiggins, *Introduction to Applied Nonlinear Dynamical Systems and Chaos*. Springer-Verlag New York, Inc, second ed., 2003.

[14] M. di Bernardo, F. Garofalo, L. Glielmo, and F. Vasca, "Switchings, bifurcations, and chaos in DC/DC converters," *IEEE Transactions on Circuits and Systems*, vol. 45, no. 2, pp. 133–141, 1998.

[15] J. Guckenheimer and P. Holmes, *Nonlinear Oscillations, Dynamical Systems, and Bifurcations of Vector Fields*. New York: Springer-Verlag, 1983.

[16] C. Pugh and M. Shub, "Linearization of Normally Hyperbolic Diffeomorphisms and Flows," *Inventiones mathematicae*, vol. 10, pp. 187–198, 1970.

[17] J. M. T. Thompson, H. B. Stewart, and Y. Ueda, "Safe, explosive, and dangerous bifurcations in dissipative dynamical systems," *Physical Review E*, vol. 49, no. 2, pp. 1019–1027, 1994.

[18] N. Berglund and B. Gentz, *Noise-Induced Phenomena in Slow-Fast Dynamical Systems*. London: Springer, 2006.

[19] J. Carr, *Applications of Centre Manifold Theory*. Springer-Verlag New York Inc., 1981.

[20] J.-P. Eckmann and D. Ruelle, "Ergodic theory of chaos and strange attractors," *Reviews of Modern Physics*, vol. 57, no. 3, pp. 617–656, 1985.

[21] K. Geist, U. Parlitz, and W. Lauterborn, "Comparison of Different Methods for Computing Lyapunov Exponents," *Progress of Theoretical Physics*, vol. 83, no. 5, pp. 875–893, 1990.

[22] K. E. Atkinson, *An Introduction to Numerical Analysis*. John Wiley & Sons, 1989.

[23] B. Ermentrout, *Simulating, Analyzing, and Animating Dynamical Systems: A Guide to XPPAUT for Researchers and Students*. Philadelphia, PA, USA: SIAM, 2002.

[24] B. Øksendal, *Stochastic Differential Equations: An Introduction with Applications*. Berlin: Springer, 2003.

[25] P. E. Kloeden and E. Platen, *Numerical solution of stochastic differential equations*. Berlin Heidelberg: Springer-Verlag, 1992.

[26] S. Smale, "Catastrophe theory: Selected papers, 1972-1977, by E.C. Zeeman," *Bulletin of the American Mathematical Society*, vol. 84, no. 6, pp. 1360–1368, 1978.

[27] M. Gladwell, *The Tipping Point*. Little, Brown and Company, 2000.

[28] D. Sornette, *Why Stock Markets Crash*. Princeton University, Princeton, 2003.

[29] T. Kaizoji and D. Sornette, "Market Bubbles and Crashes," *Encyclopedia of Quantitative Finance*, 2008.

[30] A. Kirilenko, A. S. Kyle, M. Samadi, and T. Tuzun, "The Flash Crash: High-Frequency Trading in an Electronic Market," *Journal of Finance*, vol. 72, no. 3, pp. 967–998, 2017.

[31] A. Johansen and D. Sornette, "Stock market crashes are outliers," *The European Physical Journal B*, vol. 1, pp. 141–143, 1998.

[32] A. Johansen and D. Sornette, "Large Stock Market Price Drawdowns Are Outliers," *Journal of Risk*, vol. 4, no. 2, pp. 69–110, 2001.

[33] D. Sornette and A. Johansen, "Significance of log-periodic precursors to financial crashes," *Quantitative Finance*, vol. 1, no. 4, pp. 452–471, 2001.

[34] A. Johansen and D. Sornette, "Shocks , Crashes and Bubbles in Financial Markets," *Brussels Economic Review*, vol. 53, no. 2, pp. 201–253, 2010.

[35] D. Sornette, "Dragon-kings, black swans, and the prediction of crises," *International Journal of Terraspace Science and Engineering*, vol. 2, no. 1, pp. 1–18, 2009.

[36] A. Hüsler, D. Sornette, and C. H. Hommes, “Super-exponential bubbles in lab experiments: Evidence for anchoring over-optimistic expectations on price,” *Journal of Economic Behavior and Organization*, vol. 92, pp. 304–316, 2013.

[37] D. Sornette, R. Woodard, W. Yan, and W.-X. Zhou, “Clarifications to questions and criticisms on the Johansen-Ledoit-Sornette financial bubble model,” *Physica A*, vol. 392, pp. 4417–4428, 2013.

[38] J. V. Andersen and D. Sornette, “Fearless versus fearful speculative financial bubbles,” *Physica A: Statistical Mechanics and its Applications*, vol. 337, no. 3-4, pp. 565–585, 2004.

[39] M. Schatz and D. Sornette, “Inefficient bubbles and efficient drawdowns in financial markets,” *Swiss Finance Institute Research Paper No. 18-49*, 2018.

[40] E. C. Zeeman, “On the unstable behaviour of stock exchanges,” *Journal of Mathematical Economics*, vol. 1, pp. 39–49, 1974.

[41] T. Lux, “Herd behaviour, bubbles and crashes,” *The Economic Journal*, vol. 105, pp. 881–896, 1995.

[42] B. van der Pol, “The Nonlinear Theory of Electric Oscillations,” *Proceedings of the IRE*, vol. 22, no. 9, pp. 1051–1086, 1934.

[43] W. A. Brock and C. H. Hommes, “Heterogeneous beliefs and routes to chaos in a simple asset pricing model,” *Journal of Economic Dynamics and Control*, vol. 22, no. 8, pp. 1235–1274, 1998.

[44] V. I. Yukalov, D. Sornette, and E. P. Yukalova, “Nonlinear Dynamical Model of Regime Switching Between Conventions and Business Cycles,” *J. Econ. Behav. Org.*, vol. 70, pp. 206–230, 2009.

[45] G. I. Bischi, M. Gallegati, L. Gardini, R. Leombruni, and A. Palestrini, “Herd behavior and nonfundamental asset price fluctuations in financial markets,” *Microeconomic Dynamics*, vol. 10, pp. 502–528, 2006.

[46] C. Chiarella, R. Dieci, and L. Gardini, “Asset price and wealth dynamics in a financial market with heterogeneous agents,” *Journal of Economic Dynamics and Control*, vol. 30, pp. 1755–1786, 2006.

[47] F. Tramontana, F. Westerhoff, and L. Gardini, “On the complicated price dynamics of a simple one-dimensional discontinuous financial market model with heterogeneous interacting traders,” *Journal of Economic Behavior and Organization*, vol. 74, pp. 187–205, 2010.

[48] M. Ollikainen, *Multiple market regimes in an equilibrium model of fundamentalist and noise traders*. Master’s thesis, ETH Zürich, 2016.

[49] A. Corcos, J.-P. Eckmann, A. Malaspinas, Y. Malevergne, and D. Sornette, “Imitation and contrarian behavior: hyperbolic bubbles, crashes and chaos,” *Quantitative Finance*, vol. 2, pp. 264–281, 2002.

[50] A. Omurtag and L. Sirovich, “Modeling a large population of traders: Mimesis and stability,” *Journal of Economic Behavior and Organization*, vol. 61, no. 4, pp. 562–576, 2006.

[51] V. Cheriyan and A. J. Kleywegt, “A dynamical systems model of price bubbles and cycles,” *Quantitative Finance*, vol. 16, no. 2, pp. 309–336, 2016.

[52] D. Sornette and J. V. Andersen, “A Nonlinear Super-Exponential Rational Model of Speculative Financial Bubbles,” *Int. J. Mod. Phys.*, vol. C 13, no. 2, pp. 171–188, 2002.

[53] W. A. Brock, D. A. Hsieh, and B. D. LeBaron, “Nonlinear dynamics, chaos, and instability: statistical theory and economic evidence,” *MIT press*, 1991.

[54] W. A. Brock and C. H. Hommes, “A rational route to randomness,” *Econometrica*, vol. 65, no. 5, pp. 1059–1095, 1997.

[55] W. A. Brock and S. N. Durlauf, “Discrete choice with social interactions,” *The Review of Economic Studies*, vol. 68, no. 2, pp. 235–260, 2001.

[56] W. A. Brock and S. N. Durlauf, “Interactions-based models,” *Handbook of econometrics*, vol. 5, pp. 3297–3380, 2001.

[57] W. A. Brock, C. H. Hommes, and F. O. O. Wagener, “Evolutionary dynamics in markets with many trader types,” *Journal of Mathematical Economics*, vol. 41, no. 1, pp. 7–42, 2005.

[58] A. Hüsler, D. Sornette, and C. H. Hommes, “Super-exponential bubbles in lab experiments: Evidence for anchoring over-optimistic expectations on price,” *Journal of Economic Behavior and Organization*, vol. 92, pp. 304–316, 2013.

[59] M. Leiss, H. H. Nax, and D. Sornette, “Super-Exponential Growth Expectations and the Global Financial Crisis,” *Journal of Economic Dynamics and Control*, vol. 55, pp. 1–13, 2015.

[60] D. Sornette and P. Cauwels, “Financial bubbles: mechanisms and diagnostics,” *Review of Behavioral Economics*, vol. 2, no. 3, pp. 279–305, 2015.

[61] A. Johansen, O. Ledoit, and D. Sornette, “Crashes as critical points,” *International Journal of Theoretical and Applied Finance*, vol. 3, pp. 219–255, 2000.

[62] A. Johansen and D. Sornette, “Finite-time singularity in the dynamics of the world population, economic and financial indices,” *Physica A*, vol. 294, no. 3-4, pp. 465–502, 2001.

[63] K. Ide and D. Sornette, “Oscillatory finite-time singularities in finance, population and rupture,” *Physica A*, vol. 307, pp. 63–106, 2002.

[64] L. Lin and D. Sornette, “Diagnostics of Rational Expectation Financial Bubbles with Stochastic Mean-Reverting Termination Times,” *The European Journal of Finance*, vol. 19, no. 5-6, pp. 344–365, 2013.

[65] L. Lin, R. E. Ren, and D. Sornette, “The Volatility-Confined LPPL Model: A Consistent Model of ‘Explosive’ Financial Bubbles With Mean-Reversing Residuals,” *International Review of Financial Analysis*, vol. 33, pp. 210–225, 2014.

[66] P. J. Holmes and D. A. Rand, “Bifurcations of the forced van der Pol oscillator,” *Quarterly of Applied Mathematics*, vol. 35, pp. 495–509, 1978.

[67] J.-M. Gambaudo, “Perturbation of a Hopf Bifurcation by an External Time-Periodic Forcing,” *Journal of Differential Equations*, vol. 57, pp. 172–199, 1985.

[68] F. O. O. Wagener, “Semilocal analysis of the k : 1 and k : 2 resonances in quasiperiodically forced systems,” in *Global Analysis of Dynamical Systems* (H. W. Broer, B. Krauskopf, and G. Vegter, eds.), pp. 113–129, Bristol and Philadelphia: Insitute of Physics Publishing, 2001.

[69] K. Saleh and F. O. O. Wagener, “Semi-global analysis of periodic and quasi-periodic normal-internal k : 1 and k : 2 resonances,” *Nonlinearity*, vol. 23, pp. 2219–2252, 2010.

[70] P. Gaspard, “Measurement of the Instability Rate of a Far-from-Equilibrium Steady State at an Infinite Period Bifurcation,” *The Journal of Physical Chemistry*, vol. 94, no. 1, 1990.

[71] R. J. Shiller and A. E. Beltratti, “Stock prices and bond yields,” *Journal of Monetary Economics*, vol. 30, no. 1, pp. 25–46, 1992.

[72] C. Krishnan, R. Petkova, and P. Ritchken, “Correlation risk,” *Journal of Empirical Finance*, vol. 16, pp. 353–367, 2009.

[73] K. Guo, W.-X. Zhou, S.-W. Cheng, and D. Sornette, “The US stock market leads the Federal funds rate and Treasury bond yields,” *PLoS ONE*, vol. 6, no. 8, 2011.

[74] H. Meng, H.-C. Xu, W.-X. Zhou, and D. Sornette, “Symmetric thermal optimal path and time-dependent lead-lag relationship: novel statistical tests and application to UK and US real-estate and monetary policies,” *Quantitative Finance*, 2016.

[75] A. Johansen, D. Sornette, and O. Ledoit, “Predicting Financial Crashes Using Discrete Scale Invariance,” *Journal of Risk*, vol. 1, no. 4, pp. 5–32, 1999.

[76] D. Sornette, R. Woodard, W. Yan, and W.-X. Zhou, “Clarifications to questions and criticisms on the Johansen-Ledoit-Sornette financial bubble model,” *Physica A*, vol. 392, no. 19, pp. 4417–4428, 2013.

[77] W.-X. Zhou and D. Sornette, “Non-Parametric Analyses of Log-Periodic Precursors to Financial Crashes,” *International Journal of Modern Physics C*, vol. 14, no. 8, pp. 1107–1126, 2003.

[78] M. Bartolozzi, S. Drożdż, D. B. Leinweber, J. Speth, and A. W. Thomas, “Self-Similar Log-Periodic Structures in Western Stock Markets from 2000,” *International Journal of Modern Physics C*, vol. 16, no. 9, pp. 1347–1361, 2005.

[79] W. H. Press, S. A. Teukolsky, W. T. Vetterling, and B. P. Flannery, *Numerical Recipes in Fortran 77: The Art of Scientific Computing*. Cambridge University Press, 2nd ed., 1992.

[80] G. B. Ermentrout and N. Kopell, “Parabolic Bursting in an Excitable System Coupled with a Slow Oscillation,” *SIAM Journal on Applied Mathematics*, vol. 46, no. 2, pp. 233–253, 1986.

[81] C. M. Bender and S. A. Orszag, *Advanced Mathematical Methods for Scientists and Engineers: Asymptotic methods and perturbation theory*. Springer-Verlag New York, Inc., 1999.

[82] D. Sornette, “Predictability of catastrophic events: material rupture, earthquakes, turbulence, financial crashes and human birth,” *Proceedings of the National Academy of Sciences USA*, vol. 99, no. 1, pp. 2522–2529, 2002.

[83] N. Israeli and N. Goldenfeld, “Computational Irreducibility and the Predictability of Complex Physical Systems,” *Phys. Rev. Lett.*, vol. 92, no. 7, 2004.

[84] N. Israeli and N. Goldenfeld, “Coarse-graining of cellular automata, emergence, and the predictability of complex systems,” *Phys. Rev. E*, vol. 73, no. 026203, 2006.

[85] E. Edlund and M. N. Jacobi, “Renormalization of Cellular Automata and Self-Similarity,” *J. Stat. Phys.*, vol. 139, pp. 972–984, 2010.

[86] B. M. McCoy and T. T. Wu, *The Two-Dimensional Ising Model*. Cambridge, Mass.: Harvard University Press, 1973.

[87] E. Callen and D. Shapero, “A theory of social imitation,” *Phys. Today*, vol. 27, no. 7, pp. 23–28, 1974.

[88] S. Galam, Y. Gefen, and Y. Shapir, “Sociophysics: A new approach of sociological collective behaviour. I. mean-behaviour description of a strike,” *The Journal of Mathematical Sociology*, vol. 9, no. 1, pp. 1–13, 1982.

[89] S. Galam and S. Moscovici, “Towards a Theory of Collective Phenomena: Consensus and Attitude Changes in Groups,” *European Journal of Social Psychology*, vol. 21, pp. 49–74, 1991.

[90] M. B. Gordon, J.-P. Nadal, D. Phan, and V. Semeshenko, “Discrete Choices under Social Influence: Generic Properties,” *Mathematical Models and Methods in Applied Sciences*, vol. 19, no. Suppl. 1, pp. 1441–1481, 2009.

[91] M. Granovetter and R. Soong, “Threshold models of diffusion and collective behavior,” *J. Math. Sociol*, vol. 9, pp. 165–179, 1983.

[92] E. W. Montroll and W. W. Badger, *Introduction to Quantitative Aspects of Social Phenomena*. New York: Gordon and Breach, 1974.

[93] J.-P. Nadal, D. Phan, M. B. Gordon, and J. Vannimenus, “Multiple equilibria in a monopoly market with heterogeneous agents and externalities,” *Quantitative Finance*, vol. 5, no. 6, pp. 557–568, 2005.

[94] A. Orléan, “Bayesian interactions and collective dynamics of opinion: Herd behavior and mimetic contagion,” *Journal of Economic Behavior & Organization*, vol. 28, pp. 257–274, 1995.

[95] D. Phan, M. B. Gordon, and J.-P. Nadal, “Social Interactions in Economic Theory: An Insight from Statistical Mechanics,” in *Cognitive Economics – An Interdisciplinary Approach*, pp. 335–354, Springer Science & Business Media, 2004.

[96] T. C. Schelling, “Dynamic models of segregation,” *J. Math. Sociol*, vol. 1, no. 2, pp. 143–186, 1971.

[97] D. Sornette, “Physics and financial economics (1776-2014): puzzles, Ising and agent-based models,” *Reports on Progress in Physics*, vol. 77, no. 6, p. 062001, 2014.

[98] W. Weidlich, “The statistical description of polarization phenomena in society,” *Br. J. Math. Stat. Psychol.*, vol. 24, pp. 251–266, 1971.

[99] W. Weidlich, “Physics and social science – the approach of synergetics,” *Phys. Rep.*, vol. 204, pp. 1–163, 1991.

[100] W. Weidlich, “Sociodynamics – a systematic approach to mathematical modelling in the social sciences,” *Chaos, Solitons and Fractals*, vol. 18, no. 3, pp. 431–437, 2003.

[101] W. Weidlich and H. Huebner, “Dynamics of political opinion formation including catastrophe theory,” *Journal of Economic Behavior & Organization*, vol. 67, pp. 1–26, 2008.

[102] G. Harras, C. J. Tessone, and D. Sornette, “Noise-induced volatility of collective dynamics,” *Phys. Rev. E*, vol. 85, p. 011150, 2012.

[103] T. Kaizoji, M. Leiss, A. Saichev, and D. Sornette, “Super-exponential endogenous bubbles in an equilibrium model of fundamentalist and chartist traders,” *Journal of Economic Behavior & Organization*, vol. 112, pp. 289–310, 2015.

[104] D. Sornette and W.-X. Zhou, “Importance of positive feedbacks and overconfidence in a self-fulfilling Ising model of financial markets,” *Physica A*, vol. 370, no. 2, pp. 704–726, 2006.

[105] W.-X. Zhou and D. Sornette, “Self-fulfilling Ising Model of Financial Markets,” *Eur. Phys. J. B*, vol. 55, pp. 175–181, 2007.

[106] R. Israel, A. Ross, T. J. Moskowitz, and L. Serban, “Implementing Momentum: What Have We Learned?,” *SSRN Electronic Journal*, 2017.

[107] Y. Lempérière, C. Deremble, P. Seager, M. Potters, and J. P. Bouchaud, “Two centuries of trend following,” *The Journal of Investment Strategies*, vol. 3, no. 3, pp. 41–61, 2014.

[108] T. Roncalli, “Keep Up The Momentum,” *SSRN Electronic Journal*, 2017.

[109] C. Baesens, “Gevrey series and dynamic bifurcations for analytic slow-fast mappings,” *Nonlinearity*, vol. 8, no. 2, pp. 179–201, 1995.

[110] P. Mandel and T. Erneux, “Laser Lorenz equations with a time-dependent parameter,” *Phys. Rev. Lett.*, vol. 53, no. 19, pp. 1818–1820, 1984.

[111] A. G. Haldane and R. M. May, “Systemic risk in banking ecosystems,” *Nature*, vol. 469, no. 7330, pp. 351–355, 2011.

[112] P. Gai and S. Kapadia, “Contagion in financial networks,” *Proceedings of the Royal Society A*, vol. 466, no. 2120, pp. 2401–2423, 2010.

[113] D. Acemoglu, A. Ozdaglar, and A. Tahbaz-Salehi, “Systemic risk and stability in financial networks,” *American Economic Review*, vol. 105, no. 2, pp. 564–608, 2015.

[114] P. Glasserman and H. P. Young, “Contagion in Financial Networks,” *Journal of Economic Literature*, vol. 54, no. 3, pp. 779–831, 2016.

[115] F. Caccioli, P. Barucca, and T. Kobayashi, “Network models of financial systemic risk: A review,” *Journal of Computational Social Science*, vol. 1, no. 1, pp. 81–114, 2018.

[116] F. Allen and D. Gale, “Financial Contagion,” *Journal of Political Economy*, vol. 108, no. 1, pp. 1–33, 2000.

[117] D. J. Watts, “A simple model of global cascades on random networks,” *PNAS*, vol. 99, no. 9, pp. 5766–5771, 2002.

[118] S. Battiston, M. Puliga, R. Kaushik, P. Tasca, and G. Caldarelli, “DebtRank: Too central to fail? Financial networks, the FED and systemic risk,” *Scientific Reports*, vol. 2, pp. 1–6, 2012.

[119] J. P. Bouchaud and R. Cont, “A Langevin approach to stock market fluctuations and crashes,” *European Physical Journal B*, vol. 6, no. 4, pp. 543–550, 1998.

[120] P. Sieczka, D. Sornette, and J. A. Holyst, “The Lehman Brothers effect and bankruptcy cascades,” *European Physical Journal B*, vol. 82, pp. 257–269, 2011.

[121] P. Ashwin, J. Creaser, and K. Tsaneva-Atanasova, “Fast and slow domino regimes in transient network dynamics,” *Physical Review E*, vol. 96, no. 5, pp. 1–14, 2017.

[122] P. Ashwin, J. Creaser, and K. Tsaneva-Atanasova, “Sequential escapes: onset of slow domino regime via a saddle connection,” *arXiv:1804.00550v1*, 2018.

[123] K. Giesecke, K. Spiliopoulos, and R. B. Sowers, “Default clustering in large portfolios: Typical events,” *Annals of Applied Probability*, vol. 23, no. 1, pp. 348–385, 2013.

[124] A. H. South and Z. R. Gurwitz, “Default, Transition, and Recovery: 2017 Annual Global Structured Finance Default Study And Rating Transitions,” tech. rep., Standard & Poor, 2018.

[125] N. Berglund, “Kramers’ law: Validity, derivations and generalisations,” *Markov Processes Relat. Fields*, no. 19, 2013.

[126] S. Azizpour, K. Giesecke, and G. Schwenkler, “Exploring the sources of default clustering,” *Journal of Financial Economics*, vol. 129, no. 1, pp. 154–183, 2018.

[127] N. G. Van Kampen, *Stochastic Processes in Physics and Chemistry*. Elsevier B.V., third ed., 2007.

[128] K. Spiliopoulos, J. A. Sirignano, and K. Giesecke, “Fluctuation analysis for the loss from default,” *Stochastic Processes and their Applications*, vol. 124, no. 7, pp. 2322–2362, 2014.

[129] H. Joe, *Multivariate Models and Dependence Concepts*. London: Chapman and Hall, 1997.

[130] R. B. Nelsen, *An Introduction to Copulas*. New York: Springer, 2nd ed., 2006.

[131] N. Balakrishnan and C.-D. Lai, *Continuous Bivariate Distributions*. Springer, 2009.

[132] Y. Malevergne and D. Sornette, *Extreme Financial Risks*. Springer-Verlag Berlin Heidelberg, 2006.

[133] K. Giesecke, “Correlated default with incomplete information,” *Journal of Banking and Finance*, vol. 28, no. 7, pp. 1521–1545, 2004.

[134] R Foundation for Statistical Computing: R Core Team, “R: A Language and Environment for Statistical Computing,” 2018.

[135] M. Hofert, I. Kojadinovic, M. Maechler, and J. Yan, “copula: Multivariate Dependence with Copulas,” 2017.

[136] H. L. d. S. Cavalcante, M. Oria, D. Sornette, E. Ott, and D. J. Gauthier, “Predictability and suppression of extreme events in a chaotic system,” *Physical Review Letters*, vol. 111, no. 198701, 2013.

[137] S. Battiston, D. Delli Gatti, M. Gallegati, B. Greenwald, and J. E. Stiglitz, “Credit chains and bankruptcy propagation in production networks,” *Journal of Economic Dynamics and Control*, vol. 31, no. 6, pp. 2061–2084, 2007.